UNIVERSITY OF BELGRADE

FACULTY OF PHYSICS

Aleksandar Ž. Tomović

Electronic properties and morphologies of thin films of organic molecules obtained by combinatorial deposition from gaseous phase

Doctoral Dissertation

Belgrade, 2015

БЕОГРАДСКИ УНИВЕРЗИТЕТ
ФИЗИЧКИ ФАКУЛТЕТ

Александар Ж. Томовић

Електронске особине и морфологија танких филмова органских материјала добијених комбинаторијалним напаравањем из гасне фазе

Докторска Дисертација

Београд, 2015

Подаци о ментору и члановима комисије

Ментор: др Владимир П. Јовановић, научни сарадник
Институт за мултидисциплинарна истраживања

Чланови комисије

Проф. др Душан Поповић
Ванредни професор, Физички Факултет, Београд

Проф. др Горан Попарић
Ванредни професор, Физички Факултет, Београд

Проф. др Стеван Стојадиновић
Ванредни професор, Физички Факултет, Београд

Проф. др Војислав Срданов
Пензионисани професор на Калифорнијском Универзитету, Санта Барбара, САД

др Наташа Бибић
Научни саветник, Институт за нуклеарне науке Винча

др Владимир Јовановић
Научни сарадник, Институт за мултидисциплинарна истраживања, Београд

Acknowledgments

First I am grateful to my mentor dr Vladimir P. Jovanović for his support, encourgment and above all patience during our trip trough the dire straits of the field of organic materials, which was new to both of us. Without him this work would be impossible.

I owe my gratitude to,

...dr Radomir Žikić for opening doors of his laboratory to me, for teaching me about physcis and life, and supporting decisions that i have made during my work.

...dr Vojislav Srdanov who generously shared his knowledge and experience in the fields of organic materials and spectroscopy and also his love for science.

...dr Laszlo Forro for his support with pentacene study and to his coworkers Dr. Jacim Jacimovic and Dr. Benmessaoud Iness for measurement of conductive properties and IR spectra of micro rods, respectively.

I would like to thank following people for their collaboration and contribution to this work:

dr James Pavlovich from the department of Chemistry and Biochemistry of the University of California Santa Barbara for mass spectroscopy of TPD samples.

dr Paolo Milani and his group from the department of physics, The University of Milan for NMR of TPD samples.

dr Gabor Bortel and dr Gyula Faigel from Institute for Solid State Physics and Optics, Budapest for XRD measurements performed on pentacene samples.

dr Dragan Dramlić and Zoran Velikić for use of their UV-VIS spectrometer and many fruitful discussions.

dr Katarina Radulović for measurement of IR spectra of TPD and DPVBi.

dr Suzana Velicković and Branislav Nastasijević for collaboration, patience and mass spectroscopy measurement of DPVBi and pentacene samples.

I would like to thank my present and former lab colleagues Ivana, Milan, Radmila, Viktor, Nemanja M., Nemanja K. and Jaca who created pleasant working environment, I have thoroughly enjoyed working, discussing and laughing with you.

Last but not least I am deeply grateful to my family and friends for continuous support and understanding during my studies.

I would like to dedicate this thesis to my parents Milica and Života.

Electronic properties and morphologies of thin films of organic molecules obtained by combinatorial deposition from gaseous phase

Abstract

There is an ongoing interest in organic materials due to their application in various organic electronic devices. However stability of organic materials limits their potential use. They are prone to degradation both during the working life and storage. One of the main causes is extrinsic degradation, under the influence of oxygen and moisture. This problem can be solved by encapsulation of devices. However no encapsulation is perfect.

In the first part of this work a study of degradation of thin films of N,N′-bis(3-methylphenyl)-N,N′-bis(phenyl)benzidine (TPD) and 4,4′-bis(2,2-diphenylvinyl)-1,1′-biphenyl (DPVBi) under UV irradiation in air is given. Films of both materials are stable in vacuum, but readily degrade in the presence of oxygen. Thus, the necessary condition for degradation is *the simultaneous presence of UV light and oxygen*. Chemical analysis of irradiated films by NMR, mass and infrared spectroscopy revealed presence of oxidized species (impurities). These impurities are responsible for increased morphological stability of irradiated films and quenching of photoluminescence. Only small amount of impurities, 0.4 % (0.2 %) for TPD (DPVBi), causes 50 % decrease of photoluminescence. This implies a non-trivial mechanism of quenching. For both molecules it was found that distance between impurities is smaller or equal to exciton diffusion length, which is the necessary condition for quenching. Following mechanism of quenching is proposed: exciton diffuses by hopping form one DPVBi (TPD) to another through FRET in a random walk manner. If, during its lifetime, it comes to proximity of an impurity, a Dexter-type energy transfer occurs and PL is quenched.

Findings of DPVBi study are important because they show that even a small amount of oxygen that penetrates a DPVBi layer would impair luminescence efficiency of a device. Moreover, the absorption of own radiation (for DPVBi and TPD both) would additionally contribute to the rate of degradation of a device. It is reasonable to expect that transport properties would also be affected when materials are used as a hole-transporting layer in OLEDs.

The second part of the work concerns characterization of micro rods and small crystals on the surface of pentacene films annealed in air. These structures are interesting as they could be easily integrated into devices due to their shape and size. Micro rods seem to have crystalline structure and are composed of oxidized pentacene species. Further experiments are needed in order to resolve the exact chemical composition and structure of micro rods.

Keywords: TPD, DPVBi, Pentacene, thin films, organic materials, degradation, oxidation, PL quenching, UV-VIS spectroscopy, mass spectroscopy.
Scientific field: Physics
Field of academic expertise: Physics of condensend matter
UDC number: 538.9(043.3)

Електронске особине и морфологија танких филмова органских материјала добијених комбинаторијалним напаравањем из гасне фазе

Резиме

Постоји велики интерес за органске материјале због њихове примене у различитим органским електронским уређајима. Међутим стабилност орагнских материјала ограничава њихову примену. Они су подложни деградацији не само за време операције уређаја већ и за време складиштења. Један од главних узрока је деградација услед спољних утицаја: светлости, влаге и кисеоника. Овај проблем може да се превазиђе путем енкапсулације уређаја, али ниједан вид енкапсулације није савршен.

У првом делу рада биће изложена студија деградације танких филмова N,N′-bis(3-methylphenyl)-N,N′-bis(phenyl)benzidine (TPD) и 4,4′-bis(2,2-diphenylvinyl)-1,1′-biphenyl (DPVBi) под утицајем УВ зрачења у ваздуху. Филмови оба материјала су стабилни у вакууму, али деградирају у присуству кисеоника. Дакле, непоходан услов за деградацију, потребно је *истовремено присуство УВ светлости и кисеоника*. Хемијска анализа осветљених филмова извршена уз помоћ NMR, масене и инфрацрвене спектроскопије показала је присуство оксидованих врста (нечистоћа). Нечистоће су одговорне за повећану морфолошку

стабилност осветљених филмова и гашење фотолуминесценције. Мала количина нечистоћа, 0.4 % (0.2 %) у случају TPD (DPVBi), изазива пад интензитета фотолуминесценције од 50 %. Ово имплицира нетривијални механизам гашења фотолуминесценције. За оба молекула је нађено да је растојања између нечистоћа мање или приближно једнако дужини дифузије ексцитона што је неопходан услов за гашење фотолуминесценције. Предложен је механизам гашења: ексцитони дифундују у скоковима од једног до другог молекула DPVBi (TPD) случајним ходом путем Форстеровог резонатног трансфера енергије. Ако у току свог времена живота ексцитон дође у близину нечистоће долази до Декстеровог трансфера енергије и гашења фотолуминесценције.

Резултати студије за DPVBi молекул су важни зато што показују да и мала количина кисеоника у слоју DPVBi може озбиљно да утиче на фотолуминесцентну ефикасност уређаја. Штавише, апсорпција сопственог зрачења (код оба молекула, DPVBi и TPD) ће додатно да допринесе брзини деградације уређаја. Разумно је претпоставити да ће и транспортне особине бити нарушене у случају када се ови материјали користе као слој за транспорт шупљина у органским светлећим диодама.

Други део рада тиче се карактеризације микро штапића и малих кристала насталих на површини пентаценских филмова током грејања у ваздуху. Добијене структуре су интересатне будући да би због своје величине и облика лако могле да буду интегрисана у електронске уређаје. Микро штапићи поседују кристалну структуру и сачињени су од молекула који су последица оксидације пентацена. Додатни експерименти су неопходни како би се утврдио тачан хемијски састав штапића и њихова структура.

Кључне речи: TPD, DPVBi, пентацен, танки филмови, органски материјали, деградација, оксидација, гашење фотолуминесценције, UV-VIS спектроскопија, масена спектроскопија.

Научна област: Физика

Ужа научна област: Физика кондезоване материје

УДК број: 538.9(043.3)

Table of contents

1. Introduction 1
   1.1 Brief history of organic electronics 1
   1.2 Thin films 2
   1.3 Organic materials 2
      1.3.1 Advantages of organic materials 3
      1.3.2 Disadvantages of organic materials 3
   1.4 Extrinsic degradation of thin organic films 5
   1.5 Dissertation outline 6
      References for Chapter 1 6
2. Experimental details 10
   2.1 Materials 10
   2.2 Physical vapor deposition 11
      2.2.1 Deposition apparatus 11
      2.2.2 Combinatorial physical vapor deposition 13
      2.2.3 Preparation of substrates 15
      2.2.4 Evaporation procedure 16
   2.3 Irradiation of thin films 17
   2.4 Experimental setups for spectroscopic measurement 17
      2.4.1 Infrared spectroscopy (IR) 18
      2.4.2 Raman spectroscopy 18
      2.4.3 UV –VIS and photoluminescence spectroscopy 19
   2.5 Spectroscopic data acquisition and manipulation 23
      2.5.1 Absorbance 23
         2.5.1.1 Profile of thickness measurement 24
         2.5.1.2 Absorbance vs. irradiation time 25
      2.5.2 Photoluminescence 25
         2.5.2.1 PL spectra vs. irradiation time 26
      2.5.3 Raman 26

2.6 Atomic Force Microscopy (AFM) 26
2.7 ^{1}H nuclear magnetic resonance (NMR) spectroscopy 27
2.8 Mass spectroscopy 27
2.8.1 Atmospheric Solid Analysis Probe (ASAP) 27
2.8.2 Laser Desorption Ionization Time of Flight (LDI TOF) mass spectroscopy 28
2.8.3 FI/FD Time of Flight 29
2.9 X-ray diffraction (XRD) 29
References for Chapter 2 29
3. Influence of UV irradiation on morphologies and chemical composition of thin amorphous films of TPD and DPVBi 31
3.1 Morphology of pristine and UV irradiated thin amorphous TPD and DPVBi films 31
3.1.1 Morphology of pristine thin amorphous TPD and DPVBi films 31
3.1.2 Influence of UV irradiation on morphologies of thin TPD and DPVBi films 36
3.2 Investigation of chemical changes 39
3.2.1 Mass spectroscopy 40
3.2.2 ^{1}H NMR spectroscopy 44
3.2.3 Vibrational spectroscopy 46
References for Chapter 3 49
4. Quenching of photoluminescence 51
4.1 Absorbance and photoluminescence of thin TPD and DPVBi films 51
4.1.1 Spectral characteristics of pristine films 51
4.1.2 Influence of irradiation on absorbance and photoluminescence 54
4.1.2.1 Influence of different UV light intensities in the case of DPVBi 58
4.1.2.2 Irradiation of DPVBi under different oxygen pressures 59
4.2 The mechanism of PL quenching 61
References for Chapter 4 64
5. Nano and micro rods obtained by annealing of thin pentacene films in air 67
5.1 Characterization of pentacene thin films 67
5.2 Annealing of pentacene thin films and crystal growth 72
5.3 Characterization of MRs and CSs 74

5.4 Explanation of crystal growth 80
References of Chapter 5 81
6. Conclusions 83
Appendix A: Assignation of NMR peaks 85
References for Appendix A 88
Appendix B: Evidences for formation of complexes upon irradiation of DPVBi films with UV light in air 89
B.1 Evidence for formation of complexes found in PL spectra 89
B.2 Evidences for formation of complexes observed by Raman spectroscopy 89
B.3 Partial reversibility of photoluminescence 91
References for Appendix B 91
Appendix C: Raman and IR spectra of TPD and DPVBi 92
References for Appendix C 93

1. Introduction

1.1 Brief history of organic electronics

There is an ongoing interest in organic materials and electronics because of their unique properties; someone may ask when did it all start? According to Wudl [1] records of photoconductivity of organic materials go as far back as the beginning of the 20th century. Electroluminescence was observed in the 1950s by André Bernanose *et al*. [2], followed by Martin Pope *et al.* [3] in 1960s when the electroluminescence was obtained from anthracene single crystals under high voltages. High voltages and problems related with production of large single crystals suggested that there is no practical use of this discovery. Attempts were made to produce an electroluminescent device from a thin amorphous film of an organic material, but all devices were short lived. That changed with the pioneering work of Tang and Van Slyke [4] on production of first organic light emitting diode in 1987, which is considered by the many as the birth of organic electronics. The same year saw production of the first organic filed effect transistor by Koezuke *et al*. which was made of thin polythiophene film [5]. In the year 2000 Alan. G. McDiarmid, Alan J. Heeger, and H. Shirakawa received the Nobel Prize for their work on the discovery and development of conductive polymers. Two out of three laureates of the 2010 Millennium technology prize made their contribution in the field of organic electronics: Sir Richard Friend for his work in field of organic light emitting diodes (OLEDs) and Michael Grätzel for his work with dye-sensitized solar cells.

There was an expansion of organic electronics in the last decade, various types of organic devices are being produced nowadays: OLEDs, organic field effect transistors (OFETs), organic photovoltaics (OPVs) etc. There are many products containing organic materials already available to consumers such as TVs and mobile phones which contain OLED displays. Price of the OLED TV is still very high when compared to the standard technology. The largest benefit would be achieved with the mass production of OPVs, however many of the challenges remain before the true potential of the organic materials is reached.

1.2 Thin films

Thin films of organic materials are building blocks for all of the organic electronic devices. The number of different layers varies in the different devices, for example the first OLED built by Tang and Van Slyke consisted of only two layers of organic materials. Modern designs usually incorporate seven layers of organics and sometimes even more than that. Performance of the device depends not only on the materials that are used in the layers but also on the thickness of the respective layers. For example in OPVs active layer should be as thick as possible to absorb enough light (produce enough charge carriers) but at the same time sufficiently thin for charge carriers to reach corresponding transporting layer.

Depending on the application, for example in OLEDs, it is better to use amorphous films than polycrystalline, due to easy and reproducible deposition and spatial homogeneity of optical and transport properties [6]. Organic thin films are usually obtained either by spin-coating or by physical vapor deposition (PVD). Both processes lead to thermodynamically unstable amorphous films that are prone to various types of structural degradation. These include changes in thin film morphology, which may occur at considerably lower temperatures in comparison to the bulk glass transition temperature T_g [7]. In the first part of this work we will deal with morphological stability of organic thin films. To optimize the performance of organic electronic devices one has to balance optoelectronic properties with morphological properties of materials.

1.3 Organic materials

Richness of organic chemistry enables design of new molecules and modifications of the existing ones in order to enhance wanted and remove unwanted properties. Organic materials can be naturally divided into two distinct groups: polymers and small molecules. Both of the groups have their own advantages and disadvantages.

1.3.1 Advantages of organic materials

What makes the organic electronics so appealing are properties of the organic materials which give possibility for easier and cheaper production:

- low temperature processing,
- large area applications,
- molecules and polymers can be designed or modified,
- doping.

Organic materials can be evaporated at much lower temperatures; this is an advantage over traditional CMOS technology where high temperature processes are involved which require temperature resistant materials and crystalline silicon as substrate. Solubility of organic materials (mainly polymers) also enables alternative types of deposition such as spin coating and printing. This is very convenient as not only it does not require use of vacuum but the clean room requirements are much less stringent. Both spin coating and printing are suitable for large area applications, with printing being more cost effective as the material is applied only where it is needed, which omits use of patterning techniques. All of these processes are compatible with use of plastic and flexible substrates, which is not only cheaper but also opens a whole new area of applications.

Optical and transport properties of organic materials can be controlled through doping, which is easier than in the case of inorganic materials. Organic molecules can also be designed and modified in order to achieve wanted or remove unwanted properties. The existing library of functional organic materials is vast, and the new materials are produced on regular basis.

1.3.2 Disadvantages of organic materials

There are also problems which come with use of organic materials:

- low carrier mobility,
- incompatibility with processes in classical semiconductor industry,
- stability of organic materials, with consequences to their optical and electronic properties.

Low carrier mobility of organic materials is one of the main factors which limit their possible area of application. So far pentacene and rubrene hold the record for the highest mobility achieved with organic materials. In the case of the rubrene the value is 20 $cm^2V^{-1}s^{-1}$ and it was achieved with the device made out of single crystal. The highest mobility obtained in a FET containing a thin film of pentacene is around 5 $cm^2V^{-1}s^{-1}$. While both values surpass amorphous silicon they fall short when compared to the values for crystalline or polycrystalline silicon which are 1000 $cm^2V^{-1}s^{-1}$ and 100 $cm^2V^{-1}s^{-1}$, respectively.

The fact that all of the organic materials are unstable at high temperatures makes them incompatible with processes that are used in the classical semiconductor industry. Incompatibility between organic and inorganic materials is also reflected at their interfaces in electronic devices through formation of dark spots, electrode delamination, etc. [8, 9].

Stability of organic materials is one of the problems that limit their use. Devices that contain polymers or small molecules are prone to degradation both during their shelf life and operation. Thus the understanding of the processes that lead to degradation of devices and thin films from which they are made of is of great importance. There is no unified theory that covers degradation of devices that contain organic materials, as there are numerous different ways in which organic materials or devices can degrade. Many causes that are responsible for degradation of devices have been identified and they can be divided in two groups: intrinsic and extrinsic [8]. Both types of degradation result in the loss of device luminance in time. Intrinsic degradation manifests itself as uniform loss of luminance in time without visible changes in the device and is very complex topic. Extrinsic degradation, which is consequence of external factors (oxygen, humidity, sunlight) is usually manifested through formation of dark non-emissive spots because of cathode or organic layer deterioration [8, 9].

Degradation of devices and materials from which they are made of became an important topic. However polymers and small molecules did not receive equal coverage. Most of the available literature mainly covers degradation of polymer materials both as films and incorporated in the devices, while in the case of small molecules degradation of whole devices is much more studied. Information regarding degradation of commonly used small organic molecules is lacking.

1.4 Extrinsic degradation of thin organic films

It is known that organic materials degrade easily when light, moisture and/or oxygen are present simultaneously [10–14], which is the reason that organic electronic devices such as organic light emitting diodes (OLEDs) need to be encapsulated. Despite a continuous progress in this area [15–17], the entropy always wins so that lifetime of an OLED mainly depends on air diffusion rate through encapsulation barrier. Most of the studies regarding the device degradation are related to operational degradation, i.e. film material is not studied alone but as an integral part of a working device [9,18]. Learning about degradation pathway of a *single component* and about its durability can help differentiate between various materials and unwanted processes that can occur during operation of a device.

Simultaneous presence of air and light may lead to degradation of organic thin films by interaction of the photo-excited molecules with oxygen [13, 19–24]. This interaction results in newly formed species – the impurities hereafter – which can significantly affect various film properties such as exciton diffusion length, luminescence, thermal (morphological) stability, etc. In favorable cases, like in anthracene-tetracene mixed crystals, the sensitized fluorescence measurements can detect impurity concentrations as low as one impurity molecule per ten billion host molecules [25]. This is possible because excited electronic states, i.e. the excitons in some molecular solids can diffuse during their radiative lifetime to reach quenching site at the distances that are comparable to the exciton diffusion length [26]. The understanding of the behavior under the influence of impurities may lead to technological progress that could extend the lifetime of organic electronic devices.

Extrinsic degradation of single component thin organic films is the main subject of this thesis. Besides the study of morphological stability of amorphous N,N′-bis(3-methylphenyl)-N,N′-bis(phenyl)benzidine (TPD) and 4,4′-bis(2,2-diphenylvinyl)-1,1′-biphenyl (DPVBi)thin films, widely used in production of OLEDs, we also study steady-state photoluminescence (PL) under different external conditions of these films. Electroluminescent devices with blue emitters are particularly prompt to photo-degradation in the presence of oxygen because of a high photon energy that can trigger photo-oxidation. Simultaneous exposure to UV light and oxygen introduces photo-

oxidized molecules (the impurities) in the DPVBi (TPD) films, leading to an efficient quenching of the steady-state PL with very low concentration of the impurities. This work offers a new insight on degradation mechanism of thin films of DPVBi and TPD, while other studies concerning these materials [18,27, 28] deal with operational degradation of OLEDs that contain these thin films. DPVBi and TPD have similar characteristics like molecular structure, UV-Vis absorbance [29,30] and glass transition temperatures [7,31], but changes under UV light and oxygen are faster in DPVBi, which makes it easier to study.

1.5 Dissertation outline

The second chapter of this work will be dedicated to overview of experimental techniques and setups used in this work. Then results regarding degradation of amorphous films of TPD and DPVBi will be presented in chapter three. First a study of morphologies of pristine TPD and DPVBi film will be given, followed by the influence of UV irradiation on formation of morphologies. After that results regarding chemical changes in the irradiated films obtained with use of MS, NMR, Raman and IR spectroscopy will be given. In the fourth chapter mechanism of the luminescence quenching in the irradiated films will be explained.

Chapter five will deal with the degradation of polycrystalline pentacene films, characterized with UV-VIS, Raman and AFM. Then a study concerning annealing of thin pentacene films in air will be presented. This will be followed by characterization of annealing products and explanation of their growth.

In the last chapter results will summarized and conclusions will be given. Explanation of assignment of NMR peaks and additional results will be given in appendices A and B, respectively.

References for Chapter 1

[1] F. Wudl, *Spiers Memorial Lecture: Organic electronics: an organic materials perspective,* Faraday Discuss. **174** (2014) 9-20.

[2] A. Bernanose, M. Comte, P. Vouaux, *A new method of light emission by certain organic compounds*, J. Chim. Phys. **50** (1953) 64.

[3] S. Mizuka, P. Martin, K. Hartmut, *Electroluminescence and Band Gap in Anthracene*, J. Chem. Phys. **43** (1965) 2920.

[4] C. W. Tang and S. A. VanSlyke, *Organic electroluminescent diodes*, Appl. Phys. Lett. **51** (1987) 913.

[5] H. Koezuka, A. Tsumura, T. Ando, *Field-effect transistor with polythiophene thin film*, Synthetic Metals **18** (1987) 699–704.

[6] T. P. I. Saragi, T. Spehr, A. Siebert, T. Fuhrmann-Lieker, J. Salbeck, Chem. Rev. **107** (2007) 1011.

[7] K. Naito, A. Miura, *Molecular design for non-polymeric organic dye glasses with thermal stability: relations between thermodynamic parameters and amorphous properties*, J. Phys. Chem. **97** (1993) 6240.

[8] H. Aziz and Z. D. Popovic, *Degradation phenomena in small-molecule organic light emitting devices*, Chem. Mater. **16** (2004) 4522-4532.

[9] F. So and D. Kondakov, *Degradation mechanisms in small-molecule and polymer organic light emitting diodes*, Adv. Mater. **22** (2010) 3762-3777

[10] H. Neugebauer, C. Brabec, J.C. Hummelen, N.S. Sariciftci, *Stability and photodegradation mechanisms of conjugated polymer/fullerene plastic solar cells*, Sol. Energy Mater. Sol. Cells **61** (2000) 35-42.

[11] K. Kawano, R. Pacios, D. Poplavskyy, J. Nelson, D.D.C. Bradley, J.R. Durrant, *Degradation of organic solar cells due to air exposure*, Sol. Energy Mater. Sol. Cells **90** (2006) 3520-3530.

[12] R. Pacios, A.J. Chatten, K. Kawano, J.R. Durrant, D.D. C. Bradley, J. Nelson, *Effects of photo-oxidation on the performance of poly[2-methoxy-5-(3',7'-dimethyloctyloxy)-1,4-phenylene vinylene]:[6,6]-phenyl C61-butyric acid methyl ester solar cells*, Adv. Funct. Mater. **16** (2006) 2117–2126.

[13] S. Cook, A. Furube, R. Katoh, *Matter of minutes degradation of poly(3-hexylthiophene) under illumination in air*, J. Mater. Chem. **22** (2012) 4282-4289.

[14] S. Schmidbauer, A. Hohenleutner, B. König, *Studies on the photodegradation of red, green and blue phosphorescent OLED emitters*, Beilstein. J. Org. Chem. **9** (2013) 2088–2096.

[15] P.E. Burrows, V. Bulovic, S.R. Forrest, L.S. Sapochak, D.M. McCarty, M.E. Thompson, *Reliability and degradation of organic light emitting devices*, Appl. Phys. Lett. **65** (1994) 2922-2924.

[16] A.B. Chwang, M.A. Rothman, S.Y. Mao, R.H. Hewitt, M.S. Weaver, J.A. Silvernail, K. Rajan, M. Hack, J.J. Brown, X. Chu, L. Moro, T. Krajewski, N. Rutherford, *Thin film encapsulated flexible organic electroluminescent displays*, Appl. Phys. Lett. **83** (2003) 413-415.

[17] J.-S. Park, H. Chae, H.K. Chung, S.I. Lee, *Thin film encapsulation for flexible AM-OLED: a review*, Semicond. Sci. Technol. **26** (2011) 034001.

[18] R. Siefert, S. Scholz, B. Lüssem, K. Leo, *Comparison of ultraviolet- and charge-induced degradation phenomena in blue fluorescent organic light emitting diodes*, Appl. Phys. Lett. **97** (2010) 013308.

[19] A. Maliakal, K. Raghavachari, H. Katz, E. Chandross, T. Siegrist, *Photochemical stability of pentacene and a substituted pentacene in solution and in thin films*, Chem. Mater. **16** (2004) 4980-4986.

[20] A.B. Djurišić, T.W. Lau, C.Y. Kwong, L.S.M. Lam, W.K. Chan, *Evolution of optical properties of tris (8-hydroxyquinoline) aluminum (Alq3) with atmosphere exposure*, Proc. SPIE **4800** (2003) 200-207.

[21] V.K. Shukla, S. Kumar, D. Deva, *Light induced effects on the morphology and optical properties of tris-(8-hydroxyquinoline) aluminium (Alq3) small molecular thin film*, Synth. Metals **156** (2006) 387-391.

[22] T. Zyung, J.-J. Kim, *Photodegradation of poly(p-phenylenevinylene) by laser light at the peak wavelength of electroluminescence*, Appl. Phys. Lett. **67** (1995) 3420-3422.

[23] H. Hintz, H.-J. Egelhaaf, L. Lüer, J. Hauch, H. Peisert, T. Chassé, *Photodegradation of P3HT – a systematic study of environmental factors*, Chem. Mater. **23** (2011) 145-154.

[24] L. Lüer, H.-J.Egelhaaf, D. Oelkrug, G. Cerullo, G. Lanzani, B.-H. Huisman, D. de Leeuw, *Oxygen-induced quenching of photoexcited states in polythiophene films*, Org. Electron. **5** (2004) 83-89.

[25] Von K.W. Benz, H.C. Wolf, *Die konzentrationsabhängigkeit der energie-übertragung in anthracen-tetracen-mischkristallen*, Z. Naturforschg. **19a** (1964) 177-181.

[26] M. Pope, C.E. Swenberg, *Electronic processes in organic crystals and polymers, second ed.*, Oxford University Press, New York, 1999.

[27] S. Winter, S. Reineke, K. Walzer, K. Leo, *Photoluminescence degradation of blue OLED emitters*, Proc. SPIE **6999** (2008) 69992N.

[28] G. Nenna, M. Barra, A. Cassinese, R. Miscioscia, T. Fasolino, P. Tassini, C. Minarini, and D. della Sala, *Insights into thermal degradation of organic light emitting diodes induced by glass transition through impedance spectroscopy*, J. App. Phys. **105**, (2009) 123511.

[29] H. Mattoussi, H. Murata, C.D. Merritt, Y. Iizumi, J. Kido, Z.H. Kafafi, *Photoluminescence quantum yield of pure and molecularly doped organic solid films*, J. App. Phys. **86** (1999) 2642.

[30] T. Fukuda, B. Wei, M. Ichikawa, Y. Taniguchi, *Transient characteristics of organic light-emitting diodes with efficient energy transfer in emitting material*, Thin Solid Films **518** (2009) 567-570.

[31] S. Wang, W.J. Oldham Jr., R.A. Hudack Jr., G. C. Bazan, *Synthesis, morphology, and optical properties of tetrahedral oligo(phenylenevinylene) materials*, J. Am. Chem. Soc. **122** (2000) 5695-5709.

2. Experimental details

2.1 Materials

Following materials were studied: TPD, DPVBi and pentacene, all of them being p-type semiconductors. They have a wide spread use in the field of organic electronics, mainly in the production of OLEDs (TPD and DPVBi) and OTFTs (pentacene).

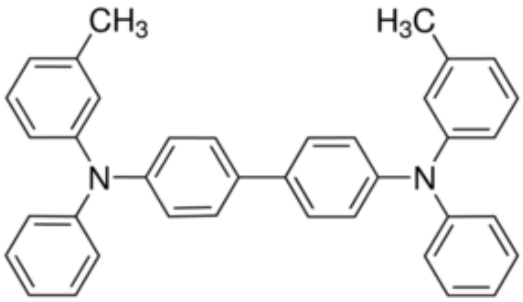

Fig. 2.1 Molecular structure of TPD

N,N′-Bis(3-methylphenyl)-N,N′-diphenylbenzidine ($C_{38}H_{32}N_2$) (Fig. 2.1) also known as TPD is a well-known hole transporting material widely used for production of OLEDs. It was part of the first OLED produced by Tang and Van Slyke [1]. Major drawback of TPD is its low glass transition temperature T_g= 65 °C[2]. Owing to its low T_g thin TPD films undergo morphological changes even at room temperature.

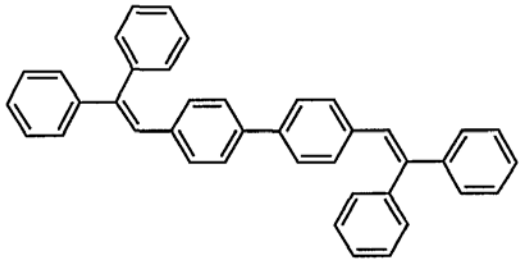

Fig. 2.2 Molecular structure of DPVBi

4,4'-Bis(2,2-diphenylvinyl)-1,1'-biphenylDPVBi (Fig. 2.2) is another hole transporting material and a blue emitter, mainly is used in production of white and blue OLEDs[3-6]. It has the same glass transition temperature T_g= 65 °C as TPD [7].

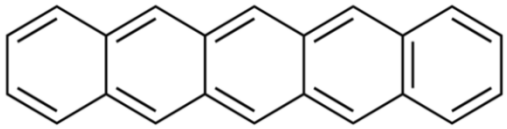

Fig. 2.3 Molecular structure of pentacene

Pentacene ($C_{22}H_{14}$) is a well-known organic semiconductor; it consists of five fused benzene rings (Fig. 2.3). Due to its high mobility second only to rubrene it is predominantly used for production of thin film transistors (TFT) [8]. Pentacene used in this research was purchased from Fluka and Sigma Aldrich and used as received.

2.2 Physical vapor deposition (PVD)

Physical vapor deposition is a process in which solid material is transformed to gaseous phase and then deposited on to a substrate under vacuum conditions. Evaporation of desired material can be achieved with different methods such as: e-beam, pulsed laser deposition, sputtering and thermal evaporation which was used in this research. Term physical stems from absence of any chemical reactions both in gaseous phase and at substrate surface. It is a simple technique suitable for deposition of thin films of organic materials which evaporate at low temperatures.

2.2.1 Deposition apparatus

The deposition apparatus, shown in Fig2.1a, consists of a homemade stainless steel deposition chamber brought to Serbia by Professor Vojislav Srdanov from University of California Santa Barbara. Main part is steel cross with four 10 cm and two 5 cm ports for flanges (Fig 2.1b), which enables several ways to position the substrate and shutter. This type of chamber design proved to be convenient for mounting of quartz viewports

shown in Fig 2.4c. Use of viewports is convenient because evaporation process can be crudely monitored with hand held UV lamp as materials used in this research are luminescent or colored. This also provides possibility for measurement of absorbance and photoluminescence of thin films *in situ*.

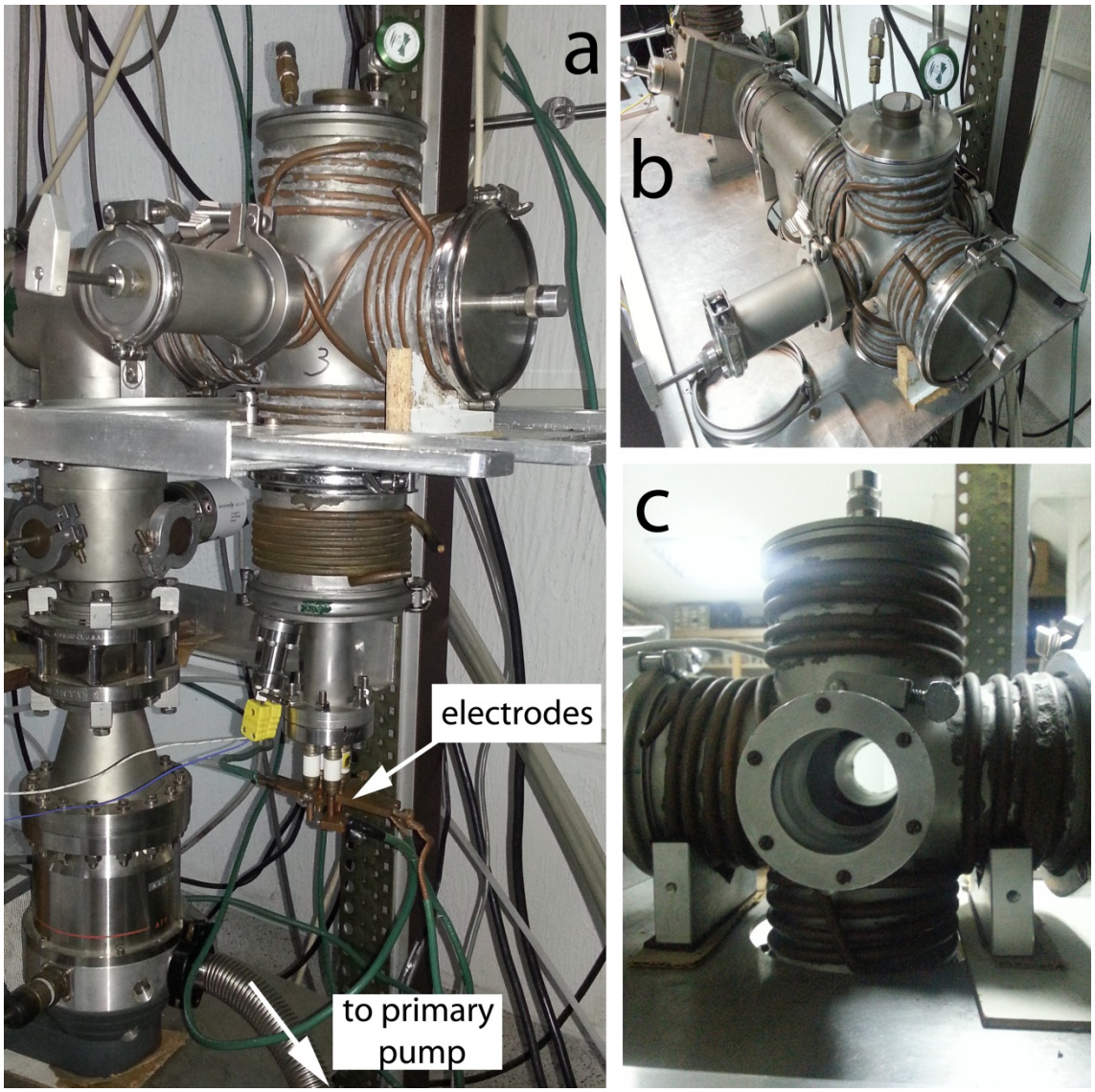

Fig. 2.4 a) Turbo pump (down left) with evaporation chamber (side view)b) evaporation chamber, shutter leaver is visible on the left (top view) and c) evaporation chamber with mounted quartz viewports.

In order to achieve and maintain high vacuum necessary for evaporation, two stage pumping was used: primary mechanical pump and turbo molecular pump. Vacuum was

monitored with Cold Cathode Pirani Gauge: this is a combination gauge which uses Pirani gauge for low range (down to the $1x10^{-3}$ Torr) and the cold cathode gauge for the high range (10^{-3} to 10^{-7} Torr).Maximum pressure achievable with this system was $5x10^{-7}$ Torr. Films used in this study were evaporated under pressure of $5x10^{-6}$ Torr which is suitable for this type of application and was easily achieved in time span of 45 minutes.

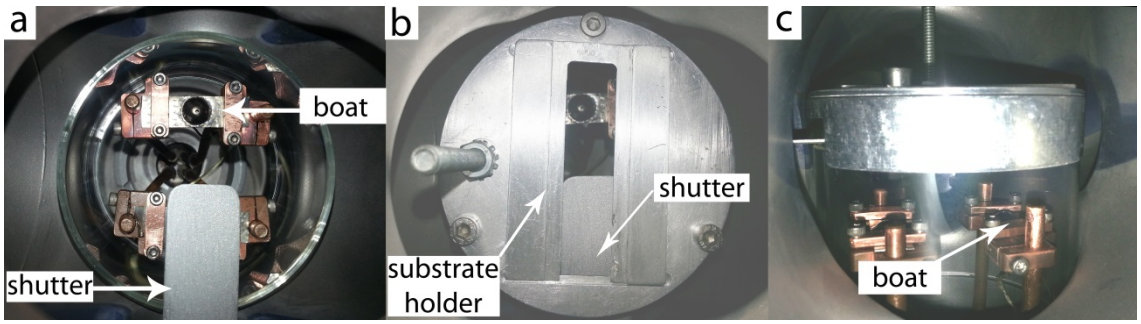

Fig. 2.5 a) Evaporation boat mounted onto the copper electrodes with a retracted shutter (top view), b) substrate holder placed above the evaporation boat (top view), c) substrate holder and boat (side view) inside the evaporation chamber.

Materials were evaporated from Knudsen type sources made from INOX 311 steel. Picture of the typical boat attached to copper electrodes is shown in Fig. 2.5. Thermocouple wires which were welded at the bottom of each boat enabled monitoring of the source thermocouple wires were welded at the bottom of each boat. Boats were resistively heated by passing current through them which was supplied by D.C. power supply (*Sorensen DCS8-125E*). The process of evaporation was controlled by LABVIEW program, which controlled output of a power supply through a feedback loop and in turn enabled evaporation at constant temperature with an error of ±1°C.

2.2.2 Combinatorial Physical Vapor Deposition

Combinatorial synthesis and analysis is a well-known method used in combinatorial chemistry for production of new drugs and materials. Similar principle can be applied for production OLEDs where large number of devices can be prepared under same conditions while parameters such as composition and thickness of different layers can be varied [9, 10].

Combinatorial method can also be used for preparation of single component films as shown by E. Suljovrujic *et al.*[11], in the sense that it is possible to acquire library of thickness from a single evaporation, under identical conditions (chamber pressure, evaporator temperature, substrate) in order to study relations between film thickness and morphology.

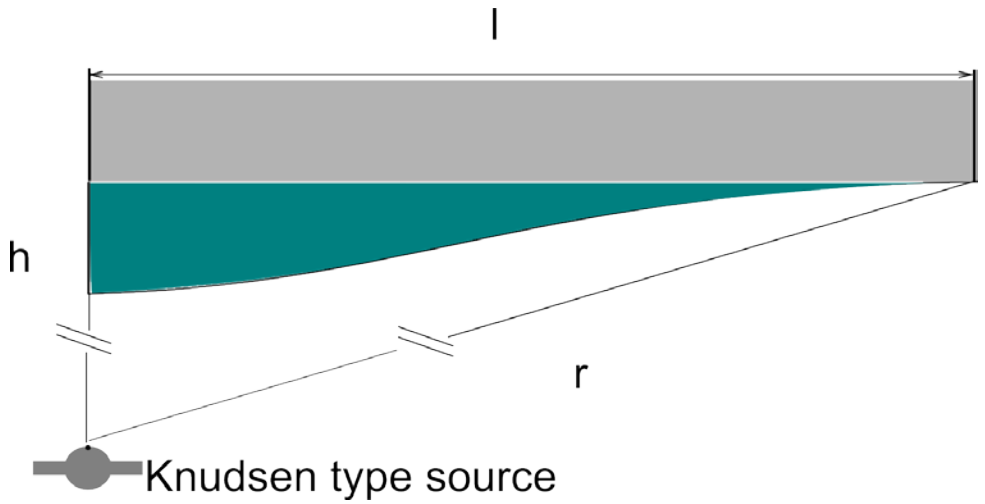

Fig. 2.6 Schematic representation of evaporation from Knudsen source.

Practically library of thickness is achieved with use of a Knudsen source (quasi point source) which has an angle dependent deposition rate [11]. The motion of the molecules from the source is effusive (there no collision between the molecules) under condition that the mean free path of the molecules is much larger than the orifice and the distance between source and the substrate. Profile of thickness (Fig. 2.6) of thin films abides Knudsen law given by equation:

$$d = d_0 \cos^n(arctg(l/h)),$$

where d_0 is film thickness directly over the evaporator, $\boldsymbol{r}$ distance between a given point on the substrate and evaporator, h distance between evaporator and the substrate and n is a parameter that depends on geometry of the source. Parameter n is different for each boat and can be obtained from a fit of experimentally measured data to Knudsen law.

2.2.3 Preparation of substrates

Following substrates were used in this work: glass 25mm x 75mm, fused silica 25mm x 25mm and KBr substrates.

For Raman spectroscopy glass substrates were used in the case of pentacene samples, while gold substrates were used for DPVBi and TPD. Gold substrates had to be used due to small Raman signal that was completely covered by the background signal which originates from glass substrates.

KBr substrates for infrared spectroscopy were purchased from Sigma Aldrich and used as is.

Glass substrates were used in order to study morphologies of thin films, for monitoring changes in absorbance and photoluminescence caused by UV irradiation. For AFM imaging glass substrates were cut in to 10mm x 25mm strips before cleaning. This was necessary because AFM construction would not permit use of larger samples and cutting a substrate after evaporation would possibly cause unwanted sample damage.

In order to acquire absorbance spectra in the full range (UV-VIS) fused silica substrates were used because they are transparent to UV light down to 250nm (unlike glass substrates). Following procedure was used for cleaning of glass, fused silica and gold substrates, whose steps are listed in order of application:

- 10 minutes of sonic bath in detergent and distilled water,
- rinse with distilled water,
- 10 minutes of sonic bath in methanol,
- rinse with ultra-pure water 18.2 MΩcm,
- 10 minutes of sonic bath in ultra-pure water.

Substrates were dried under nitrogen flow and then mounted on the substrate holder before being placed in vacuum chamber.

2.2.4 Evaporation procedure

Evaporation boat (see Fig. 2.5) is usually filled with 2 to 4 mg of desired material through a small funnel made from weighing paper. Depending on the used material these amounts were sufficient for several evaporations. Substrates were mounted above the boat (see Fig. 2.5b) at the distance of 30 mm and the mechanical shutter (see Fig. 2.5a, b)was placed the between the evaporator and substrate. Purpose of the shutter is to act as a barrier to prevent the deposition of the material until the desired temperature acquired. Once the vacuum of $5x10^{-6}$ Torr is reached, boat is heated in the following protocol: first temperature is elevated to 110 ºC and held there for 10 minutes to remove any residual moisture from the boat, after that temperature is gradually raised until the evaporation temperature is reached. Boat is kept few minutes at the evaporation temperature in order to get uniformly heated, shutter is then moved and deposition of the material on to the substrate begins.

Materials were evaporated under following temperatures:

- DPVBi (Sigma Aldrich) films were evaporated at source temperature of 210°C yielding evaporation rate of around $3Ås^{-1}$ at maximum of film thickness.
- TPD (Sigma Aldrich) was evaporated at source temperature of 190°C which gave evaporation rate of 1 $Ås^{-1}$ at maximum of film thickness. For all depositions substrate was kept at room temperature. Obtained films were amorphous as evidenced by AFM, surface of films was flat with no grain boundaries.
- Pentacene (Sigma Aldrich, Fluka) films were evaporated at source temperatures of 240°C and 220 °C, yielding peak evaporation rates of 2 $Ås^{-1}$and 0.5 $Ås^{-1}$respectively.

For all the evaporations substrates were kept at room temperature. Films that were obtained in this way are amorphous: under said conditions there are two possible outcomes. Films could either be polycrystalline or amorphous. If they were polycrystalline then grain structure would be observed by AFM, but we found only flat film surface.

2.3 Irradiation of thin films

For irradiation of thin TPD and DPVBi films two light sources were used, an Hg lamp and 350 nm UV LED (Fig. 2.7), with a maximum power density of in the 300–400 nm range of 1.7mWcm^{-2} and 3 mWcm^{-2}, respectively, as determined by a Solar Light Co. PMA 2110 UVA sensor. Hg lamp was used for irradiation of large areas of a film, that is for morphology studies, while light from UV LED was usually focused on a sample and used to follow changes in absorbance and PL spectra with irradiation time.

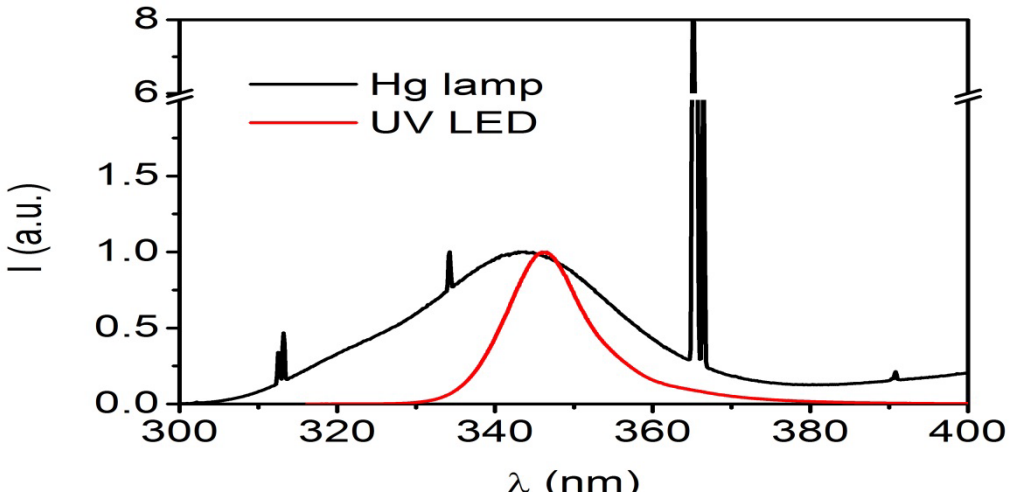

Fig. 2.7 Spectra of Hg and UV LED lamps used for irradiation of thin films.

2.4 Experimental setups for spectroscopic measurements

Apart from IR spectroscopy and some of the UV-VIS spectra which were acquired on commercial devices, all of the other measurements were performed using custom setups which will be explained here. Core of the setup that was used in this research consisted of Acton Research Corporation SpectraPro-2500i monochromator and a Princeton Instruments Pixis 100 Peltier cooled CCD detector and different light sources (standard tungsten lamp, white LED and UV LED, He-Ne laser). Monochromator is equipped with three gratings (300, 600, 1200 grooves per mm with 500 nm blaze). CCD detector has 1340 x 100 pixels with dimension of 20 μm x 20 μm and was used in spectroscopic mode (integration by 100 vertical pixels). The range of wavelengths (spectral window) which is detected by CCD is determined by its horizontal dimension

(26.8 mm) and the position of the grating. This will also determine the resolution of the system which calculated by ratio of width of a spectral window (for a given grating) and number of horizontal pixels. Typical resolution is approximately 0.12, 0.06 and 0.03 nm for gratings 300, 600 and 1200 respectively.

Sensitivity of the system depends on the efficiency of CCD detector and a chosen grating, both of which are wavelength dependent. Due to that obtained spectra are inaccurate. In order to correct this inaccuracy an efficiency calibration curve (efficiency vs. wavelength) was obtained with use of a known light source. All of the obtained spectra were then corrected for the response of the device. Absorbance spectra obtained on commercial device and our custom setup were compared and found to be in good agreement.

2.4.1 Infrared spectroscopy (IR)

IR measurements were performed on Nicolet iN10 infrared microscope with a cooled detector, 300μm x 300 μm sampling area, 256 scans and resolution of 4cm^{-1} on pristine and irradiated (one hour of exposure to UV light with a power I_{UV}= 2$mWcm^{-2}$) 400 nm thick DPVBi films deposited on KBr substrates. Before measurement of the samples background signal was obtained from the clean part of the KBr substrate. Obtained spectra for pristine and irradiated sample were corrected for the background signal.

2.4.2 Raman spectroscopy

Raman measurements were performed with a He-Ne laser with wavelength λ= 633nm and nominal laser power of P= 17mW in configuration shown in Fig. 2.8. The sample holder, lenses L1 and L2 together with monochromator and CCD represent a base setup which is used in all experiments. Lens L1 is used to collect scattered light from the sample and L2 for projection of light on to the slit of monochromator and is chosen in such way to match its aperture number f /6.5. The sample itself is placed on a XYZ sample holder which enables positioning in the focus of L1 with high precision.

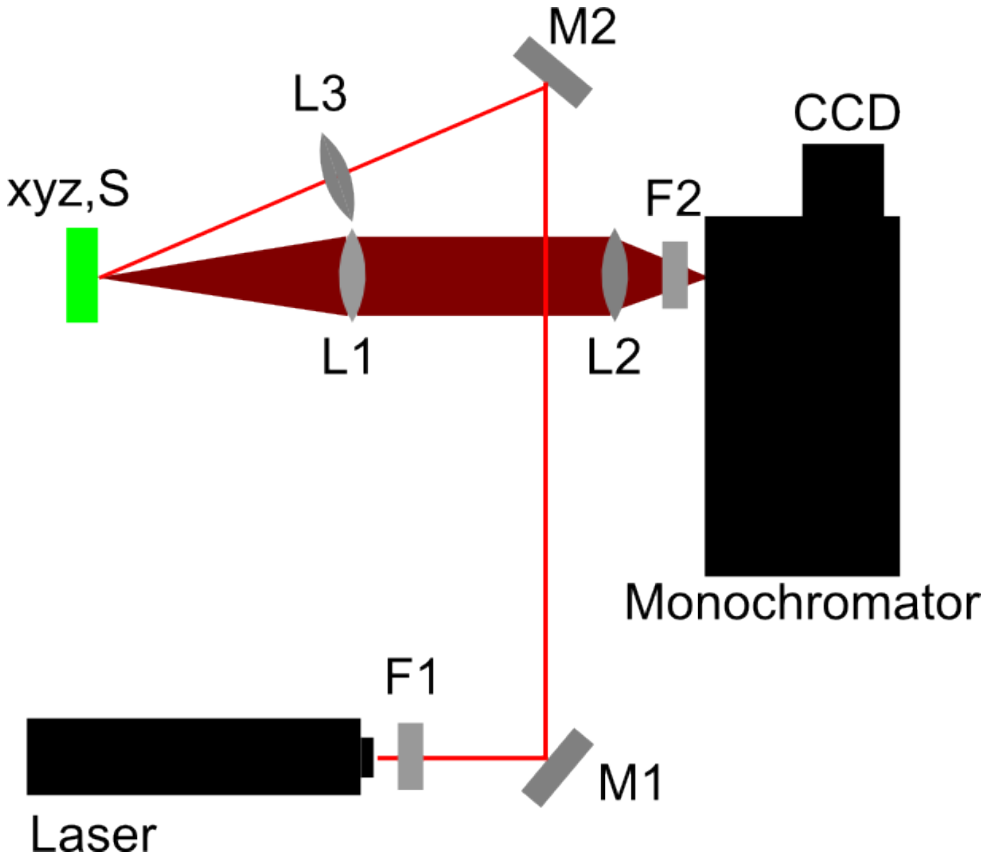

Fig. 2.8 Schematic representation of Raman setup: F1 – anti notch filter, M1 and M2 – mirrors, L1 – lens for focusing of laser beam on to the sample, L2 and L3 lenses, F2 notch filter.

Two filters were used; the first, F1, is anti-notch filter for the rejection of all wavelengths other than 633nm coming from laser and the second, F2, is notch filter which rejects 633 nm coming from Rayleigh scattering. Notch filter is necessary to enhance much smaller Raman signal and to protect the detector.

2.4.3 UV –VIS and photoluminescence spectroscopy

For acquisition of full UV-VIS spectra Beckman Coulter DU 700 single beam spectrophotometer was used with the resolution of 1 nm. This device is designed for measurement of absorbance of solutions and only has a mount for quartz cuvettes. In order to use it for measurements of the absorbance of thin films a small modification

was made. Substrate holder with a 3mm hole was made in our lab so it could easily be attached in front of a detector and enabled recording absorbance of thin films. The limited space available in the device did not permit any further modification so it was only able to record spectra at one point of the sample.

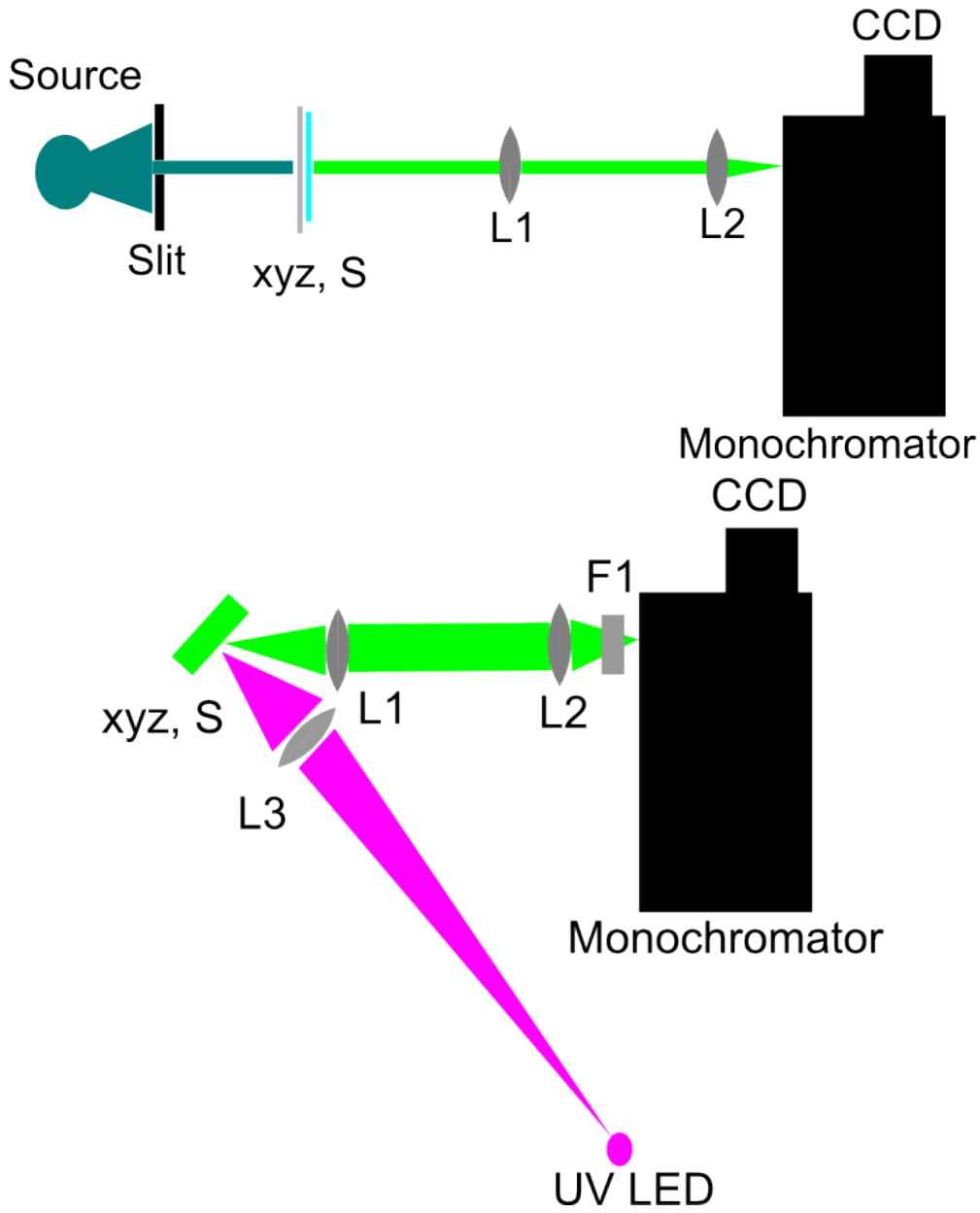

Fig. 2.9 Schematic representation of basic setup for UV Vis spectroscopy (top): light source, slit used for collimation of light and making the probe beam smaller, S- sample; photoluminescence setup (bottom): S – sample, L1 – lens used for focusing UV light on to the sample, F1 – filter.

Most of the spectra were recorded on a custom setup as it allowed for much more flexibility. The setup was used with substrate holder that has XYZ motion capability and thus enabled easy focusing and recording of a thickness profile of thin film samples or with a vacuum chamber which enabled monitoring of absorbance and photoluminescence in vacuum. Setup could be easily modified to acquire absorbance, photoluminescence and Raman spectra either separately or at the same spot on sample. Basic setups for absorbance and photoluminescence spectroscopy are shown in Fig. 2.9.

For absorbance a suitable light (UV LED for TPD and DPVBi, white LED for pentacene) source is added followed with a 1 mm slit in order to collimate the light and probe only a small portion of the sample. For photoluminescence spectroscopy a UV LED diode with a peak wavelength λ = 365 nm was used as light source focused on to the sample with an additional lens L3.

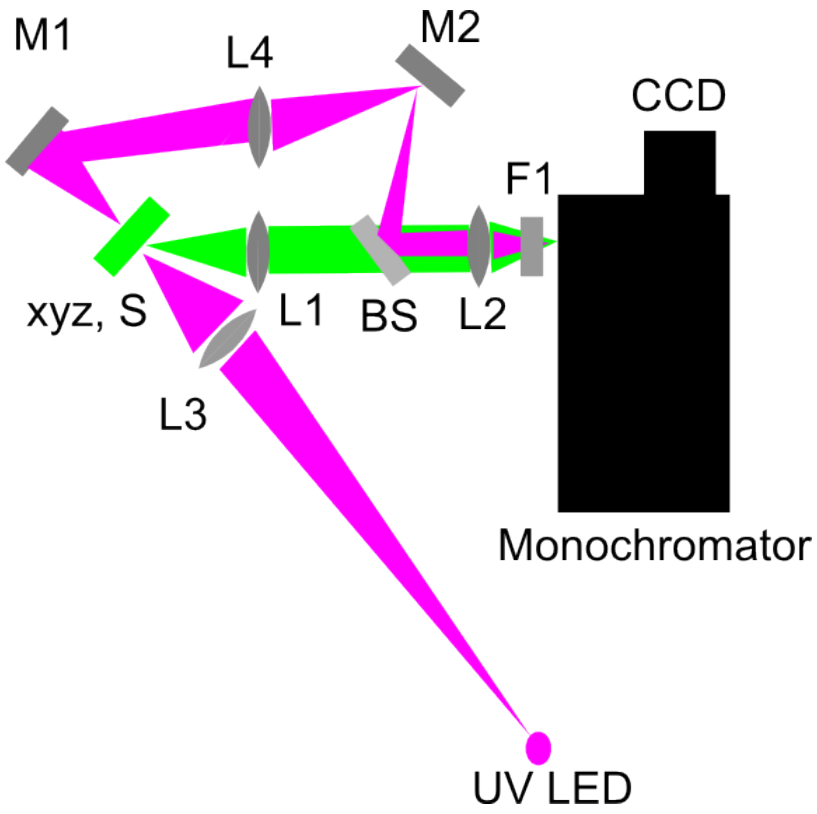

Fig.2.10 Schematic representation of setup for absorbance and photoluminescence measurement on the same spot of the sample.L3- lens for focusing probe beam onto the sample. M1, M2 – mirrors, BS – beam splitter.

More advanced setup was made in order to measure absorbance and photoluminescence spectra on the same point of the sample; schematic representation of this setup is shown in Fig. 2.10. This was very important for the study of chemical changes induced by UV irradiation in thin DPVBi films as absorbance spectra provided estimation for the number of the new species which are responsible for quenching of photoluminescence. Modification of the basic photoluminescence setup was made in order to record absorbance of the portion of sample that was exposed to UV light. Mirror M1 was placed behind the sample in order to collect the transmitted light which was then projected on to a lens L4 and from there to a second mirror M2; light was then diverted to a glass beam splitter and from there delivered to monochromator by a lens L2. When photoluminescence was recorded the light path used for absorbance was blocked before M2, and for absorbance measurement blocker was placed after L1.

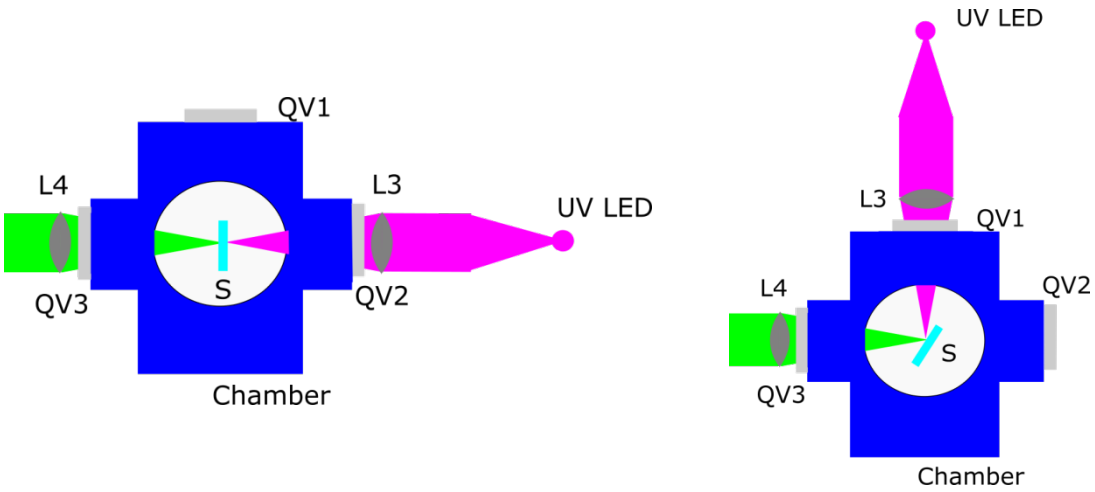

Fig. 2.11 Setup for measurement of absorbance (left) and photoluminescence (right) under vacuum conditions and different oxygen pressures. QV1, 2, 3 are quartz viewports, L3 and L4 lenses.

For measurement of absorbance and photoluminescence in chamber under vacuum and different oxygen pressures following setups were made (Fig. 2.11). Two lenses were mounted in front of the quartz viewports. For measurement of absorbance quartz viewports QV2 and QV3 were used. Lenses L3 and L4 were mounted in front of the viewports in order to focus the UV LED at the sample and to collect transmitted light. Light collected by L4 was diverted with a mirror on to the L2 which is used to focus the

light on to the slit of the monochromator. In order to measure the PL of the sample UV LED was mounted above the chamber and viewports QV1 and QV3 were used, again two lenses L3 and L4 were used with a same purpose as in previous setup.

2.5 Spectroscopic data acquisition and manipulation

Raman, photoluminescence and absorbance spectra were acquired with WinSpec software from Princeton Instruments which is used to control both monochromator and CCD camera.

WinSpec software provides control of important functions of both devices: selection of the spectral window by changing the position of one of the three gratings (300, 600 and 1200 grooves/mm) of the monochromator and control of the CCD exposure time, number of spectra and number of accumulations being the most important for data acquisition. CCD exposure time depends on light intensity that falls on the detector and count should be less than 64000 for a single exposure (in order not to saturate it). Depending on the sample and application it can vary several orders of magnitude.

2.5.1 Absorbance

For recording absorbance of the thin film grating with 300 grooves was used and width of slit of the monochromator was set to 100 μm. First the transmitted intensity through a reference substrate I_0 of the used light source is recorded then sample is placed on the holder and the procedure is repeated in order to obtain intensity of light transmitted through sample *I*. As CCD poses dark current (inherent count that is always present as a consequence of thermal energy within the silicon lattice comprising the CCD) its value has to be subtracted first before any other data manipulation. Curves obtained for reference and sample are then used for calculation of transmittance which is given by relation:

$$T = I/I_0, \qquad (1.1)$$

while absorbance is obtained from transmittance using (contribution of reflectance is omitted):

$$A = -\log T. \qquad (1.2)$$

2.5.1.1 Profile of thickness measurement

Film thickness was calculated, using Beer-Lambert law $I = I_0 e^{-\mu d}$, from absorbance (Eq. 1.2) at certain wavelength and corresponding value of absorption coefficient μ:

$$d = A \ln 10/\mu \qquad (1.3)$$

In order to find maximum of thickness following procedure was performed: first sample was scanned along the short axis in order to find the maximum value of absorbance and then along the long axis in order to acquire profile of thickness (Fig. 2.12).

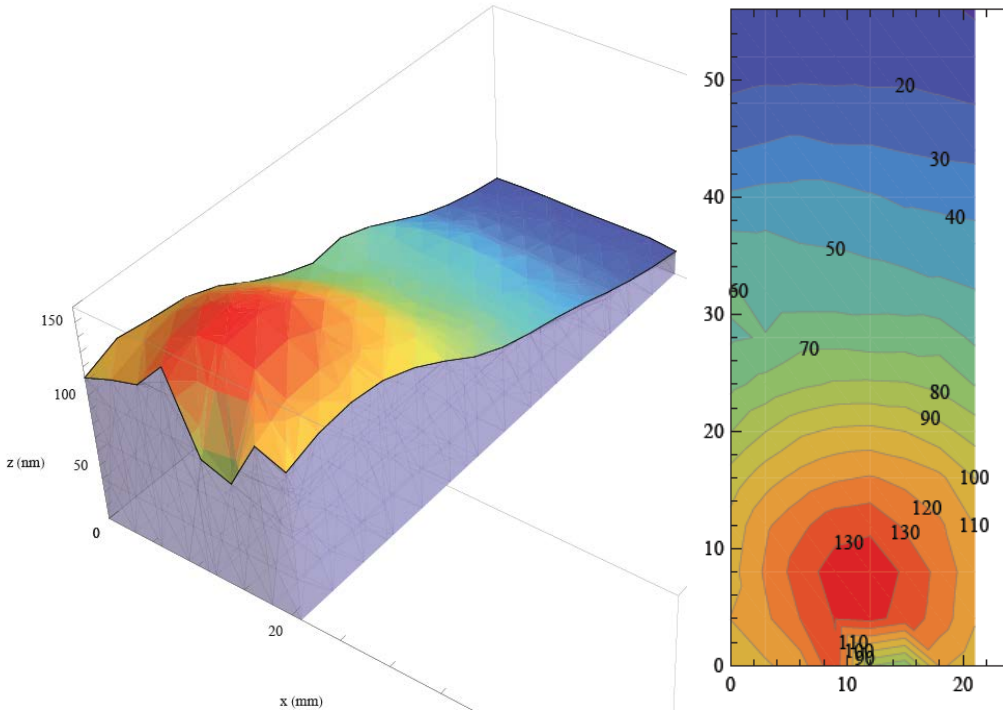

Fig. 2.12 Example of the 2D profile obtained by recording absorbance of the thin TPD film at 60 points on the sample.

2.5.1.2 Absorbance vs. irradiation time

In order to study the influence of UV irradiation on absorbance for different irradiation times and UV light intensities following procedure was used. Same UV LED was used both for degradation and acquisition of absorbance spectra. This means that effectively sample is degraded while its absorbance is recorded. CCD exposure times were chosen in such way that the degradation during spectra acquisition is minimal.

2.5.2 Photoluminescence

Photoluminescence spectra were acquired with grating that has 300 grooves per mm as it gives the largest spectral window (around 160 nm) and the width of the slit was set to 100 μm. Depending on the width of the spectra at least two windows were necessary in order to acquire the whole PL spectrum of the sample. For that purpose macro was created using WinSpec which automatically switched between the different spectral windows and recorded the curves. Acquired curves were corrected for dark current (Fig. 2.13a) of CCD and smoothed if necessary.

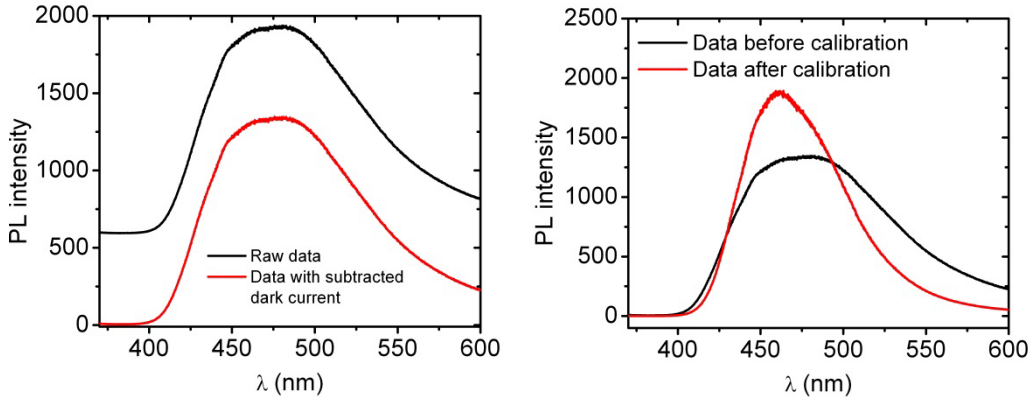

Fig. 2.13 a) Raw PL spectra (black curve) and PL spectra after the subtraction of dark current signal. b) PL spectra before (black) and after (red) calibration for the system response.

After that, obtained data were corrected for system response using a previously obtained efficiency calibration curve (Fig 2.13b).

2.5.2.1 PL spectra vs. irradiation time

In order to study the behavior of PL with the UV irradiation time following procedure was used. Only the spectral window in which the maximum of PL spectra is located is recorded. Before placing the new sample path between the sample and light source is blocked. The exposure time of CCD needs to be short because of the fast PL quenching of the sample but long enough in order to have significant signal. Acquisition is set to multiple spectra with a typical CCD exposure time of 0.2 s and started before removing the blocker. Usually several hundred spectra were obtained and exported to Origin. Dark current is subtracted and all the spectra are smoothed before further processing. Peak values of the PL are then plotted versus time in order to obtain curve of the PL evolution.

2.5.3 Raman

Raman spectra are recorded with grating with 600 grooves per mm (resolution of 1.4 rel. cm^{-1}) and the width of the slit of 50 μm. For this grating the center of the first spectral window was set to 685 nm in order to avoid the signal from laser. If several spectral windows were recorded they were joined before manipulation. Obtained spectra were baseline corrected using Origin software.

2.6 Atomic Force Microscopy (AFM)

The AFM used in research was commercial Nanotec Cervantes AFM. System consists of electronics, chassis, head, cantilever holder and PC which controls the AFM through WSxM freeware software [13] developed by Nanotec company. AFM was equipped with small piezo scanner which enabled imaging of 12μm x 12μm x 2μm with capabilities of achieving atomic resolution. Two types of cantilevers were used, both for tapping mode, Budget Sensors Tap150-G[14] with resonant frequency of 150kHz, force constant 5N/m and tip radius less than 10nm and NANOSENSORS PPP-NCH[15] with resonant frequency of 330kHz, force constant 42N/m and tip radius less than

10nm. Tapping mode was chosen for imaging as it minimizes contact between probe and sample and thus prevents sample damage.

2.7 ^{1}H nuclear magnetic resonance (NMR) spectroscopy

Proton NMR spectroscopy was performed by group of Paolo Milani from the department of physics, The University of Milan. Results were obtained on Varian 400 MHz spectrometer. The NMR spectra were recorded at room temperature after dissolving TPD pristine and irradiated films in deuterated chloroform. Analysis of the NMR spectra was done in our laboratory.

2.8 Mass spectroscopy

Mass spectroscopy was used in order to follow chemical changes induced by UV light irradiation of thin films in cases of TPD and DPVBi and annealing in the case of thin pentacene film. Results obtained in the study of TPD films were recorded with time-of-flight mass spectrometer. In the study of thin DPVBi two different types of mass spectroscopy were used: Atmospheric Solid Analysis Probe (ASAP) and Laser Desorption Ionization Time of Flight (LDI TOF) which will be described here.

2.8.1 Atmospheric Solid Analysis Probe (ASAP)

Atmospheric Solid Analysis Probe (ASAP) is a modification of a Waters Acquity system with a tandem quadrupole detector. Waters Acquity system uses Electrospray Ionization (ESI) technique, however in the case of pentacene and pentacequinone it showed to be inadequate and unable to provide reliable results. As ASAP gave good results with both compounds it was also used with DPVBi. ASAP technique allows introduction of solid or liquid samples in to the chamber kept at atmospheric pressure with use of glass capillary. Schematics of ASAP is shown in in Fig.2.14. Once introduced in the chamber sample is evaporated with heated desolvation gas (N_2) and ionized by a corona discharge pin. Desolvation gas temperature, corona and cone

voltage are controllable parameters and were optimized for each material in order to acquire good spectra.

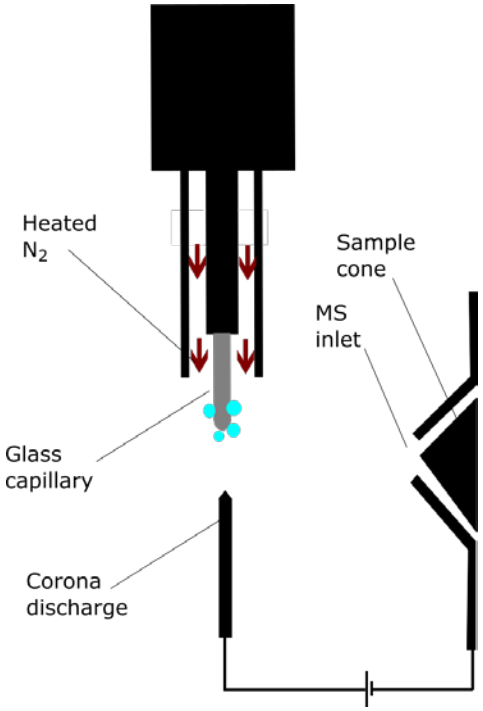

Fig. 2.14 Schematic of ASAP ion source

2.8.2 Laser Desorption Ionization Time of Flight (LDI TOF) mass spectroscopy

Laser Desorption Ionization Time of Flight (LDI TOF) was performed using the commercial matrix-assisted laser desorption and ionization time-of-flight Voyager Biospectrometry DE Pro Workstation (Perseptive Biosystems, USA). As DPVBi absorbs at the wavelength of the laser, matrix material was not used. Sample was directly evaporated onto the metallic sample holder (well plate) of the spectrometer. The pressure inside the workstation was kept at few 10^{-5}Pa so the laser, emitting at 337 nm, could not produce photo-oxidation of DPVBi films. The polarization was positive and laser intensity was 2000 with 330 shots.

2.8.3 FI/FD Time of Flight

Mass spectra of TPD films were measured by Dr. James Pavlovich from the department of Chemistry and Biochemistry of the University of California Santa Barbara. For that purpose thin TPD films were dissolved in toluene and mass spectra were recorded using a Waters GCT premier time-of-flight mass spectrometer equipped with ionization/field desorption (FI/FD) ion sources. Spectra were analyzed in our laboratory.

2.9 X-ray diffraction (XRD)

X-ray diffraction was measured in Bragg-Brentano focusing geometry. The diffractometer was equipped with a sealed Cu X-ray tube and a short linear position sensitive detector. The K_β line was suppressed by a Ni filter instead of a crystal monochromator, leading to higher intensity of the probe beam. Measurements were performed by Gabor Bortel and Gyula Faigel from Institute for Solid State Physics and Optics, Budapest.

References of Chapter 2

[1] C. W. Tang and S. A. VanSlyke, *Organic electroluminescent diodes*, Appl. Phys. Lett. **51** (1987) 913.

[2] K. Naito, A. Miura, *Molecular design for non-polymeric organic dye glasses with thermal stability: relations between thermodynamic parameters and amorphous properties*, J. Phys. Chem. **97** (1993) 6240.

[3] X. Zhang, Z. Wu, B. Jiao, D. Wang, D. Wang, X. Hou and W. Huang, *Solution-processed white organic light-emitting diodes with mixed-host structures*, J. Lumin. **132** (2012) 697–701.

[4] G. Li and J. Shinar, *Combinatorial fabrication and studies of bright white organic light-emitting devices based on emission from rubrene-doped 4,4'-bis(2,2'-diphenylvinyl)-1,1'-biphenyl*, Appl. Phys. Lett. **83** (2003) 5359-5361.

[5] S. E. Shaheen, G. E. Jabbour, M. M. Morrell, Y. Kawabe, B. Kippelen, N. Peyghambarian, M. F. Nabor, R. Schlaf, E. A. Mash, and N. R. Armstrong, *Bright blue organic light-emitting diode with improved color purity using a LiF/Al cathode*, J. Appl. Phys. **84** (1998) 2324-2327.

[6] C. Hosokawa, H. Higashi, H. Nakamura and T. Kusumoto, *Highly efficient blue electroluminescence from a distyrylarylene emitting layer with a new dopant*, Appl. Phys. Lett. **67** (1995) 3853-3855.

[7] S. Liu, F. He, H. Wang, H. Xu, C. Wang, F. Li and Y. Ma, *Cruciform DPVBi: synthesis, morphology, optical and electroluminescent properties*, J. Mater. Chem. **18** (2008) 4802-4807.

[8] D.J. Gundlach, Y.Y. Lin, T.N. Jackson, S.F. Nelson, D.G. Schlom, *Pentacene organic thin-film transistors-molecular ordering and mobility*, Electron Device Letters, IEEE **18** (1997) 87-89.

[9] H. Fukumoto, Y. Muramatsu, T. Yamamoto, J. Yamaguchi, K. Itaka, and H. Koinuma, *Combinatorial Physical Vapor Deposition of π-Conjugated Organic Thin Film Libraries*, Macromol. Rapid Commun. **25** (2004) 196.

[10] M. Thelakkat, C. Schmitz, C. Neuber, and H.-W. Schmidt, Materials Screening and Combinatorial Development of Thin Film Multilayer Electro-Optical Devices, Macromol. Rapid Commun. **25** (2004) 204.

[11] E. Suljovrujic, A. Ignjatovic, V.I. Srdanov, T.Mitsumori, F.Wudl, *Intermolecular energy transfer involving an iridium complex studied by a combinatorial method*, J. Chem. Phys. **121** (2004) 3745.

[12] Milton Ohring, *Material Science of Thin Films, 2nd Edition*, Academic Press, 2001

[13] WSxM software can be downloaded from the following address: http://www.wsxmsolutions.com/

[14] Information about Tap150-G cantilevers can be found here: http://www.budgetsensors.com/soft_tapping_mode_afm_probes.html

[15] Information about NANOSENSORS PPP-NCH cantilevers can be found here: http://www.nanosensors.com/PointProbe-Plus-Non-Contact-Tapping-Mode-High-Resonance-Frequency-afm-tip-PPP-NCH

3. Influence of UV irradiation on morphologies and chemical composition of thin amorphous films of TPD and DPVBi

Influence of UV irradiation on stability of morphology of thin TPD films was topic of previous studies done by Han *et al.* [1] and Qiu and Qiao [2]. However explanation for mechanism of increased stabilization was not given. While Qiu and Qiao have correctly recognized that UV light degrades TPD films, the type of degradation was not researched. TPD and DPVBi are used in the production of OLEDs and share some similar properties. Throughout the chapter results obtained for both materials will be compared. In the following section morphologies of pristine TPD and DPVBi films will be compared. Influence of UV irradiation on morphological stability of TPD will be confirmed and examined in the case of DPVBi. This will be followed by the study of chemical changes caused by UV irradiation of both materials; it will be shown that degradation is due to oxidation. Presence of the oxidized species will be identified as the cause for the increased stability of irradiated TPD films.

3.1 Morphology of pristine and UV irradiated thin amorphous TPD and DPVBi films

3.1.1 Morphology of pristine thin amorphous TPD and DPVBi films

Amorphous thin films of organic molecules with low glass transition temperature tend to be morphologically unstable even at room temperature. In such films the energy of non-covalent interactions is comparable to the energy of thermal fluctuations and thus can lead to morphological and structural changes driven by minimization of Gibbs free energy. Instability gives rise to different morphologies that depend on the film thickness as shown by Suljovrujic et al. [3].

General behavior of our TPD and DPVBi films is in agreement with previous observations– TPD films dewet at room temperature [3], while DPVBi crystalizes [4].Results regarding morphology at room temperature of our pristine TPD and DPVBi films will be now presented. For morphology study thin films of TPD and DPVBi were deposited on to the 75 mm x 25 mm glass substrates. Length of the substrate enabled

evaporation of thickness libraries which usually spanned an order of magnitude. Typical maximal film thickness was 100 nm for TPD and 200 nm for DPVBi.

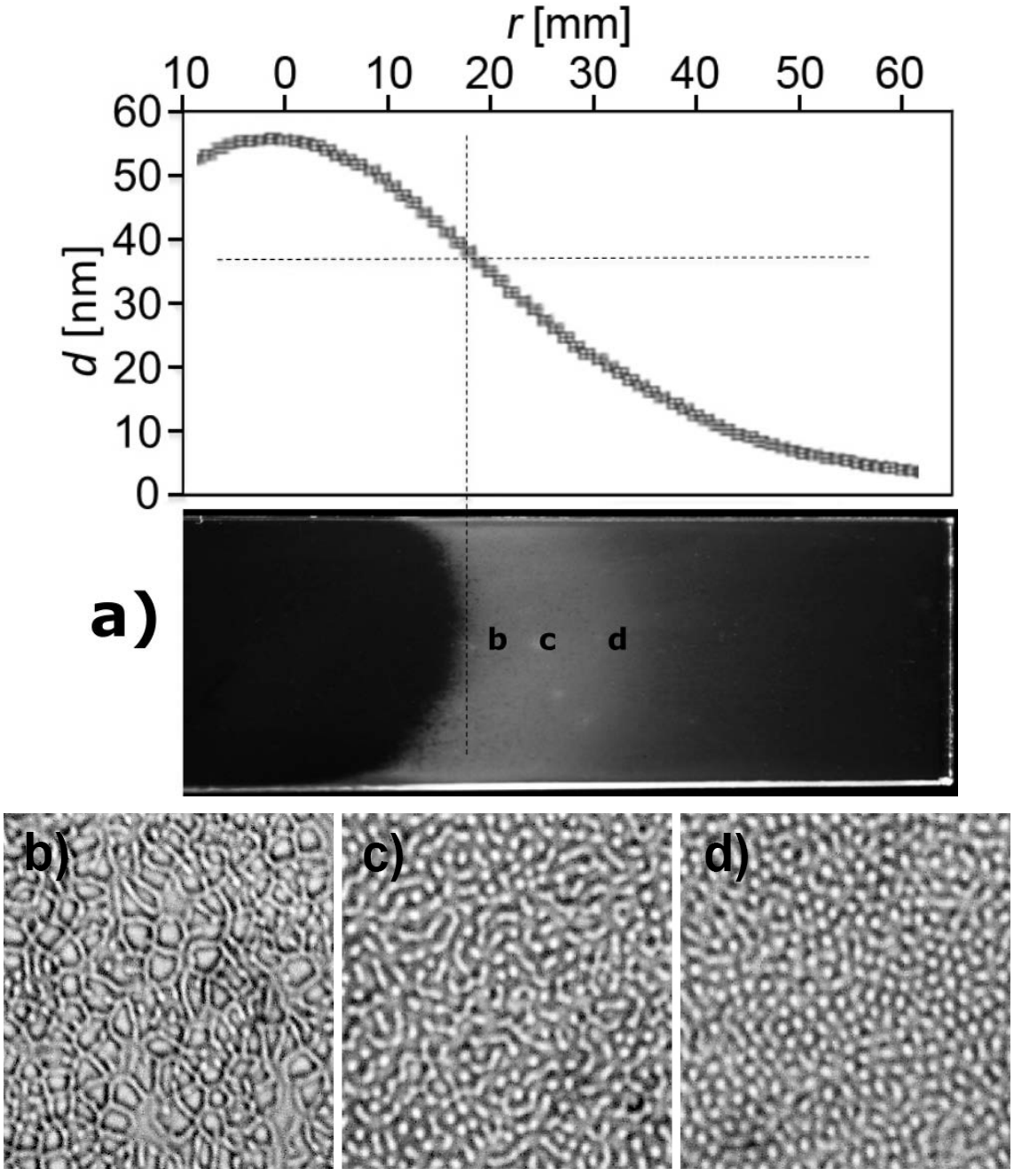

Fig. 3.1 Photograph of the 75 mm long TPD film taken after the dewetting process (approximately 48 h) aligned with its thickness profile. Two distinct parts can be seen: transparent, thick part and opalescent, thin part under the 40 nm which had undergone dewetting process. Micrographs (200 μm x 200 μm) are showing relation between morphologies and thickness of the film.

Upon deposition thin TPD films were completely transparent under visible light for the whole library of thickness. Approximately one day after the deposition of the thin TPD film two distinct parts could be observed as shown in Fig. 3.1a. On the left hand side is a thicker part of the film which remained transparent. A sharp line separating dewetted section from smooth part of the film follows constant film thickness of around 40 nm, while its curvature reflects axial symmetry of the film deposited from a Knudsen source. The right hand portion of the film has a frosted glass look (opalescent) which is a consequence of Mie scattering of light from the formed structures during the dewetting process.

As said before, the surface of the thick part (d> 40 nm) is flat and continuous (confirmed by AFM imaging). Close to this critical thickness of 40 nm interconnecting holes can be seen by optical microscope in the structure of the film (Fig. 3.1b). Going to smaller thicknesses these are followed by wormlike structures (Fig. 3.1c) and isolated droplets (Fig. 3.1d). Size of these structures is comparable to the wavelength of visible light, thus opalescence. It is reasonable to assume that dewetting of the TPD probably starts as soon as the deposition is finished, however much more time is needed for the effects to become visible on the microscopic scale. Similar morphologies and value of critical thickness were also observed by Suljovrujic et al. [3].

We observed the dewetting of DPVBi films, which is similar to, but much faster than for TPD films, as its signs are visible immediately after evaporation. That is, thinner part of the film was opalescent when removed from the evaporation chamber. However morphological changes of pristine DPVBi are more complicated than in the case of TPD, as crystallization could be observed only few hours after deposition. After a day or two both dewetting and crystallization processes are complete and a clear border between two parts of a film at the critical thickness of 70 nm appears (Fig 3.2a). Close examination of these two parts reveals that at the thicker part (d > 70 nm), which is bright white, only crystallization has happened (Fig. 3.2b, c) while on at the rest of the film both process are present (Fig. 3.2d, e).

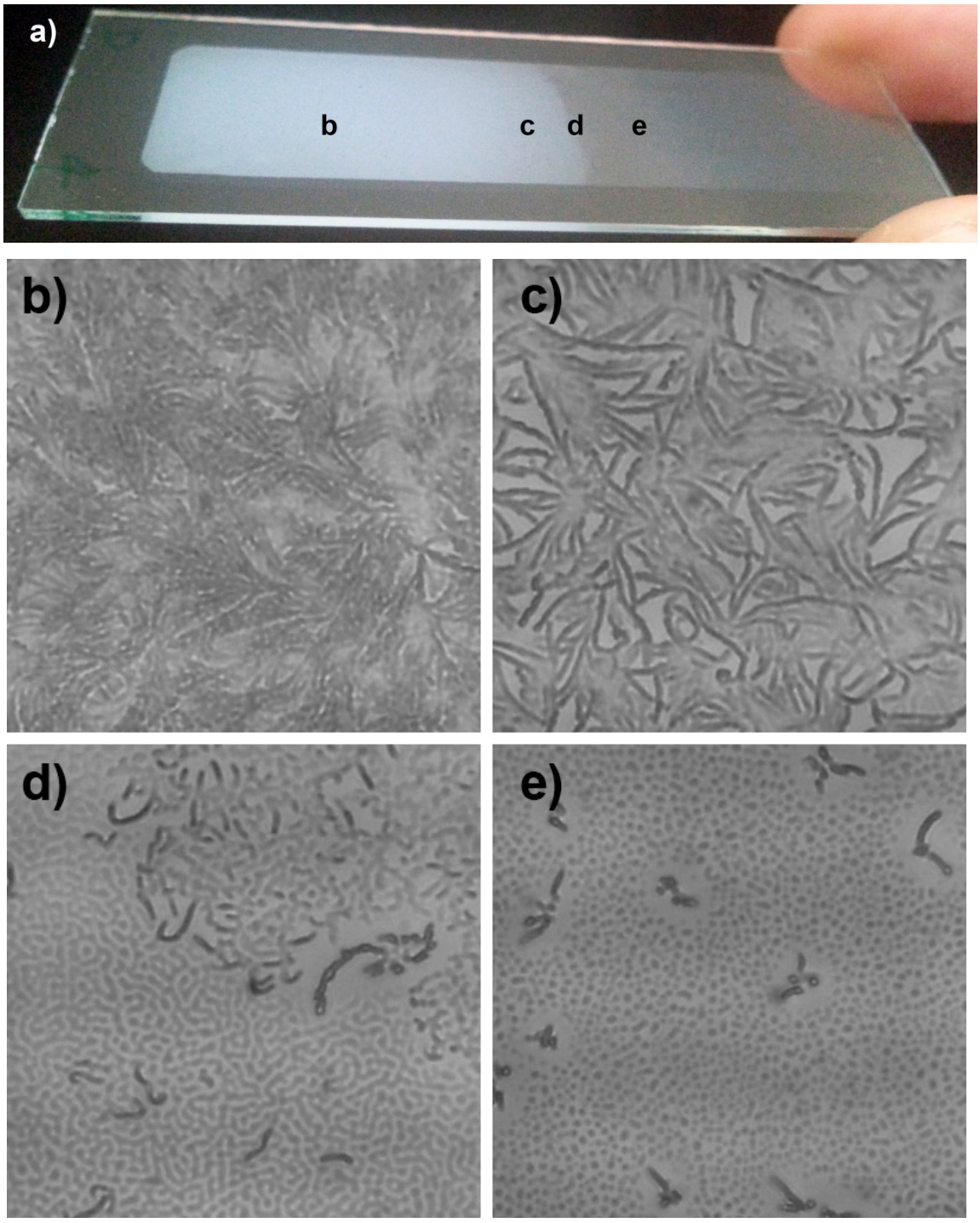

Fig.3.2 a) Photograph of the thin DPVBi film on a glass substrate taken few days after deposition. Border between dewetted part on the right and crystalized part on the left side is clearly visible. Micrographs of different thicknesses of DPVBi film under different magnification b) 135 nm, c) 90 nm, d) 70 nm and e) 50 nm.

On thick part of DPVBi, crystallization proceeds through formation of spherulites. Their number and size gradually grow and they start to coalesce. This process is finished once the whole surface of film is covered, which approximately takes two days (Fig.3.2b, c). These crystallites are extended and intertwined and, due to their size and random orientation, scatter light strongly. Crystallization can also be observed on the thinner part of the film in the form of small dendritic-like structures embedded in the dewetted background. Their size is limited by the amount of the available material and they are scarce as the competing process of dewetting prevents their formation (Fig. 3.2d, e).

TPD films can also crystallize (at the thick part), but this process is much slower than for DPVBi films. It takes few months at room temperature to observe formation of first spheriluties by naked eye.

While both molecules possess the same T_g, the dynamics of morphological changes is different. This suggests that DPVBi molecules are much more mobile than TPD which enables fast dewetting and crystallization of thin films. That is why the critical thickness below which dewetting appears is higher for DPVBi film (70 nm) compared to TPD, where it is 40 nm. Explanation of different dynamics possibly lies in the fact that TPD has a lone pair of electrons on the nitrogen atom and can form hydrogen bonds. Thus it is expected that interactions between TPD molecules among themselves and substrate are stronger than the ones in the case of DPVBi.

TPD and DPVBi are nearly non-polar hydrophobic molecules [5] whose interaction with the glass substrate is weaker than van der Waals interaction with their own species. This is the main reason why thin films of these materials on polar substrates have lower T_g than in the bulk. The dewetting process in TPD (DPVBi) appears very similar to dewetting of polystyrene thin films on SiO_2 substrate [6], which is considered as a model system for dewetting phenomena in thin films. For this system, there is an excellent agreement between theory and experiment which is presented in the review article written by R. Blossey [6]. It applies not only to morphology details but also to dynamics of the dewetting process.

3.1.2 Influence of UV irradiation on morphologies of thin TPD and DPVBi films

As mentioned before, Han *et al.* [1] have shown that UV light treatment of TPD films leads to the increased morphological stability. They have subjected irradiated TPD films to elevated temperatures and high humidity, as these conditions promote their dewetting and crystallization. Their AFM study of the pristine and irradiated films exposed to named conditions proved that UV light treatment can prevent dewetting or crystallization. We assume that similar effect would be seen in the case of DPVBi films.

Influence of the UV irradiation on formation of observed morphologies of our TPD and DPVBi films was examined. In accordance to previous studies by Han *et al.* it was found that irradiation by UV light in air inhibits morphological changes in TPD films, as well in DPVBi.

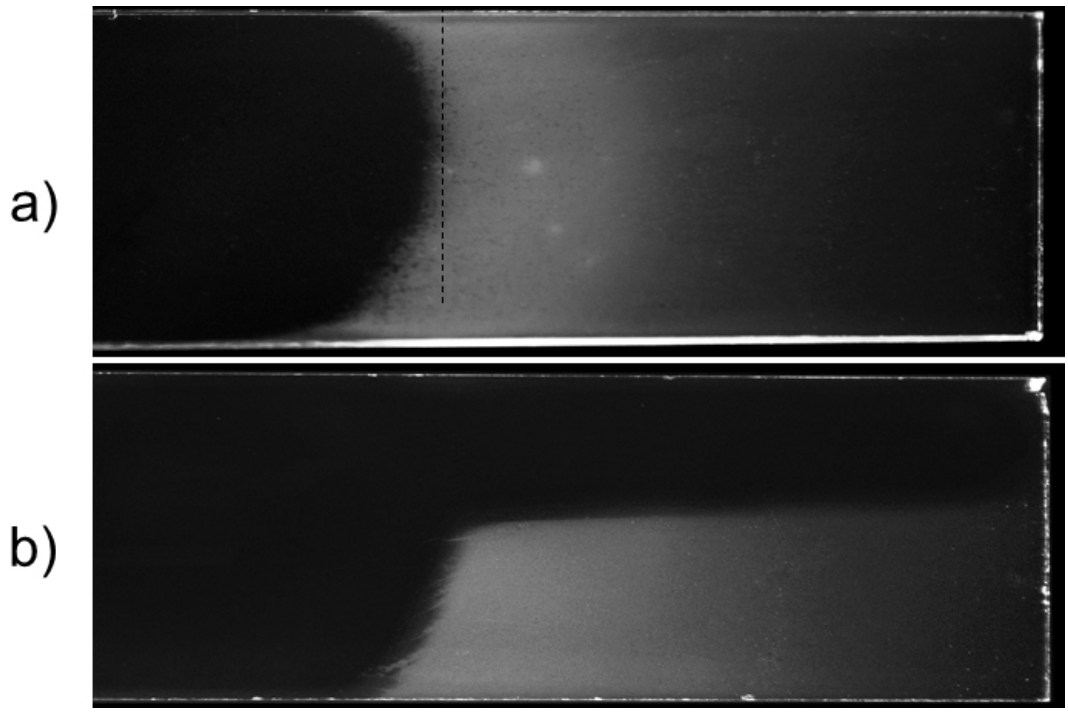

Fig. 3.3 a) Photograph of the TPD film after dewetting. Shown in b) is a photograph of another TPD film of a nearly identical thickness profile whose upper half was exposed for 2 h to UV radiation immediately after deposition. For dewetting to be completed it takes approximately 48 h.

In order to compare the behavior of morphological changes in pristine and irradiated films, one half of TPD film was covered with a mechanical mask while the other half was exposed of UV light intensity I_{UV} = 1.7mWcm^{-2}for two hours. Fig 3.3 shows two TPD films, one which did not receive the UV treatment (a) and the other which was partially irradiated (b).Inspection by naked eye clearly shows that irradiated part of the film remained transparent. This indicates that UV irradiation had stopped the dewetting process of the thin part of the TPD film as it remained transparent. Further characterization by AFM confirms that morphological changes are stopped by UV treatment (Fig. 3.4). Treated film was irradiated by UV light immediately after evaporation. Both samples were imaged one day after evaporation/treatment. While pristine film completely dewetted (separated droplets are formed) the other film shows that irradiation has stopped the dewetting process at some point[1].

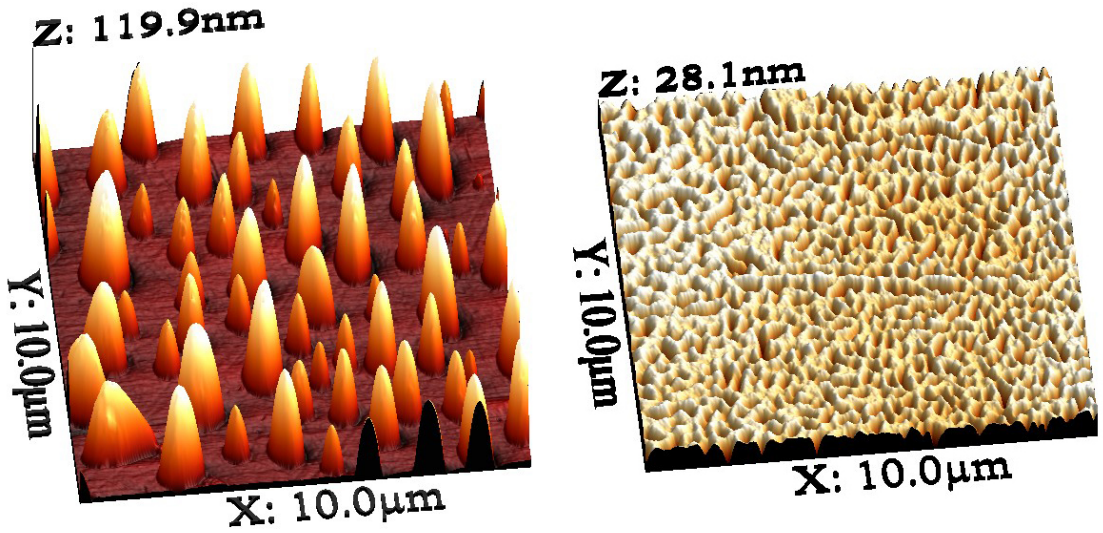

Fig. 3.4 AFM image of non-irradiated (left) and UV irradiated (right) of 20 nm thick TPD films, which were held in air and dark for one day before imaging. Surface roughnesses are around 17 nm and 4 nm for pristine and irradiated film, respectively.

[1]In the AFM image of the UV treated sample we can see the sings of the dewetting process that probably took place during short time before irradiation. As the sample is very thin such changes cannot be observed by naked eye. However it is clear that the further dewetting is stopped by application of UV light.

No sign of dewetting was found for illuminated films even if subjected to temperatures as high as 90°C which is significantly higher than the T_g of the TPD. This may be of importance for technological applications. We note that UV radiation does not stabilize morphology of TPD thin films if irradiated in vacuum after the deposition under otherwise same experimental conditions.

Similarly to TPD, DPVBi also shows signs of stabilization. However it was not possible to focus on the stabilization of the dewetting process as it was already over by the time deposition is finished. Thus we focused our attention on inhibition of crystallization of DPVBi films. For that purpose one half of freshly made DPVBi film was covered with a mechanical mask while the other half was exposed of UV light intensity I_{UV} = 1.7mWcm^{-2}for half an hour. Photographs of pristine and the partially exposed films taken two days after evaporation/exposition are shown in Fig. 3.5a and b,

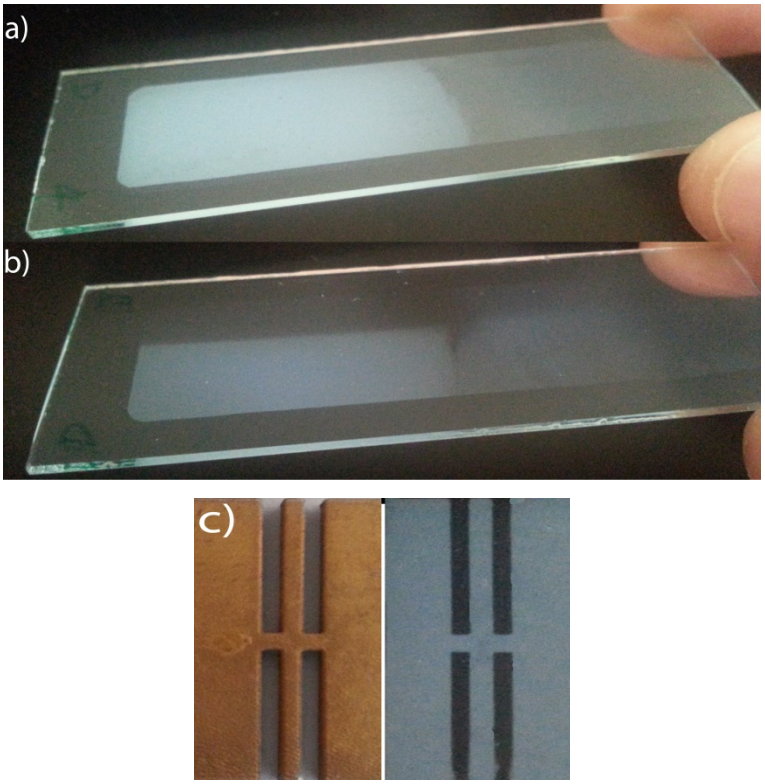

Fig. 3.5 a) Photographs of two thin DPVBi films taken few days after deposition: a) non-irradiated film and b) film whose upper half was UV irradiated. c) Image of a mechanical mask (left), 140nm thick DPVBi film irradiated with 400nm UV LED through a mechanical mask. Parts of the film that have received UV treatment appear to black in the image as they remained transparent.

respectively. It can be seen from Fig. 3.5b that irradiated part of the film (upper portion) remained partially transparent. That is UV light had more prominent effect on crystallization then on dewetting of the film.

It was interesting to see if it was possible to use the effect of UV light for patterning of thin films. For that purpose part of the film was protected with a mask shown on the left in Fig. 3.5c, while the film which was left to crystalize for two days is shown on the right. It can readily be observed that irradiation has stopped crystallization and that the pattern of the mask is well transferred: the part of the film that appears to be black is irradiated and because of that it remained transparent. The rest of the film was protected by the mask has crystalized. However, effect showed to be only temporary: after approximately two months crystallization of the irradiated parts was observed.

We have seen that UV irradiation of TPD films resulted in increase of T_g and stopped formation of morphologies and in the case of DPVBi temporarily stopped crystallization. This is a result of chemical changes that were induced by UV light irradiation in the presence of oxygen (see the next section). Formation of oxidized species is responsible for increased stability of TPD and DPVBi films. The photo-oxidized TPD and DPVBi molecules are likely to have a polar character. Such species can interact strongly with terminal −OH groups from the substrate, which will stabilize film in respect to dewetting or crystallization. One can also expect that the presence of dipole–dipole and dipole-induced-dipole interactions between different species in the film will further increase its thermal stability.

3.2 Investigation of chemical changes

It is known that exposure of thin organic films to UV light in air can lead to oxidation of material and formation of radicals or dimmers [7, 8]. Thus, we expect that our films, exposed to UV light in air, have suffered chemical changes in their composition. In order to investigate these changes, mass, NMR and IR spectrometry were performed on pristine and irradiated films of TPD, while MS and IR were done in the case of DPVBi films.

3.2.1 Mass spectroscopy

Mass spectrum of pristine TPD film showed only presence of one mass M = 516.2 gmol^{-1}, which is the mass of TPD molecule. Spectrum of a UV irradiated film (Fig. 3.6) shows presence of two new masses, first at M_1 = 530.2 gmol^{-1} and the second at M_2 = 532.2 gmol^{-1}. Both are accompanied by two satellite peaks due to isotope effect.

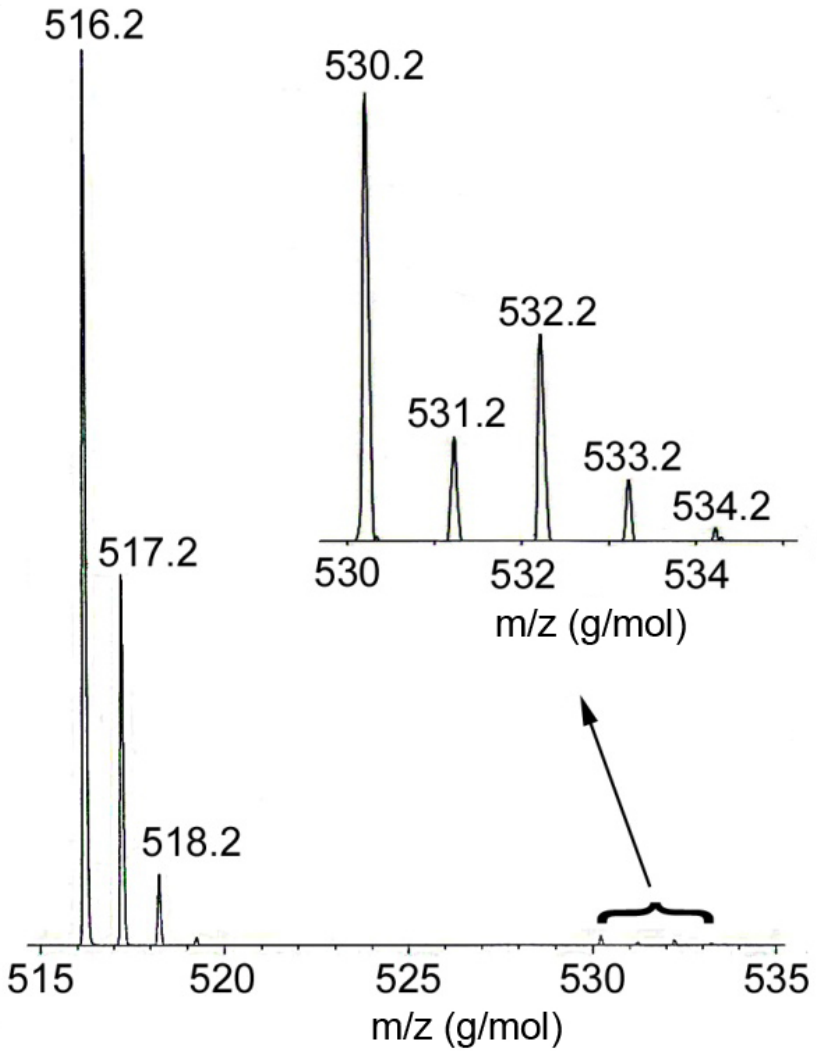

Fig.3.6 Mass spectrum of TPD film exposed to UV light. Besides the ones of TPD molecule, we observe tiny peaks at 530.2 and 532.2 g/mol. Note that each of these peaks is accompanied by two satellite peaks due to isotope species whose relative intensities are in quantitative agreement with theoretical predictions.

Difference between new masses and the mass of TPD molecule is ΔM_1 = 14 gmol^{-1} and the second is ΔM_2 = 16 gmol^{-1} respectively. The first one can be explained by loss of two hydrogen atoms and addition of one oxygen atom and the other one by addition of one oxygen atom which participates in formation of hydroxyl group. Thus it is possible to ascribe following molecular formulas to the new masses $C_{38}H_{30}N_2O$ and $C_{38}H_{32}N_2O$. Calculated isotope effect for the new molecules is in agreement with experimental results. The new molecules are a result of photo-oxidation of TPD.

Thin DPVBi films were examined by LDI-TOF and ASAP mass spectroscopy techniques. For LDI-TOF MS thin DPVBi film with a thickness of around 200 nm was deposited onto steel sample plate. Usually a matrix material which absorbs at λ = 337 nm is used, however as DPVBi absorbs light in this region use of matrix material was not necessary.

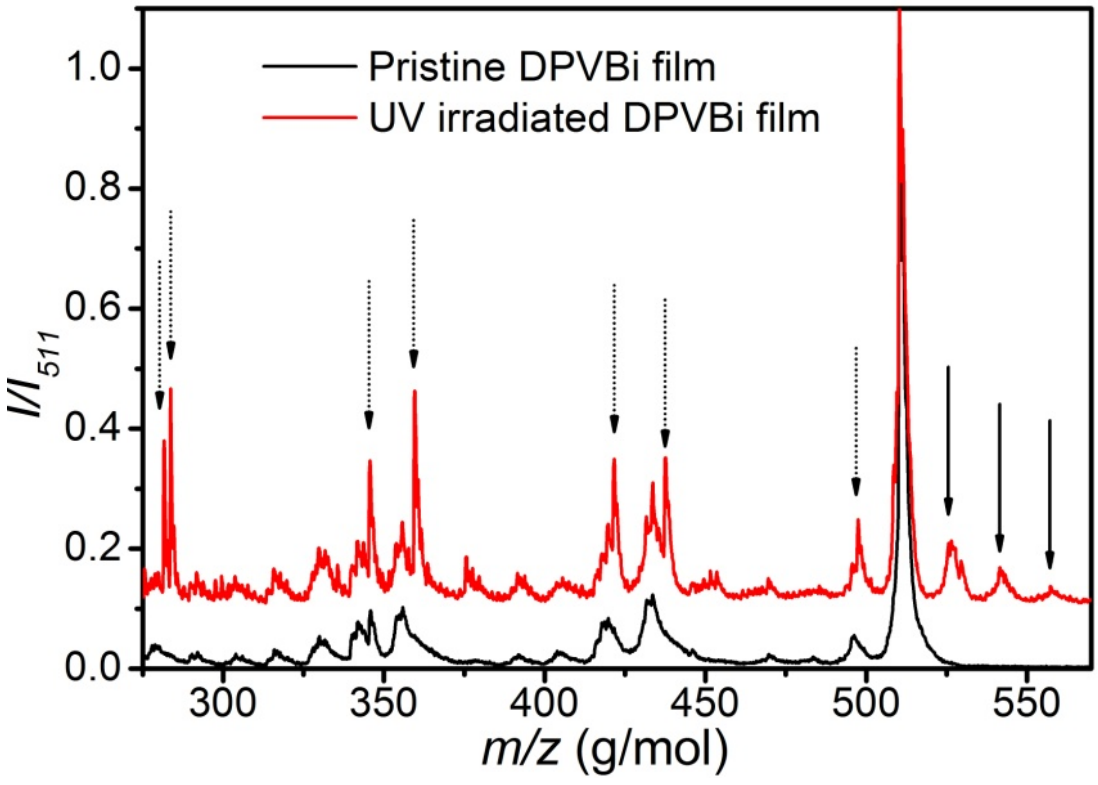

Fig. 3.7 LDI-TOF MS intensities *I* of pristine (bottom curve) and UV irradiated (top curve) films normalized to their intensity I_{511} at m/z = 511 gmol^{-1}, the mass of DPVBi and offset by 0.1 for clarity.

Mass spectra of DPVBi pristine thin films show dominant peak at 510.6gmol^{-1}, which is the mass of DPVBi molecule. Besides this peak, other lower masses can be observed, which are the fragments of DPVBi (Fig. 3.7). Irradiated samples show the presence of numerous new species, which can be divided into two groups. First group with $M>M_{\mathrm{DPVBi}}$, indicated by solid arrows, which are products of oxidation of DPVBi molecules. The other, with $M<M_{\mathrm{DPVBi}}$, indicated by dotted arrows, consists of molecular fragments of oxygenated DPVBi and/or some photo-oxidation products. Masses larger than M_{DPVBi} seem to follow a pattern: $M_{x,y,z} = M_{\mathrm{DPVBi}} + x\Delta M_1 + y\Delta M_2 + z\Delta M_3$, where $M_{x,y,z}$ is the mass of new specie and x,y and z take integer values 0, 1, 2 or 3.Masses ΔM_1 = 14gmol^{-1}, ΔM_2 = 15 gmol^{-1}and ΔM_3= 16 gmol^{-1} correspond to the molecule gaining one oxygen atom and losing two, one or zero hydrogen atoms, respectively. The loss of two H atoms may imply that O atom formed a bridge between two C atoms. If one H atom is lost, than it is expected that O forms a double bond with C and if none H atoms are lost, it is plausible that -OH group is attached to C atom.

The presence of dimers of DPVBi was not detected. Relative intensity of peaks in MS spectra does not necessarily reflect relative number of different molecules present in a film, as different species do not necessarily have the same ionization potentials. Thus, it is not possible to deduce which type of impurity is predominant.

It was interesting to see if it is possible to correlate the changes in absorbance (number of changed molecules) with the results of mass spectroscopy. For that purpose three DPVBi films of the same thickness were evaporated in the single evaporation using a special mask and movable substrate holder. One of the films did not receive any treatment while the two others were irradiated with same UV light intensity for different amounts of time. The absorbance of the two films was changed for 40 and 65 percent respectively. Mass spectra of pristine and two irradiated films are shown in Fig. 3.8, with the focus on impurities with the most intensive signal. Background signal (obtained with a clean capillary) was subtracted from all three curves. Then they were normalized to their intensity I_{511} at m/z = 511gmol^{-1}. Results suggest that the number of the impurities is rising with irradiation time which can be seen from the growing intensity of the peaks. The inset of Fig. 3.8shows how the relative number of DPVBi to the number of all detected ions varies with the degree of degradation. Mass spectra taken in the interval of m/z between 350 and 600gmol^{-1}, outside which no significant

signal was detected, were integrated to obtain the area S under curves. Subsequently, all the spectra were divided by the corresponding area S. The ratio of intensities of F1 and F2 with that of pristine film is around 35 and 66%, respectively. This means that the percent of change in the number of DPVBi molecules obtained by MS is fairly close to the one obtained by absorbance, i.e. the change in absorbance is a good measure of the change in the number of DPVBi molecules induced by UV irradiation in air.

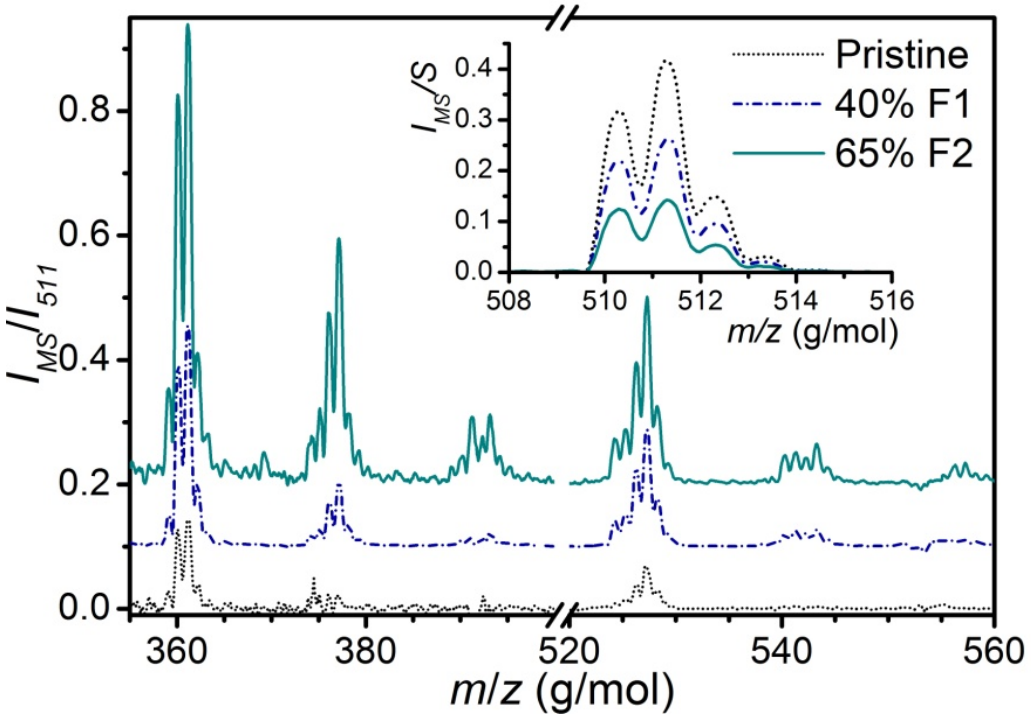

Fig. 3.8 ASAP MS intensities I_{MS} of pristine and UV irradiated films normalized to their intensity I_{511} at m/z = 511gmol^{-1}, the mass of DPVBi. Irradiated films F1 and F2 have suffered **40** and **65%** of change in absorbance, respectively. Curves are shifted for clarity by 0.1 and 0.2 for F1 and F2, respectively. Background signal (no material scratched with the capillary) was subtracted from the curves. Inset shows I_{MS} of DPVBi normalized to the surface S under spectra in the range of m/z between 350 and 600gmol^{-1}. Note that at 511 gmol^{-1}normalized intensities I_{MS}/S stand in ratio 0.42 : 0.26 : 0.14 = 100 : (100 – **38**) : (100 – **67**) for pristine, F1 and F2 films, respectively.

ASAP has confirmed the results obtained with LDI TOF, the same new masses were observed in the irradiated samples with both methods. However small amount of impurities located around the m/z = 525 gmol^{-1} was also observed in the pristine film

with the ASAP method. This could be explained by the oxidation of DPVBi during the experiment, as the presence of water in the chamber operated at the atmospheric pressure was noted previously [9].This was not the case with LDI TOF experiment which operates under high vacuum conditions.

Mass spectroscopy gave evidence for oxidation of thin films of both molecules; it is interesting to see that in the case of TPD only the species with one oxygen atom were observed, while in the case of DPVBi oxygenated species containing from one to four oxygen atoms were detected. It is possible that there are also oxidized TPD species that have more oxygen atoms attached but they are too few to be detected.

3.2.2 ^{1}H NMR spectroscopy

Further evidence for photo-oxidation of TPD was obtained by ^{1}H NMR. Proton NMR spectra of TPD powder, pristine and UV irradiated films were measured. The same results were obtained for TPD powder and pristine thin film which show that evaporation did not induce any changes in the material. Results obtained for pristine and irradiated TPD film together with assignation of peaks are shown in Fig.3.9. The assignation of peaks is explained in detail in Appendix A. Differences between pristine and irradiated film that are consequence of UV treatment are indicated with black arrows. Only the unique protons are labeled for clarity. Resonance at 2.3 ppm belongs to protons (1) from two methyl groups while a large number of resonances centered at 7 ppm belong to protons (2-10) from phenyl rings. The smaller ppm values of the chemical shift the larger electron density around the proton; hence it is plausible that the methyl group is the most susceptible to oxidation. Such an outcome not only would produce a new set of resonances from protons of -H_2COH group but also would cause a small downfield shift of the proton resonances associated with phenyl rings. This is a consequence of so-called induction effect, which manifests through a shift in the local electron density due to introduction of a distant atom of a different electron affinity.

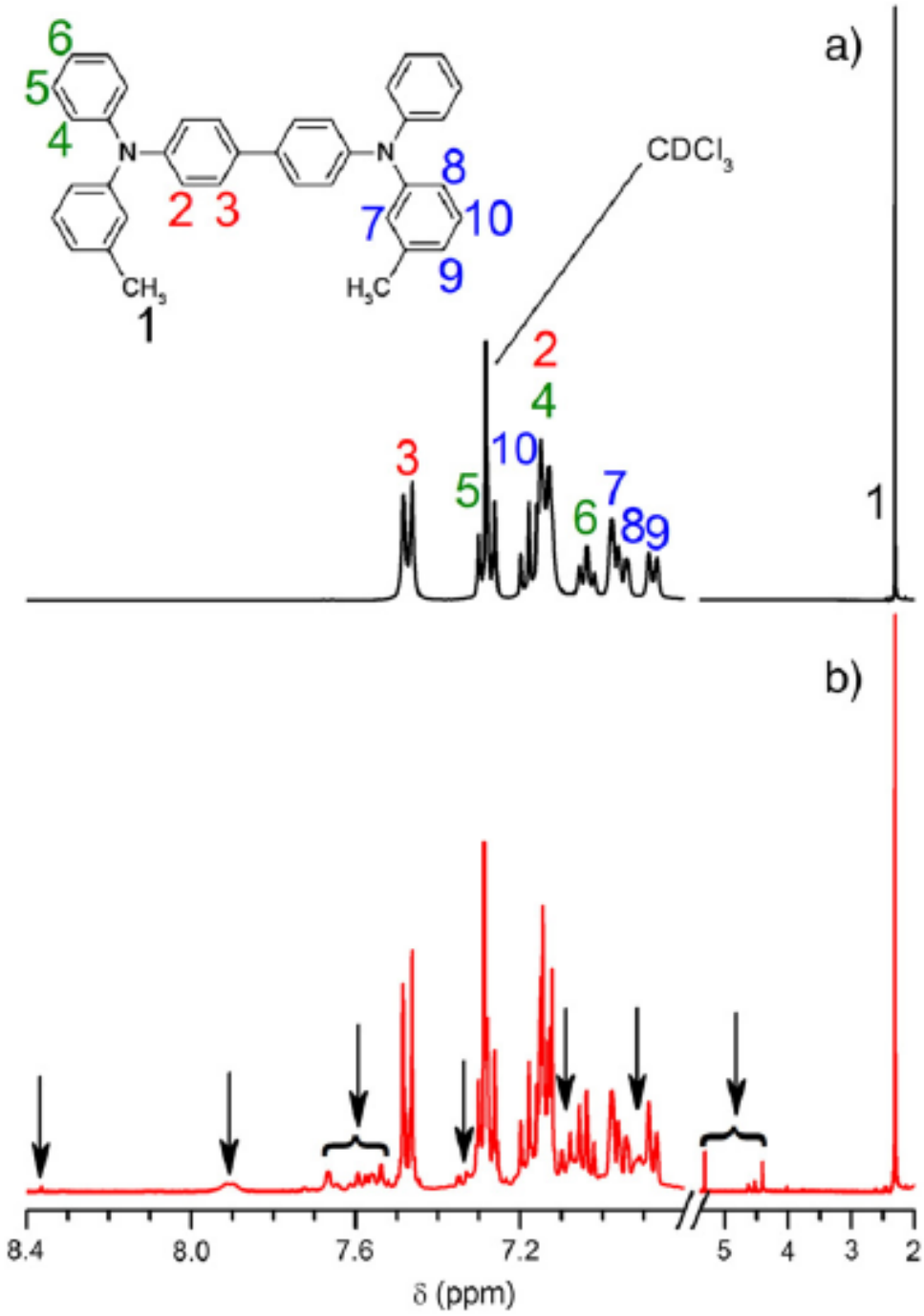

Fig.3.9 ^{1}H NMR spectrum of a dissolved pristine TPD film with the main resonance assigned to protons attached to 10 unique carbon atoms in TPD; see the drawing of TPD molecular structure in the inset. b) The corresponding spectrum of UV irradiated TPD film with additional resonances (indicated by arrows and braces) due to photo-oxidized TPD species.

The trends observed in ^{1}H NMR spectrum of UV irradiated TPD sample in Fig. 3.9 bare in qualitative agreement with above expectations. The resonances of pristine TPD sample are still dominant but a number of additional weak resonances of photo-oxidized TPD species are clearly visible. Unfortunately, most of them are buried under intense TPD resonances thus making their assignment impossible. We can speculate that the resonances between 4.5 ppm and 5.5 ppm belong to protons from $-H_2COH$ group, in analogy with ^{1}H NMR spectrum of phenylmethanol [10], where these resonances are found at 4.58 ppm. The group of additional dense resonances at around 7.6 ppm should be ascribed to protons from phenyl rings of photo-oxidized TPD species. These resonances are shifted downfield for up to 0.2 ppm from the resonances of TPD protons with smallest electron density (3). In addition, there are some weak resonances at 7.9 ppm and 8.4 ppm which should also belong to the protons from phenyl rings. It is unlikely that distant $-H_2COH$ group can cause such a large downfield shift; hence we suppose that phenyl rings of TPD are also susceptible to photo-oxidation. Whether we have one or more different species of that kind remains an open question.

3.2.3 Vibrational spectroscopy

NMR study of irradiated TPD film showed that assignation of peaks is difficult task when several different molecules are present in the sample as there is significant overlap between resonances. Results of MS performed on irradiated thin films of DPVBi showed presence of numerous new species, it was clear that NMR would not be able to give relevant results without special sample preparation which would require separation of species and large sample quantities. In order to provide more evidence for the case of photo-oxidation IR spectroscopy was performed instead. The measured IR spectra of pristine and irradiated TPD and DPVBi film are shown in Fig.3.10.

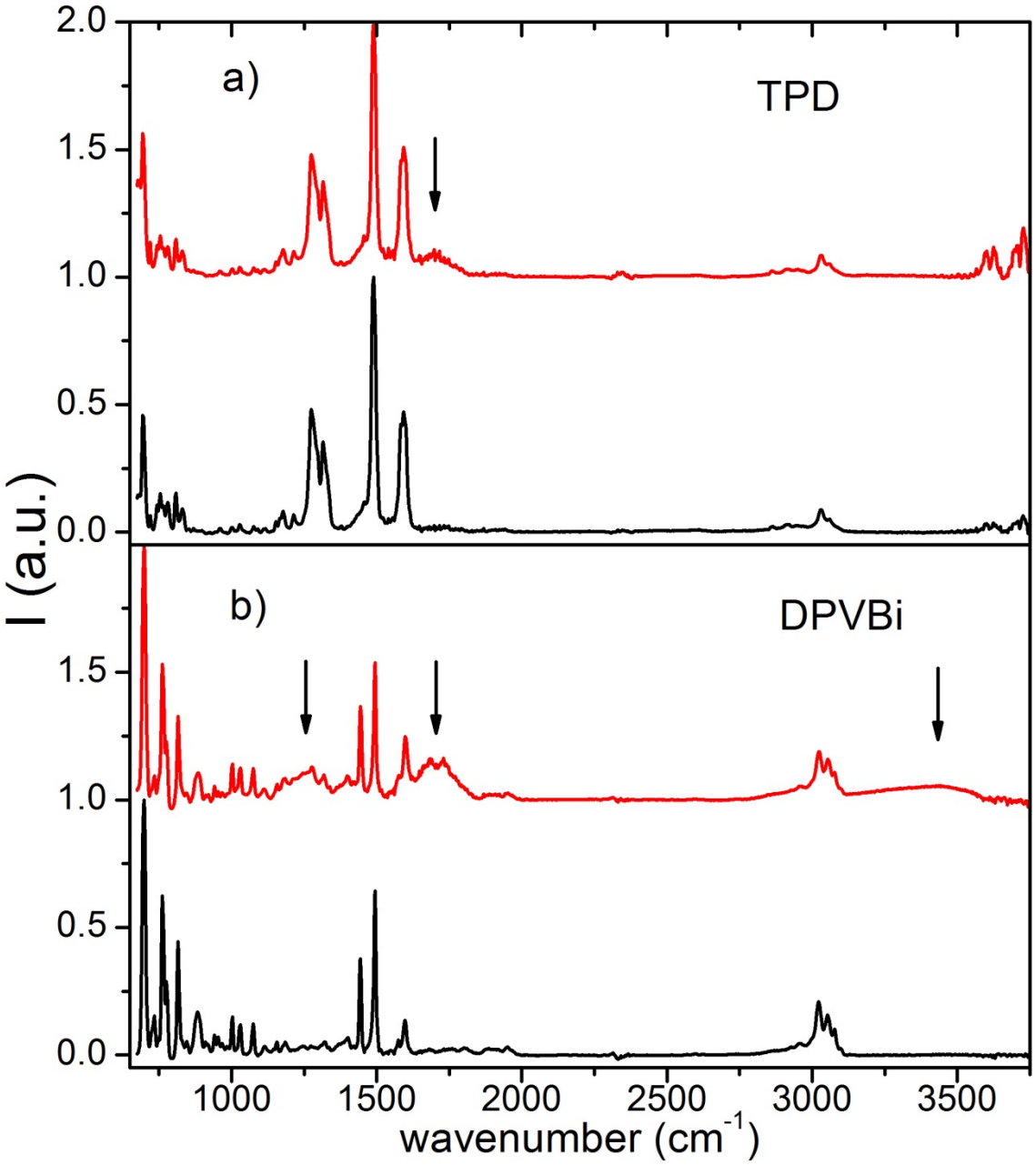

Fig. 3.10 IR spectra of a) TPD and b) DPVBi films. Black curves denote pristine and red curves UV exposed films, irradiated for 90 min with I_{UV} = 1 mWcm^{-2}. Spectra are offset 1 a.u. for clarity. Changes in spectra of exposed films compared to pristine films are indicated with arrows.

In the case of exposed TPD there is only one new feature, around 1700 cm^{-1}, compared to the pristine film (Fig. 3.10a). For UV exposed DPVBi new broad features can be observed in the regions around 1250, 1700 and 3300 cm^{-1} (Fig. 3.10b). The new

features have large width as a consequence of inhomogeneous broadening in the amorphous medium of DPVBi film.IR spectra are in agreement with results obtained from MS: we assume that the feature around 1700 cm^{-1} belongs to C=O bond (ΔM_2), while the one around 1250 cm^{-1} can be ascribed to C-O bond (ΔM_1, if O bound to two C atoms or ΔM_3). Broad feature around 3300 cm^{-1} could be explained by the presence of -OH groups (ΔM_3), possibly participating in hydrogen bonding [11]. While MS shows the presence of new masses, which correspond to formation of hydroxyl groups, IR spectra do not show pronounced -OH peak.

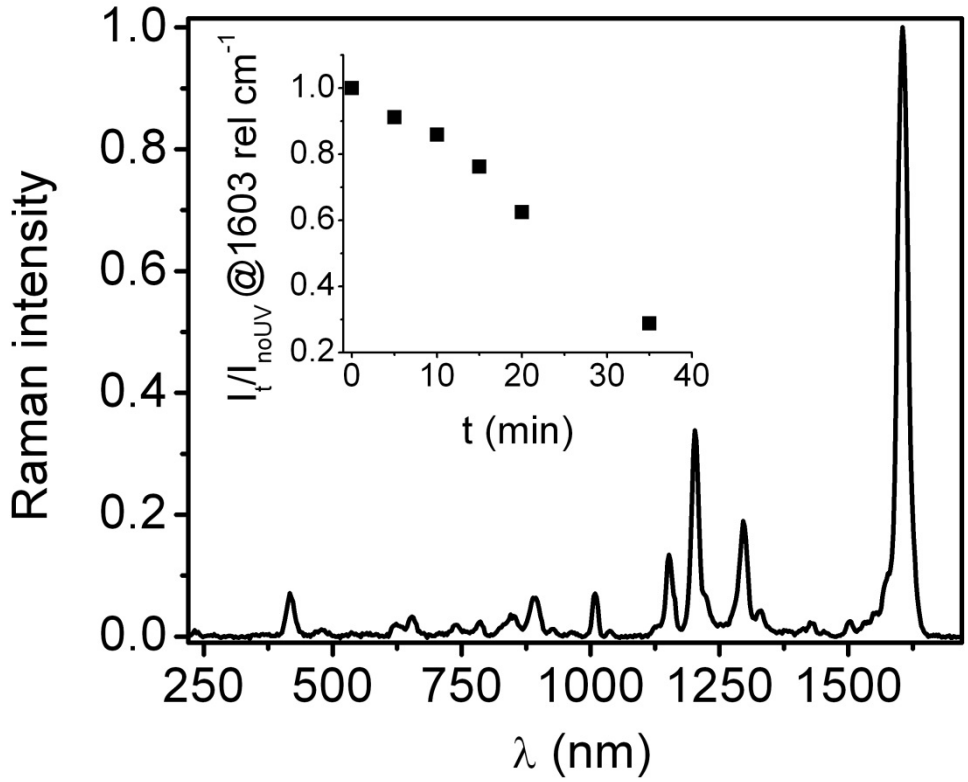

Fig. 3.11 Typical Raman spectra of DPVBi normalized to the intensity of the peak at 1603 rel cm^{-1}, inset shows intensity at the peak 1603 cm^{-1} for different irradiation time normalized to the value for non-irradiated film.

Raman spectroscopy was performed on pristine and irradiated 180 nm thin DPVBi film[2]. Thin DPVBi film was irradiated with UV light (I_{UV} = 3 $mWcm^{-2}$) and its Raman

[2]For TPD it was hard to obtain Raman signal and no difference could be observed between pristine and irradiated samples due to small signal-to-noise ratio.

spectra were recorded every five minutes. Results show that intensity of Raman signal is diminishing with irradiation time while background signal, which looks like photoluminescence, is rising. Background signal is subtracted, Raman spectra obtained for different irradiation times normalized to the value at the peak 1603 $cm^{-1}$and compared to the spectrum of pristine sample: not only that no new features were observed but there were no changes in the intensity of Raman modes. Inset of the Fig. 3.11 shows value of intensity at the peak 1603 cm^{-1} for different irradiation time normalized to the value for the pristine film. For irradiation times larger than 30 minutes Raman spectra was buried in the photoluminescence background. Thus results of Raman spectroscopy were not able to show presence of new species. The origin of the background signal in the UV irradiated films will be discussed in the Appendix B. In Appendix C assignation of Raman and IR peaks for both molecules will be given.

References for Chapter 3

[1] E.M. Han, J.J. Yun, G.C. Oh, S.M. Park, N.K. Park, Y.S. Yoon, M. Fujihira, *Enhanced stability of organic thin films for electroluminescence by photoirradiation*, Opt. Mater. **21** (2002) 243.

[2] Y. Qiu, J. Qiao, *Photostability and morphological stability of hole transporting materials used in organic electroluminescence*, Thin Solid Films **372** (2000) 265.

[3]E. Suljovrujić, M. Mićić, S. Demic, V.I. Srdanov, *Combinatorial approach to morphology studies of epitaxial thin films,* Appl. Phys. Lett. **88** (2006) 121902.

[4] X. Zhang , Z.Wuan, B.Jiao, D. Wang, D. Wang, X. Hou, W. Huang, *Solution-processed white organic light-emitting diodes with mixed-host structures*, Journal of Luminescence **132** (2012) 697–701.

[5] P.M. Borsenberger, J.J. Fitzgerald, *Effects of the dipole moment on charge transport in disordered molecular solids*, J. Phys. Chem. **97** (1993) 4815.

[6] R. Blossey, *Thin film rupture and polymer flow*, Phys. Chem. Chem. Phys. **10** (2008) 5177.

[7] L. Lüer, H.-J.Egelhaaf, D. Oelkrug, G. Cerullo, G. Lanzani, B.-H. Huisman and D. de Leeuw, *Oxygen-induced quenching of photoexcited states in polythiophene films*, Org. Electron. **5** (2004) 83-89.

[8] Denis Kondakov, *Role of chemical reactions of arylamine hole transport materials in operational degradation of organic light-emitting diodes*, J. Appl. Phys. **104** (2008) 084520-084528.

[9] S.-Z. Wang, X. Fan, A.-L.Zheng, Y.-G.Wang, Y.-Q.Dou, X.-Y.Wei, Y.-P.Zhao, R.-Y. Wang, Z.-M. Zong and W. Zhao, *Evaluation of atmospheric solids analysis probe mass spectrometry for the analysis of coal-related model compounds*, Fuel **117** (2014) 556.

[10] M. Balci, *Basic ^{1}H- and ^{13}C-NMR Spectroscopy*, Elsevier, Amsterdam, 2005.

[11] J. Workman Jr., *The handbook of organic compounds*, Academic Press, San Diego 2000.

4. Quenching of photoluminescence

Results have shown that irradiation of thin TPD and DPVBi films with UV light in air leads to their oxidation. The presence of oxidized species, i.e. impurities can also be seen through changes in absorption and photoluminescence spectra. The change of photoluminescence follows exponential decrease while the absorbance decreases linearly with irradiation time. While the change in absorbance is barely detectable photoluminescence is quenched significantly. This implies that there is non-trivial mechanism of photoluminescence quenching. It will be shown that the quenching is not the consequence of direct long range Förster energy transfer from host to impurity molecule, rather it goes through exciton self-diffusion.

Results regarding changes of absorbance and photoluminescence will be presented for TPD and DPVBi thin films for different irradiation times, UV light intensities and in different atmospheres. The study of DPVBi is more detailed as these changes are much faster than for TPD and conclusions drawn from it can be extended to the case of TPD. Based on these results the mechanism of PL quenching will be proposed.

4.1 Absorbance and photoluminescence of thin TPD and DPVBi films

4.1.1 Spectral characteristics of pristine films

For absorbance measurement thin TPD and DPVBi films were deposited on to fused silica substrates. Fig.4.1 shows typical absorption and photoluminescence spectra of pristine TPD (top curves) and DPVBi (bottom curves) films normalized to their peak values, in good agreement with those found in literature [1, 2]. In absorption spectra two bands at 315 nm and 356 nm (242 nm and 355 nm) are observed, which correspond to two lowest excited electronic states of TPD (DPVBi) [3]. Energy gaps were estimated from the long-wavelength absorption edge [4]: (3.0 ± 0.1) eV for DPVBi and (3.14 ± 0.1) eV for TPD. While photoluminescence spectrum of DPVBi is structureless, the one for TPD shows distinct vibrational bands. Both PL spectra are strongly red shifted compared to absorbance, the values of difference between the first absorbance and PL maxima being 0.4 eV for TPD and 0.8 eV for DPVBi.

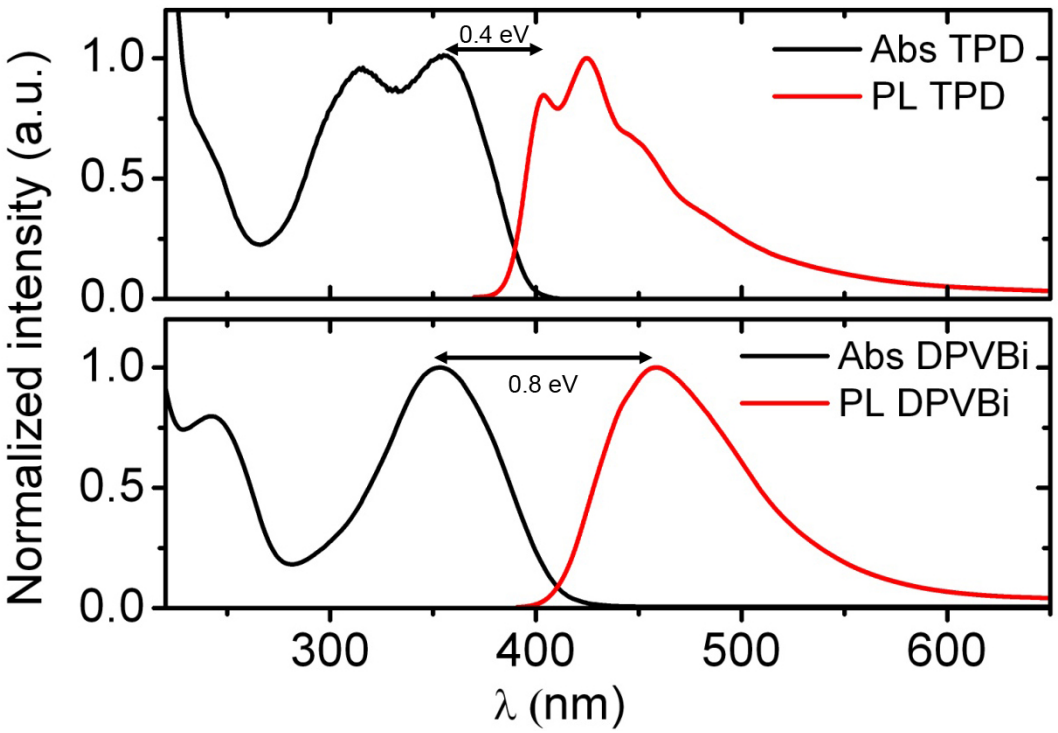

Fig. 4.1 Typical absorbance (black) and photoluminescence (red) spectra normalized to their peak values of TPD (top) and DPVBi (bottom) pristine thin films. The energy difference between peak values (indicated by arrows) of absorbance and PL is given in eV.

This shift is due to binding energy of excitons. Exciton is a bound state that is formed between electron in the lowest unoccupied molecular orbital (LUMO) excited by a photon and the hole created by its excitation in highest occupied molecular orbital (HOMO).After a characteristic lifetime, typically of an order of nanoseconds, molecule returns to its ground state by emission of a photon or phonon.

During its lifetime it is also possible for an exciton to hop from one molecule to another, via one of two possible non-radiative mechanisms, namely Dexter or Förster energy transfer (Fig. 4.2) or via radiative mechanism (which we do not consider here). For this to happen, a spectral overlap between acceptor absorbance and donor emission (PL spectrum) is necessary. In Dexter energy transfer, there is a bilateral *exchange of electrons* between excited donor and ground state acceptor molecules, in which donor goes to ground state while acceptor molecule is excited. This is a short range (typically 1-10 Å) energy transfer because an overlap between wavefunctions of acceptor and

donor is necessary, besides spectral overlap. Förster mechanism is not an electron but *energy transfer*: energy is exchanged between excited donor and ground state acceptor molecules through dipole-dipole interactions, in which donor goes to ground state while acceptor molecule is excited. As it does not require a wavefunction overlap this is a long range energy transfer (typically 10-100 Å).

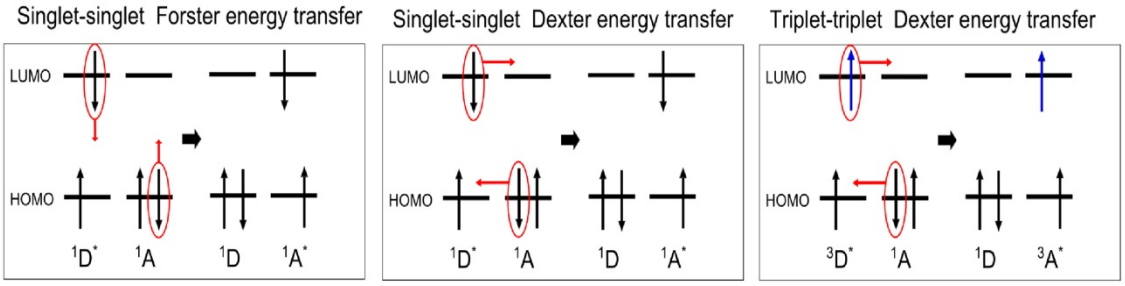

Fig. 4.2 Schematic representation of Förster and Dexter energy transfer

We will see in the following subsections that UV irradiation, i.e. the presence of photo-oxidized impurities causes the quenching of PL. In order to investigate the mechanism of quenching we need to calculate, from the overlap between absorbance and PL spectra (Fig. 4.1), Förster self-radius $R_0$for both TPD and DPVBi. Förster radius is the distance at which probability for energy transfer is 50 %. The values of $R_0$for TPD and DPVBi were calculated using the equation 4.1 [5]:

$$R_0 = 0.211\left(k^2 n^{-4} Q_D J(\lambda)\right)^{1/6}, \qquad (4.1)$$

whereκ^2 = 2/3 is the geometrical factor for random orientation of the donor and acceptor transition dipole moments, Q_D^{TPD}= 0.39and Q_D^{DPVBi} = 0.45 are PL quantum efficiencies for amorphous TPD [6] and DPVBi [7]. As, to the best of our knowledge, experimental data for the refractive index n of DPVBi are lacking, thus in both cases a value $n \approx 2$ for TPD used [8], as molecules are structurally similar. $J(\lambda)$ is the overlap integral, given by

$$J(\lambda) = \int I_\lambda^D(\lambda)\varepsilon_A(\lambda)\lambda^4 d\lambda, \qquad (4.2)$$

where $I_\lambda^D(\lambda)$ is photoluminescence spectrum of a donor normalized in such way that integral is equal to unity. Molar decadic absorption coefficient $\varepsilon_A(\lambda)$ of an acceptor is given by

$$\varepsilon_A(\lambda) = \frac{A(\lambda)}{cl}, \qquad (4.3)$$

where $A(\lambda)$ is absorbance of molecule, c is molar concentration (which can be easily calculated from the density of a given material) and l is thickness of film. As we calculate Förster self-radius, donor is the same molecule as acceptor. For overlap integrals following values were obtained $J_{TPD}(\lambda) = 9.47 \times 10^{12} (\text{nm})^4 \text{M}^{-1}\text{cm}^{-1}$ and $J_{DPVBi}(\lambda) = 4 \times 10^{12} (\text{nm})^4 \text{M}^{-1}\text{cm}^{-1}$. Thus the values of Förster self-radius for TPD and DPVBi are $R_0^{TPD} = 1.5$ nm and $R_0^{DPVBi} = 1.4$ nm.

4.1.2 Influence of irradiation on absorbance and photoluminescence

Prior studies [9-11] have shown that UV irradiation of TPD films causes changes both in absorbance and photoluminescence spectra. In this subsection results of the UV exposure on the absorbance and PL of TPD and DPVBi films will be presented.

First results for TPD will be presented. Thin TPD films were irradiated with an UV LED, which delivered about 1.7 mWcm^{-2} in the 300–400 nm range (as determined by a Solar Light Co. PMA 2110 UVA sensor). Exposure of TPD to UV light leads to a slow and steady (1% per hour) decrease in the intensity of absorption bands in 325–400 nm region (Fig. 4.3a) and much faster decrease in photoluminescence intensity (Fig. 4.3b), which is in agreement with previous studies [9-11]. Observable changes in the absorption and luminescence spectra of the films irradiated in vacuum were not found.

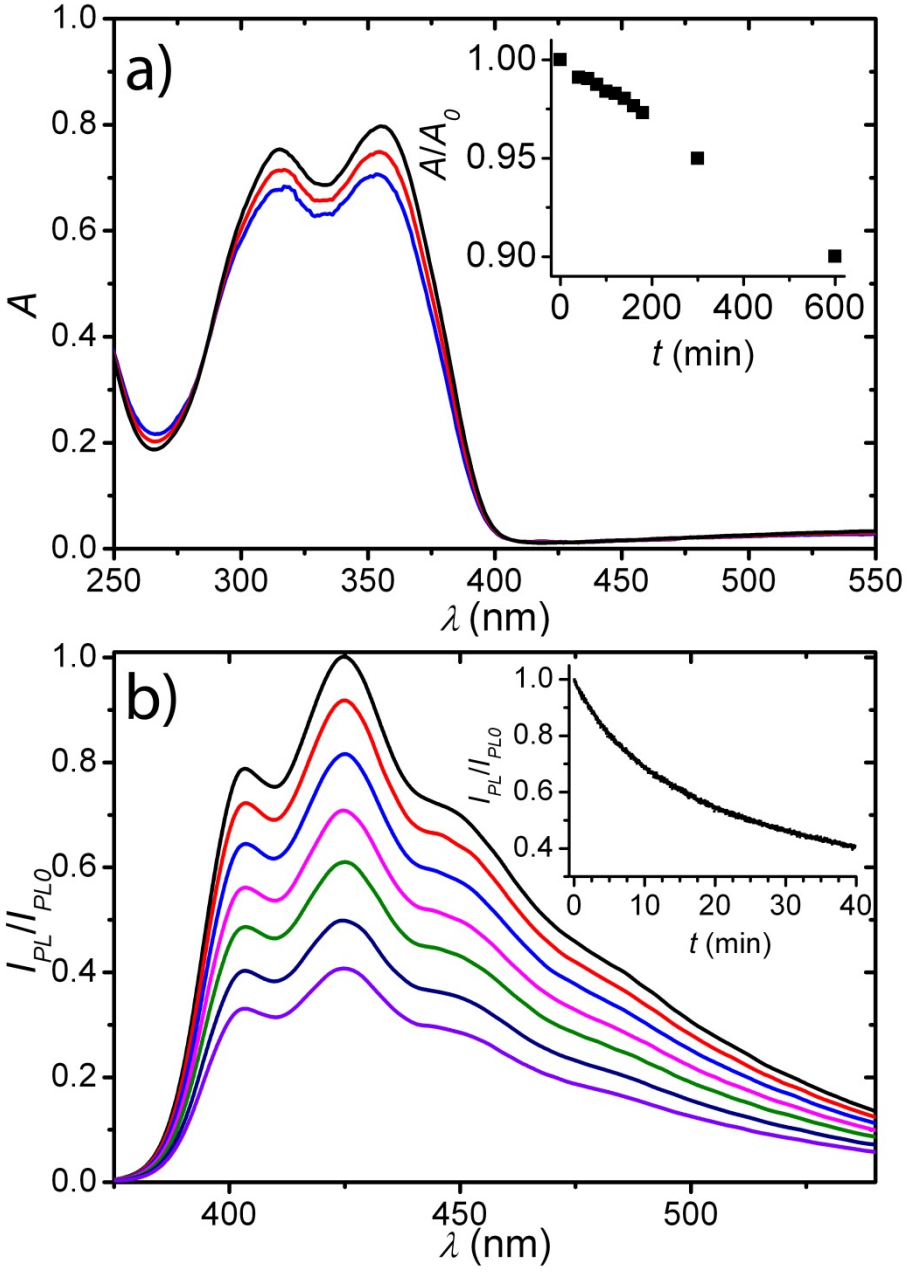

Fig. 4.3 a) Absorbance A vs. λ as a function of irradiation time t = 0, 300 and600 min, where A decreases monotonically with t. Inset in a) shows plot of absorbance A at λ = 355 nm normalized to its initial value A_0 as a function of t. b) Photoluminescence I_{PL}, normalized to the value I_{PL0} at λ = 425 nm and t = 0 s, vs. λ plotted for t = 0, 2, 5, 9.5, 15.5, 25 and 40 min, where I_{PL}/I_{PL0} decreases monotonically with t. Inset of b) shows I_{PL}/I_{PL0} at 425 nm normalized to its initial value as function of t. In both measurements 115 nm thick TPD films were irradiated in air with I_{UV} = 1.7 mWcm^{-2}.

In the case of DPVBi UV irradiation had similar effect on both absorbance and photoluminescence as in the case of TPD. However the process of degradation showed to be much faster and thus easier to study. Influence of UV irradiation on thin DPVBi films was studied thoroughly taking into account different light intensities and film thicknesses. As in the case of TPD there were no observable changes in absorbance or photoluminescence spectra of DPVBi thin films irradiated in vacuum on the time scales used in this work.

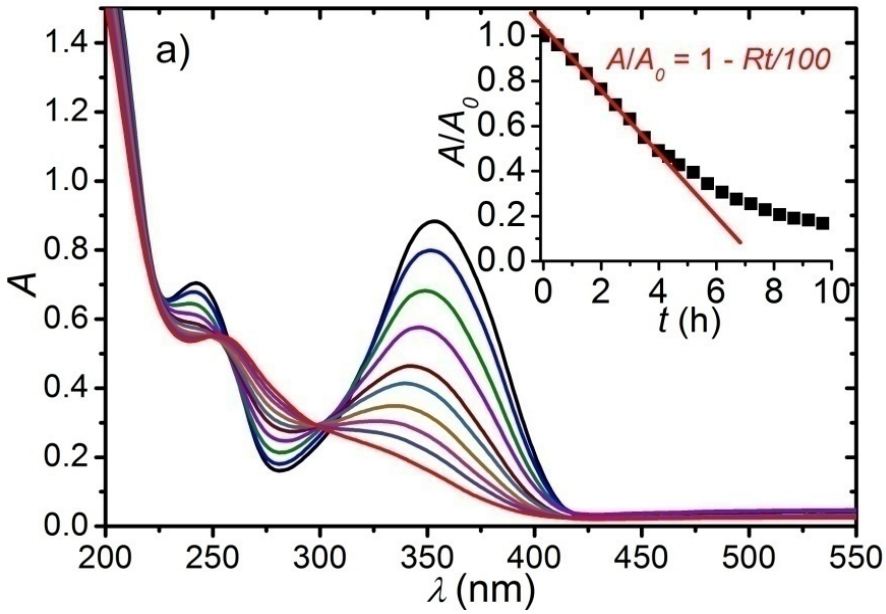

Fig. 4.4 Absorbance A vs. λ as a function of irradiation time t = 0, 1, 2, 3, 4, 4.7, 5.7, 6.7, 7.7 and 9.7 h, where A decreases monotonically with t. Inset in a) shows plot of absorbance A at λ = 355 nm normalized to its initial value A_0 as a function of t and linear fit that defines the rate R of change of absorbance.

Fig. 4.4 shows absorption spectra as a function of wavelength λ after different times of *irradiation in air* of 190 nm thick DPVBi films deposited onto fused silica substrates and irradiated with I_{UV} = 0.4 mWcm^{-2}. Irradiation with UV light induces gradual disappearance of both bands and emergence of new peak around 255 nm, reflecting a gradual chemical change in film composition (degradation of DPVBi) and a formation of new species (impurities). The percent of change in the value of absorbance A at λ = 355 nm is assumed to be roughly the same as the percent of impurities present in a film. To track this change, in the inset of Fig. 4.4 value of absorbance A taken at 355 nm,

normalized to its initial value A_0 at time t = 0, was plotted as a function of irradiation time t. The decrease in normalized absorbance A/A_0 is close to linear at the beginning and then gradually slows down. Nonlinear part of the curve can be a consequence of change in degradation process dynamics due to a significant loss of DPVBi material (around 60%). From the linear part the rate R of change of normalized absorbance $A/A_0$is defined by $A/A_0 = 1 - Rt/100$ (the inset of Fig. 4.4) and for the film from Fig. 4.4 it is around 0.22%/min.

Results of absorbance measurements suggest that DPVBi films are much more prone to oxidation than TPD, as absorbance changes 0.22% per minute for UV light intensity of 0.4mWcm^{-2}, while in the case of TPD for intensity which is four times higher we see a change in absorbance of only 1% per hour.

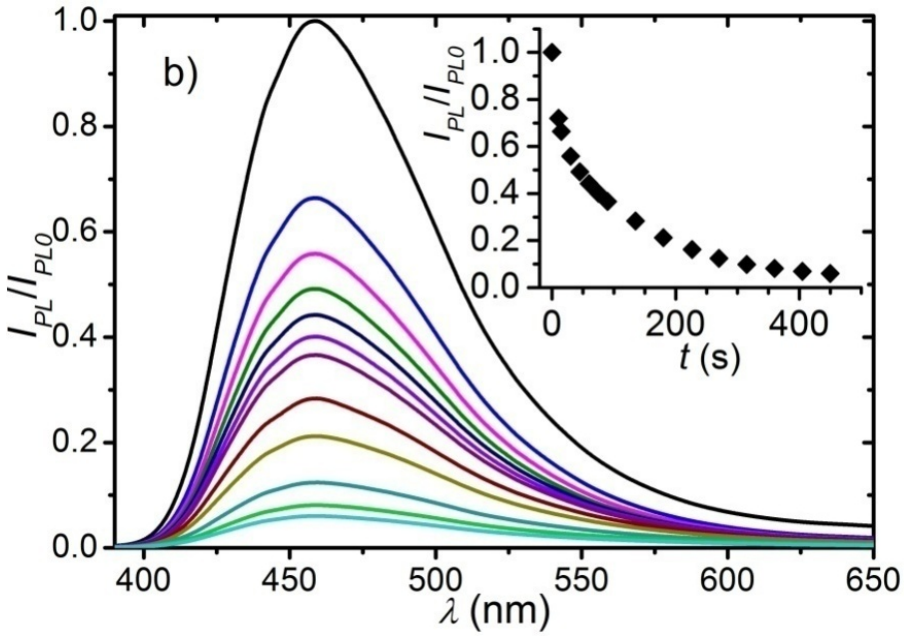

Fig. 4.5 Photoluminescence I_{PL}, normalized to the value I_{PL0} at λ = 458 nm and t = 0 s, vs. λ plotted for t = 0, 15, 30, 45, 60, 75, 90, 135, 180, 270, 360 and 450 s, where I_{PL}/I_{PL0} decreases monotonically with t. Inset of b) shows I_{PL}/I_{PL0} at 458 nm normalized to its initial value as function of t. In both measurements 190 nm thick DPVBi films were irradiated in air with I_{UV} = 0.4 mWcm^{-2}.

Effects that degradation *in air* has on the photoluminescence (PL) are shown in Fig. 4.5 as a series of spectra of a 190 nm thick film irradiated with UV intensity I_{UV} = 0.4

$mWcm^{-2}$ as function of irradiation time t. Inset of Fig. 4.5 shows that PL intensity I_{PL} at λ = 458 nm, normalized to its value I_{PL0} at t = 0, has a quick, exponential decay with t. Time necessary for PL intensity to drop to half of its initial value – half lifetime $t_{1/2}$ is 45 s. During that time, according to the value of R, absorbance changed only for a little less than 0.2%, pointing to some non-trivial mechanism of PL quenching. Somewhat higher value of 0.4 % was found in the case of TPD.

The normalization of the PL spectra from Fig. 4.5 to their maxima reveals small differences in the region above 470 nm. The difference increases with increase of the UV exposure time. This could possibly imply formation of exciplexes (the details will be given in the Appendix B).

The presence of impurities, besides having a negative effect on the photoluminescence, also can impair charge transport. Having in mind use of TPD and DPVBi, as hole-transporting and emissive layer in OLEDs, these types of side effects are highly unwanted.

4.1.2.1 Influence of different UV light intensities in the case of DPVBi

The influence of irradiation of thin DPVBi films in air with different UV light intensities was also studied: the rate R and time evolution of I_{PL}/I_{PL0} at 458 nm were measured as function of I_{UV} for 190 nm thick film. Photoluminescence I_{PL} has exponential decay that is faster for larger I_{UV} (Fig.4.6a), while the rate R is proportional to I_{UV}. In the inset of Fig. 4.6a$t_{1/2}$ was plotted versus I_{UV}/I_{UV}^{max}, along with the fit to the relation $t_{1/2} = C\ I_{UV}^{\ -1/n}$ used for OLEDs [12]; C is a constant and n is so-called acceleration parameter, whose value is (1.08 ± 0.06). This means that $t_{1/2}$ is, to a good approximation, inversely proportional to I_{UV}. The product of R and $t_{1/2}$, which is the percentage of changed absorbance or DPVBi molecules that leads to 50% decay of PL, should be then approximately independent of I_{UV}, as $R \sim I_{UV}$. This is shown in Fig. 4.6b where the product $Rt_{1/2}$ stays approximately constant and less than 0.2% when I_{UV} varies. Eventual dependence of $Rt_{1/2}$ on I_{UV} would indicate that dynamics of formation of impurities is not the same for different UV light intensities.

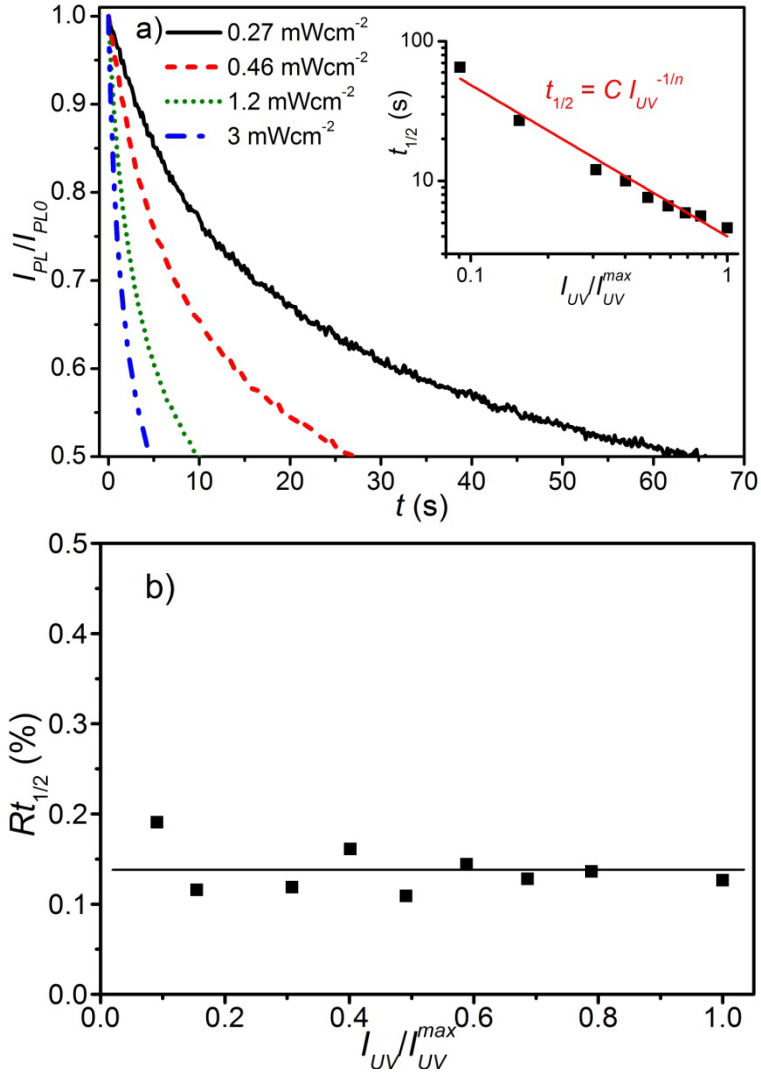

Fig. 4.6 a) Photoluminescence I_{PL} /I_{PL0} at 458 nm vs. t of 190 nm thick DPVBi films obtained for different intensities of UV light. Inset shows $t_{1/2}$ as a function of I_{UV}/I_{UV}^{max} and a fit $t_{1/2} = C\, I_{UV}^{-1/n}$ that gives n = (1.08 ± 0.06). b) The product of $Rt_{1/2}$ as a function of normalized UV light intensity I_{UV}/I_{UV}^{max}.

4.1.2.2 Irradiation of DPVBi under different oxygen pressures

In order to provide further evidence for photo-oxidation and investigate the influence of pure oxygen following experiment was performed. First DPVBi film was irradiated in the inert atmosphere of nitrogen. As expected, irradiation of thin DPVBi films in nitrogen atmosphere did not produce any changes in absorbance or photoluminescence. Then the irradiation of DPVBi films was performed with various

oxygen pressures in the chamber with maximum UV light intensity. For that purpose two films of the same thickness were evaporated, one for the measurement of absorbance and the other for photoluminescence. Results of these measurements are shown in Fig.4.7. Both rates of change of absorbance and PL increase with the increase of oxygen pressure.

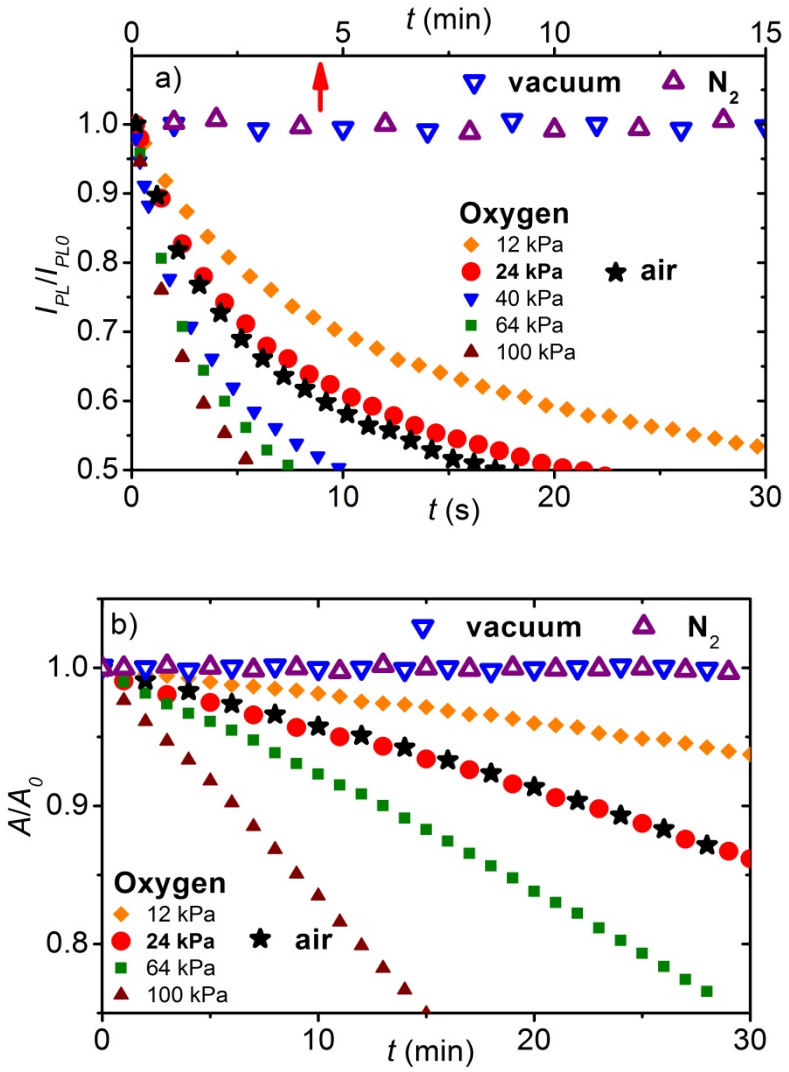

Fig. 4.7 Normalized a) PL intensity I_{PL} /$I_{PL0}$and b) absorbance A/A_0 at λ = 355 nm at 458 nm vs. t for different oxygen pressures in the chamber (solid symbols) and for nitrogen atmosphere and vacuum (open symbols).Top axis in a), which is in minutes, refers to PL data obtained in vacuum and nitrogen. Measurements are also performed in air and marked with black stars. Measurements were performed with 120 nm thick films irradiated with I_{UV}^{max} = 3 mWcm^{-2}.

It is interesting to note that the curves A/A_0 and I_{PL}/I_{PL0} for P_{O2}= 180 Torr and in air under ambient conditions are similar, as expected, since the value P_{O2}= 180 Torr is close to the partial pressure of oxygen in air. Photoluminescence spectra of DPVBi films in high vacuum (5 x 10^{-4} Pa) and nitrogen atmosphere show no change even for irradiation times of 30 minutes with I_{UV}^{max}. Under the same conditions, the rate R of change of absorbance is zero. Thus, under the conditions and on the time scale of our experiments, no change in film composition can be induced by UV light in vacuum. Likewise, PL does not change when films are exposed only to air: PL of DPVBi film was first measured in situ in vacuum (briefly exposed only to UV light), then the film was exposed only to air (no UV light) so that oxygen enters the film [13,14] and, finally, brought back to low vacuum (few Pa), where PL was recorded once again (the two measured values of PL were the same). An implication, for practical purposes, would be that even the low vacuum is sufficient for extraction of oxygen from amorphous DPVBi films of thickness of order of 200 nm. These considerations imply that the simultaneous presence of oxygen and UV light is necessary for degradation of DPVBi films and that the excited DPVBi molecules interact with oxygen to produce impurities.

4.2 The mechanism of PL quenching

From the absorbance study we have seen that irradiation of thin DPVBi films with UV light in air results in the chemical change – photo-oxidation. Measurements of absorbance under different oxygen pressures have shown that presence of oxygen plays a key role in the degradation of DPVBi. This was indeed confirmed by mass and infrared spectroscopy which gave final evidence for the case of photo-oxidation. It is clear that DPVBi molecules react with oxygen to form new impurity species *only if* excited.

In general, there are two possible pathways for chemical reaction of DPVBi and oxygen, both typical for such compounds [15, 16]. In one, excited singlet molecule gives an electron to ground-state oxygen molecule to form radical cation and the superoxide anion, which can further react chemically to form new species [16]. In the other, host molecule in excited triplet state acts as a sensitizer and transfers its energy to

ground-state triplet oxygen to form singlet oxygen and ground-state host molecule [16]. The energy needed for singlet oxygen formation is 0.97 eV. We can assume that the first excited triplet state of DPVBi lies around 2 eV based upon experimental results that Schwartz [17]has obtained for spiro-DPVBi. This energy is sufficient for singlet oxygen formation in our films. Singlet oxygen is very reactive and may further interact with other DPVBi molecules to form photo-oxidized species.

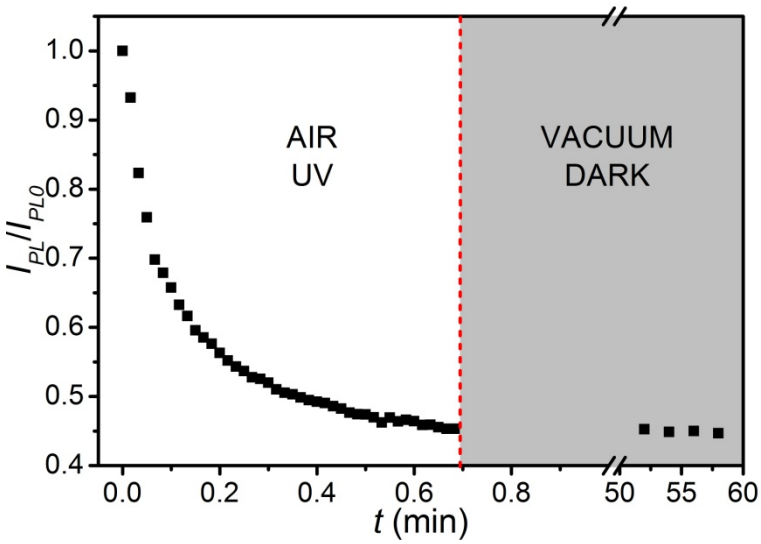

Fig. 4.8 Normalized PL intensity I_{PL}/I_{PL0} at 458 nm vs. *t* of a film exposed to I_{UV} = 0.45 mWcm^{-2}*in air* followed by a quick evacuation of air to a few Pa. Then the measurement was paused and film kept in vacuum with UV light off. After 50 minutes few PL measurements were taken in given conditions.

Oxygen is a well-known PL quencher [13, 14], however, we find no evidence for direct collisional quenching with oxygen. If this type of quenching was present, PL intensity would be (partially) reversible after removal of oxygen from the film. In the following experiment it was demonstrated that PL is not reversible (Fig.4.8): first a film was UV-degraded in air for about $t_{1/2}$, then the air was evacuated to the pressure of 10^{-2} Torr in a few seconds and the film kept in vacuum for 50 minutes in dark[3]. After 50 minutes few measurements of PL were taken which show that its value remained the

[3]The results are slightly different if the UV irradiation is continued in high vacuum and are given in Appendix B.

same as the one at the end of the degradation in air. Thus, PL quenching is only due to new photo-oxidized species.

At the level of 0.2% of impurities (that quench 50% of PL), the average distance between impurity molecules d_i is around 7 nm. This value is obtained taking the density of DPVBi to be 1.2 gcm^{-3} (that of monoclinic crystal with two molecules per unit cell) [18] and assuming that molecules form a simple cubic lattice. The long range Förster resonant energy transfer (FRET) from DPVBi to impurity molecule can be ruled out due to absence of a spectral overlap between DPVBi emission centered at 458 nm and the impurity absorption at 255 nm [19-22]. Thus, only reasonable assumption on the mechanism of PL quenching is that the excitons diffuse through the film at long distance and, if during their lifetime an impurity molecule is reached, quenching as the most probable outcome may happen [7, 23-27]. Exciton diffusion length l_D for amorphous DPVBi films is measured by Choukri et al. [28] to be (8.7 ± 0.6) nm and satisfies the condition $d_i<l_D$ required for quenching [28].

The Förster energy transfer among DPVBi molecules occurs with the probability higher than 50% when their separation is smaller than 1.4 nm as calculated previously. Excitations are localized and move by hopping from one DPVBi molecule to another via one of two possible processes: one is FRET and the other is Dexter electron transfer [30]. Dexter's mechanism requires a spatial overlap between wave functions of DPVBi molecules and it occurs only at short distances, typically not larger than 1 nm. The rate of Dexter transfer is typically much lower than the rate of FRET, as it applies to excitons with dipole-forbidden transitions, like in triplet-triplet energy transfers [7, 25]; in the case of DPVBi, PL is due to singlet excitons, thus, hopping would likely occur through FRET.

Oxygen diffuses into amorphous film, where it reacts with excited DPVBi molecule and forms an impurity, which acts as quenching site. Exciton diffuses by hopping form one DPVBi to another through FRET in a random walk manner. If, during its lifetime, it comes to proximity of an impurity, a Dexter-type energy transfer occurs and PL is quenched.

Conclusions drawn here for the case of the photoluminescence quenching of the DPVBi could be extended onto the case of TPD for which we found that 0.4 % of impurities causes 50 % in luminescence. Using the same approach as in the case of

DPVBi, distance between impurity molecules d_i was estimated to be 5.5 nm, using density 1.2 $gcm^{-3}$of TPD [31]. This value for d_i = 5.5 nm is close to exciton diffusion length l_D = 5 nm for TPD [32], and, thus, the condition $d_i<l_D$ required for quenching is nearly satisfied.

References for Chapter 4

[1] F.-C.Wu, H.-L.Cheng and W.-Y. Chou, *Studies of blue organic electroluminescent devices using the polymer/dopant systems as a light-emitting layer*, Organic Light Emitting Materials and Devices XI, edited by Zakya H. Kafafi, Franky So, Proc. of SPIE Vol. **6655** (2007) 66551P.

[2] H. Mattoussi, H. Murata, C.D. Merritt, Y. Iizumi, J. Kido, Z.H. Kafafi, *Photoluminescence quantum yield of pure and molecularly doped organic solid films,* J. App. Phys. **86** (1999) 2642.

[3] R. Scholz, L. Gisslén, C. Himcinschi, I. Vragović, E. M. Calzado, E. Louis, E. S. F. Maroto, and M. A. Díaz-García, *Asymmetry between Absorption and Photoluminescence Line Shapes of TPD: Spectroscopic Fingerprint of the Twisted Biphenyl Core*, J. Phys. Chem. A **113** (2009) 315–324

[4] P.E. Burrows, Z. Shen, V. Bulovic, D.M. McCarty, S.R. Forrest, J.A. Cronin, M.E. Thompson, *Relationship between electroluminescence and current transport in organic heterojunction light-emitting devices*, J. Appl. Phys. **79** (1996) 7991-8006.

[5] J.R. Lakowicz, *Principles of fluorescence spectroscopy,* third ed., Springer Science+Business Media, New York, 2006.

[6] T. Tsuboi, A.K. Bansal, A. Penzkofer, *Fluorescence and phosphorescence behavior of TPD doped and TPD neat films*, Thin Solid Films **518** (2009) 835–838

[7] K. O. Cheon and J. Shinar, Förster energy transfer in combinatorial arrays of selective doped organic light-emitting devices, Appl. Phys. Lett. **84** (2004) 1201-1203.

[8] W. Holzer, A. Penzkofer and H.-H.Horhold, *Travelling-wave lasing of TPD solutions and neat films*, Synth.Met. **113** (2000) 281.

[9] Y. Qiu, J. Qiao, *Photostability and morphological stability of hole transporting materials used in organic electroluminescence*, Thin Solid Films **372** (2000) 265.

[10] M.P. Joshi, S. Raj Mohan, T.S. Dhami, B. Jain, M.K. Singh, H. Ghosh, T. Shripathi, U.P. Deshpande, *Enhanced optoelectronic properties of UV-light-induced photodegraded TPD*, Appl. Phys. A **90** (2008) 351.

[11] S. Raj Mohan, M.P. Joshi, S.K. Tiwari, V.K. Dixit, T.S. Dhami, *Electrical and optical characterization of photooxidized TPD*, J. Mater. Chem. **17** (2007) 343.

[12] R. Siefert, S. Scholz, B. Lüssem and K. Leo, Comparison of ultraviolet- and charge-induced degradation phenomena in blue fluorescent organic light emitting diodes, Appl. Phys. Lett. **97** (2010) 013308.

[13] L. Lüer, H.-J.Egelhaaf, D. Oelkrug, G. Cerullo, G. Lanzani, B.-H. Huisman and D. de Leeuw, *Oxygen-induced quenching of photoexcited states in polythiophene films*, Org. Electron. **5** (2004) 83-89.

[14] H. Hintz, H.-J. Egelhaaf, L. Lüer, J. Hauch, H. Peisert and T. Chassé, *Photodegradation of P3HT – a systematic study of environmental factors*, Chem. Mater. **23** (2011) 145-154.

[15] A. Maliakal, K. Raghavachari, H. Katz, E. Chandross and T. Siegrist, P*hotochemical stability of pentacene and a substituted pentacene in solution and in thin films*, Chem. Mater. **16** (2004) 4980-4986.

[16]G. J. Kavarnos, *Fundamentals of Photoinduced Electron Transfer*, VCH Publishers, New York (1993).

[17] G. Schwartz, *Novel concepts for high-efficiency white organic light-emitting diodes*, PhD thesis, Dresden (2007).

[18] H.-N. Liu, G. Zhang, L. Hu, P.-F.Su, Y.-F. Li, *4,4′-Bis(2,2-diphenylvinyl)-1,1′-biphenyl*, Acta Cryst. E**67** (2011) o220.

[19] M. Pope, C.E. Swenberg, *Electronic processes in organic crystals and polymers*, second ed., Oxford University Press, New York, 1999.

[20] Th. Förster, 10th Spiers memorial lecture. *Transfer mechanisms of electronic excitation*, Discuss. Faraday Soc. **27** (1959) 7-17.

[21] T. Virgili, D.G. Lidzey, D. D. C. Bradley, *Efficient energy transfer from blue to red in tetraphenylporphyrin-doped poly(9,9-dioctylfluorene) light-emitting diodes*, Adv. Mater. **12** (2000) 58-62.

[22] E. Suljovrujic, A. Ignjatovic, V.I. Srdanov, T. Mitsumori, F. Wudl, *Intermolecular energy transfer involving an iridium complex studied by a combinatorial method*, J. Chem. Phys. **121** (2004) 3745-3750.

[23] W. Klöpffer, Transfer of Electronic Excitation Energy in Polyvinyl Carbazole, J. Chem. Phys. **50** (1969) 2337-2343.

[24] D.C. Northrop, O. Simpson, *Electronic Properties of Aromatic Hydrocarbons. II Fluorescence Transfer in Solid Solutions*, Proc. R. Soc. Lond. A 234 (1956) 136-149.

[25]C. Madigan, V. Bulović, *Modeling of exciton diffusion in amorphous organic thin films*, Phys. Rev. Lett. **96** (2006) 046404.

[26] T.-S. Ahn, N. Wright, C.J. Bardeen, *The effects of orientational and energetic disorder on Forster energy migration along a one-dimensional lattice*, Chem. Phys. Lett.**446** (2007) 43-48.

[27] S.M. Menke, R.J. Holmes, *Exciton diffusion in organic photovoltaic cells*, Energy Environ. Sci. **7** (2014) 499-512.

[28] H. Choukri, A. Fischer, S. Forget, S. Chénais, M.-C. Castex, D. Adès, A. Siove, B. Geffroy, *White organic light-emitting diodes with fine chromaticity tuning via ultrathin layer position shifting*, Appl. Phys. Lett. **89** (2006) 183513.

[29] O.V. Mikhnenko, M. Kuik, J. Lin, N. van der Kaap, T.-Q. Nguyen, P.W.M. Blom, *Trap-limited exciton diffusion in organic semiconductors*, Adv. Mater. **26** (2014) 1912–1917.

[30] D.L. Dexter, *A theory of sensitized luminescence in solids*, J. Chem. Phys. **21** (1953) 836-850.

[31] Z. Zhang,E. Burkholderb and J. Zubieta, *Non-merohedrally twinned crystals of N,N′-bis(3-methylphenyl)-N,N′-bis(phenyl)benzidine: an excellent triphenylamine-based hole transporter*, Acta Cryst. **C60** (2004) o452-o454.

[32] Z. H. Kafafi, H. Murata, L. C. Picciolo, H. Mattoussi, C. D. Merritt, Y. Iizumi and J. Kido, *Electroluminescent properties of functional π-electron molecular systems*, Pure Appl. Chem.**71** (1999) 2085-2094.

5. Nano and micro rods obtained by annealing of thin pentacene films in air

Unlike previous chapters that have covered degradation of thin TPD and DPVBi films and their optical properties, this chapter will cover somewhat different topic: production of nano and micro rods by annealing of thin pentacene films in air. Thus pentacene films represent a stepping stone for obtaining micro rods. Pentacene is a hole-type semiconductor well known for its high charge-carrier mobility, which is on the order of 1cm^2/Vs at room temperature. Mobility as high as 35cm^2/Vs has been obtained for ultra-pure pentacene single crystal [1]. Because of this pentacene is primarily used in production of thin film transistors [2].

It will be shown that annealing of thin pentacene films in air and dark results in formation of two types of crystal structures at the surface of pentacene films: crystallites and micro/nano rods. Characterization of crystallites and micro rods has revealed that they are composed of oxidized pentacene species: 6,13-pentacenequinone (PQ) and 5,7,12,14-pentacenetetrone (PT). While there are several studies which cover topics of degradation and annealing of pentacene films [3-5], formation of crystals was not previously reported to the best of our knowledge. Crystals of micro and nano dimensions obtained in this way may be easily integrated in devices. Lately several papers have shown that PQ has a great potential, as PQ-TiO_2 coupled semiconductor nanosystem proved to be efficient photo-catalyst active in visible light region for the production of hydrogen [6].

First results regarding UV-VIS, Raman, mass spectroscopy and AFM characterization of thin pentacene films deposited by combinatorial PVD by will be presented. Our thin pentacene films are polycrystalline. After that details of annealing of pentacene films will be discussed. Then we will proceed with characterization of annealing products. Mechanism of crystal growth will be proposed at the end.

5.1 Characterization of pentacene thin films

Under conditions we used for deposition of pentacene polycrystalline films were obtained, as witnessed by several different methods. Absorbance of thin pentacene film (Fig. 5.1) shows the presence of two peaks at 630 nm and 667 nm which is a hallmark

of orientation in thin films [7]. These peaks arise from Davydov splitting of 0-0 band and are not present in amorphous films [7].Results of absorbance measurement for different film thicknesses have shown presence of orientation throughout whole film**.** To determine the thickness at a particular point of the film, the extinction coefficient μ=4.3610^{6}m^{-1} for absorbance peak at 590 nm based on the data in reference was used [8].Band gap $E_g^{pentacene}$ = 1.8±0.1 eV was estimated from the long-wavelength absorption edge [9].

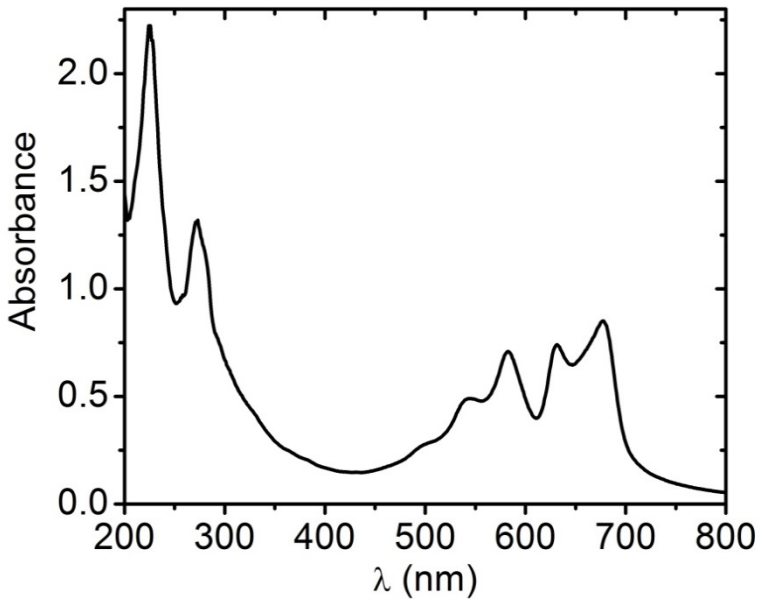

Fig. 5.1 Absorbance of 400nm thick pentacene film deposited on fused silica substrate.

These results, combined with AFM imaging (Fig 5.2) of pentacene thin film samples showing grain structure, imply that they are polycrystalline.

Unlike TPD and DPVBi, when deposited on suitable substrate, pentacene molecules arrange in the layers with a haring-bone motif, leading eventually to a polycrystalline thin film whose crystal structure can depend on the type of the substrate, substrate temperature, evaporation rate and film thickness. Four different triclinic [10, 11] crystal phases and one orthorhombic [11, 12] have been observed in pentacene films. They are commonly identified by d-spacing of the (001) plane: 14.1Å, 14.4 Å, 15.0 Å, 15.4 Å and 15.7 Å [10-12]. More than one phase can coexist in vacuum evaporated thin films [10, 12,13]. For example, phases 14.4 Å (the bulk phase), 15.4 Å (thin-film phase) and 15.7 Å (orthorhombic phase) were obtained in thin films grown on SiO_2 [10, 11], while

phases 15.0 Å and 14.1 Å were observed on kapton [10]. It is certain that fraction of the bulk phase increases with film thickness, however the question of whether the bulk phase is formed from the first layer [14] or after some critical thickness [10, 11] is still unresolved.

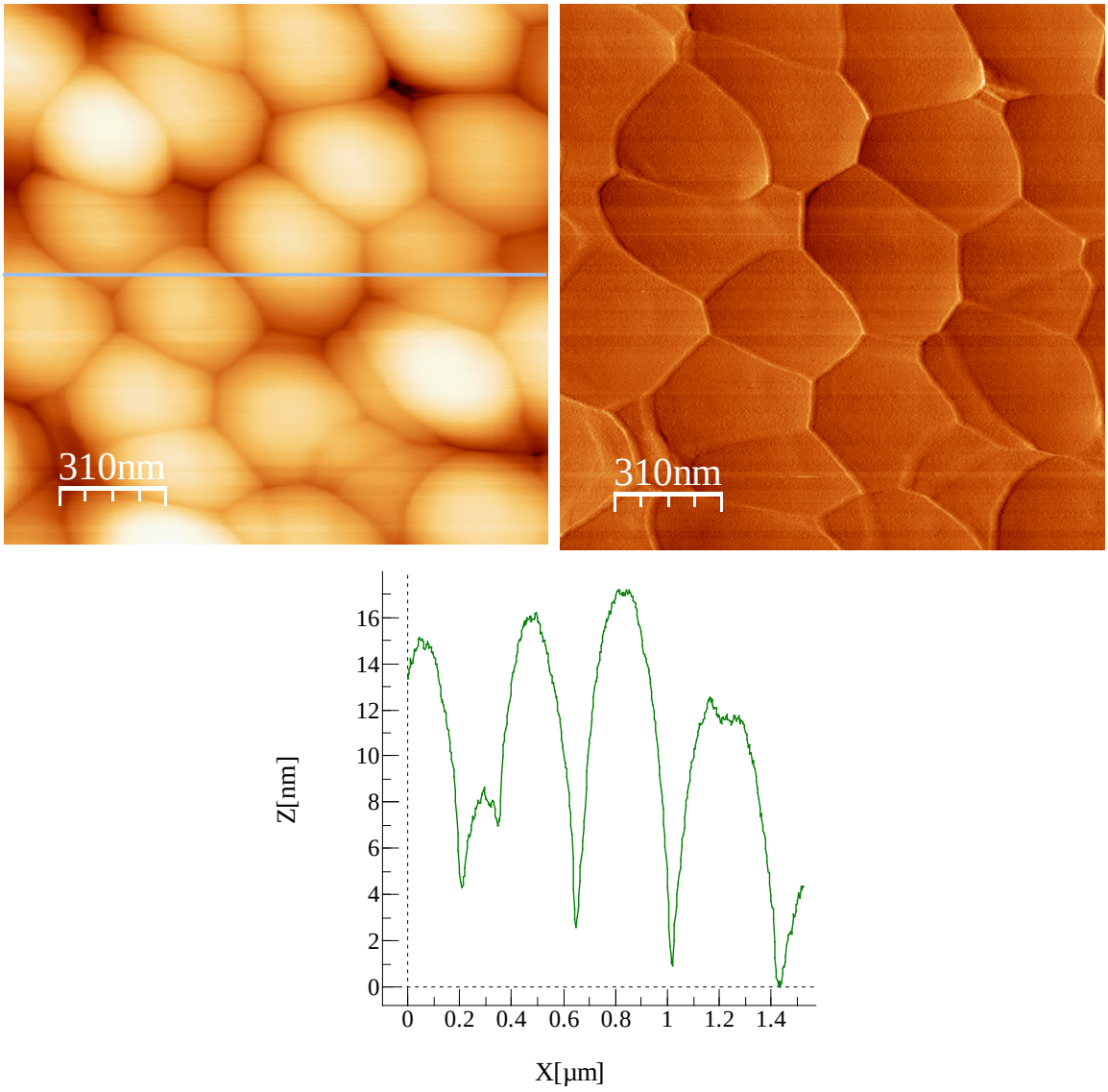

Fig. 5.2 Topographic AFM image of 1.5 µm x 1.5 µm area of a pentacene thin film on glass substrate showing grain structure (top left). Phase image of the same area (top right): boundaries between grains are more visible due to the higher contrast. Thickness profile along the blue line indicated in the first image (bottom), showing grain height and size.

XRD measurements (Fig. 5.3), performed on our 300 nm pristine pentacene film deposited on Si substrate, confirmed its polycrystalline nature. The results showed presence of two phases with d-spacing of 15.48Å and 14.69Å, in agreement with results of References 10, 12 and 13.

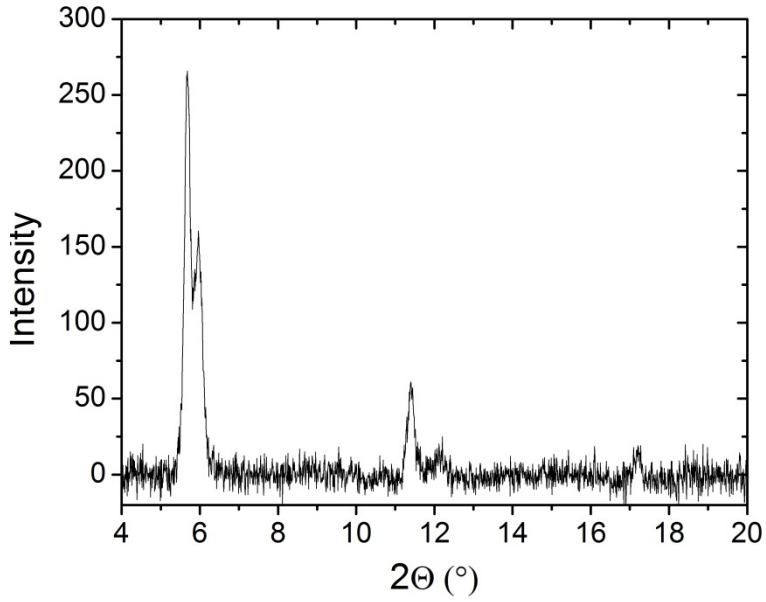

Fig. 5.3 XRD of pristine 300 nm pentacene film deposited on Si substrate having a thin layer of native SiO_2.

The fact that more than one polymorph can be present in pentacene films is witnessed also by Raman spectroscopy [11, 15]. It has been shown that Raman spectrum of pentacene thin films has thickness dependence due to this presence [11, 15]. We have also studied thickness dependence of Raman spectrum of pentacene films. Compared to DPVBi and TPD it was much easier to obtain spectra because of resonance effect: pentacene has a band gap around 1.8 eV and the energy of He-Ne laser is roughly 2 eV, which is enough to cause electronic transitions, thus enabling resonant Raman effect [16, 17]. Owing to it, it was possible to record Raman spectrum even from 10 nm thin pentacene film on glass substrate in the matter of seconds (Fig. 5.4a).

Thin pentacene film was placed on a movable substrate holder and Raman spectra were recorded along the profile of thickness. Thickness dependence can be observed, as previously reported [11, 15], in two regions around 1170 $cm^{-1}$and 1596 cm^{-1} (Fig. 5.4b, c). Peaks around 1170 cm^{-1} are assigned to C-H bending modes while the peak at 1596

cm^{-1} is related to C-C stretching mode [11].When thickness of the film increases, intensity of the peak at 1175 cm^{-1}decreases and at the same time intensity of the peak at 1596 cm^{-1}increases, which is in agreement with previous studies [11]. The mode at 1596 cm^{-1} is especially interesting because it is sensitive to the molecular orientation so it can be used for assessing the presence of different crystalline phases in thin films [11]. Performed measurement shows strength of the combinatorial method as various thicknesses could be obtained from a single evaporation.

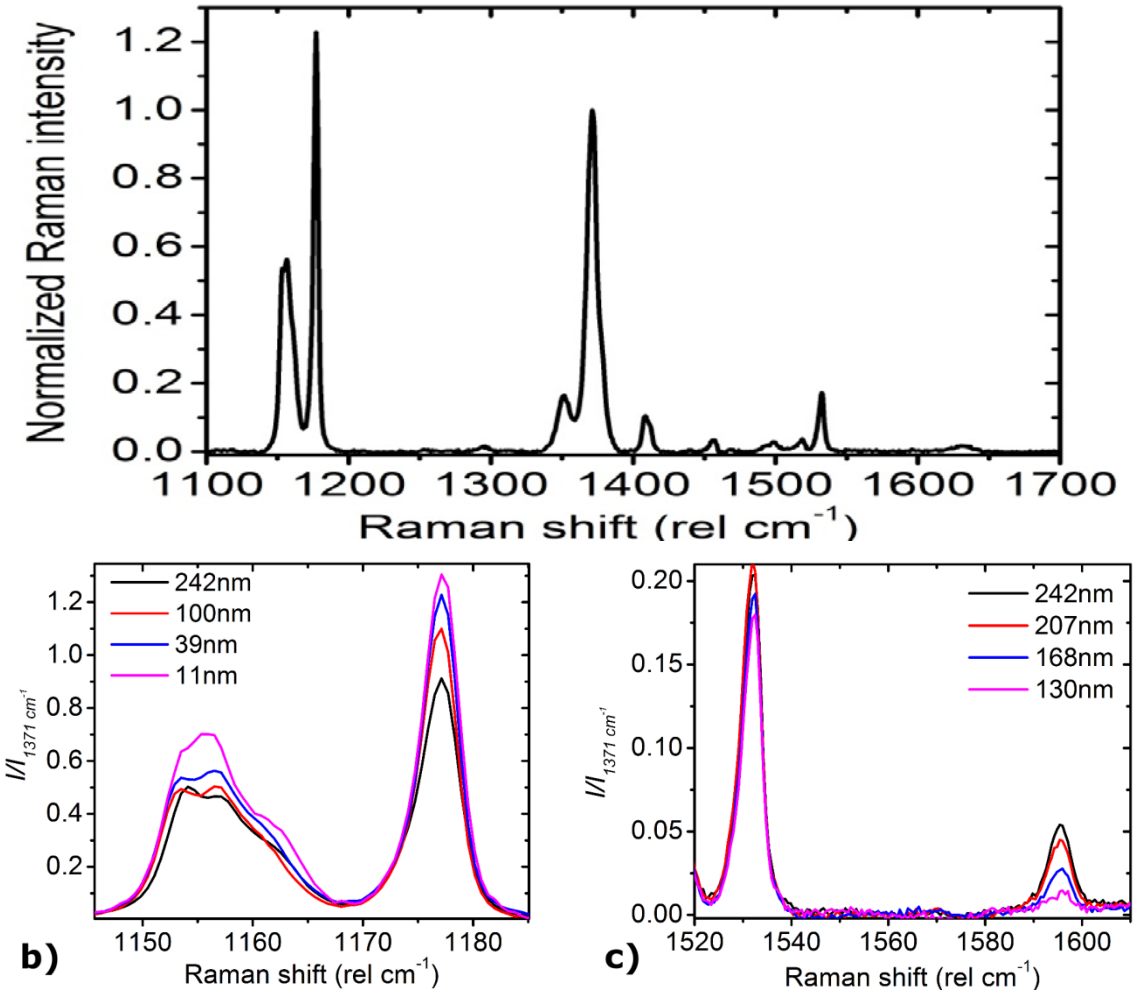

Fig. 5.4 Raman spectrum of thin pentacene film (top).Thickness dependence of Raman peaks around 1170rel cm^{-1} (bottom left) and the peak at 1596 rel cm^{-1} (bottom right) normalized to the value at 1371 rel cm^{-1}.

Thin films of pentacene obtained by combinatorial PVD were characterized by UV-VIS, XRD and Raman spectroscopy. Obtained results are in good agreement with those

found in literature. They show that more than one crystalline phase is present in our pristine polycrystalline pentacene films. Annealing in air of these films leads to formation of crystal structures on their surface, as will be described in following section.

5.2 Annealing of pentacene thin films and crystal growth

In this section we will describe procedure to grow crystallites of oxidized pentacene on the surface of thin pentacene films and their characterization. First a thin pentacene film is deposited onto the glass substrate as previously described. Then the film is enclosed in a glass container and placed in a tube furnace where it is annealed in dark and air at 130 °C for a period of 48 h. Inspection of annealed films by the optical microscopy showed presence of two types of structures (Fig 5.5a): smaller objects – crystallites (CSs) whose size is estimated to be around 5 μm x5 μm x 5 μm and rod shaped objects– micro rods (MRs), which are approximately 50 μm long and 2 μm wide. It was determined by changing focus of optical microscope that majority of MRs is freestanding and attached at their base to the crystallites. It was not uncommon to observe several MRs attached to the same crystallite. Furthermore when imaged under optical microscope using an auxiliary light source (405 nm UV LED) a yellow luminescence, uncommon for pentacene, was also observed (Fig. 5.5b). This was the first indication that MRs and CSs are not composed of pentacene.

In order to determine threshold temperature for MRs formation the duration of annealing was fixed at 20h. Annealing was then performed at T= 90, 100, 110, 120 °C. Films were then inspected with optical microscope. While crystallites were formed for all the used temperatures, MRs appeared only for temperatures ≥ 120 °C.

Duration of the annealing procedure was also varied. We have observed that the number and length of MRs depends on the annealing time. However period of two days gave the best results and if the annealing was prolonged beyond that, density and length could not be significantly improved. Instead discoloration of underlying pentacene film had changed from light blue to orange. Rods were predominantly found on the film surface, small amounts on the substrate (in the vicinity of the border between substrate and film) and on the walls of the glass container.

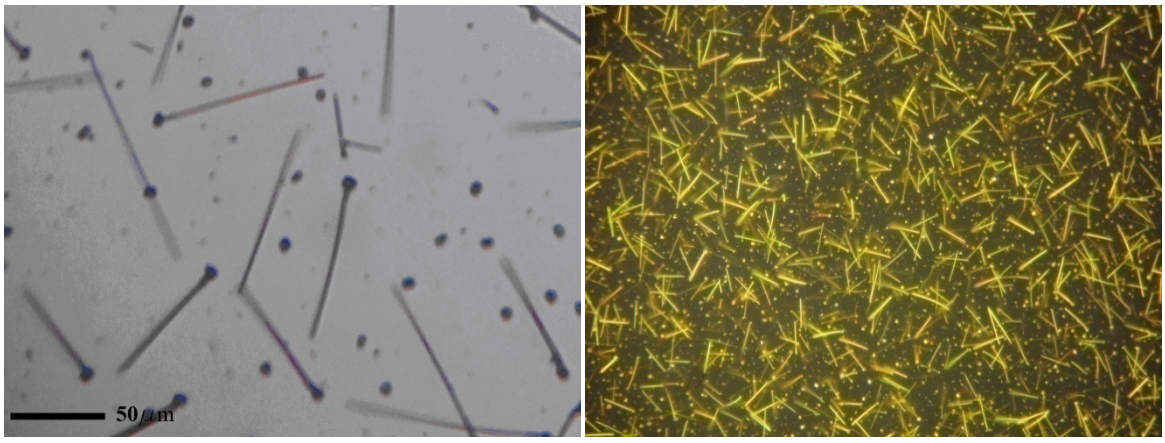

Fig. 5.5 Optical micrographs of grown crystals on pentacene films: transmission mode using a standard light source (left) and illumination with auxiliary light source 405 nm UV LED (right), where yellow luminescence emitted from crystals can be observed.

For thin pentacene films annealed in low vacuum conditions (10^{-2} Torr) growth of crystal structures was not observed. Two controls samples were also made and they did not receive annealing treatment. Instead they were kept in glass Petri dishes in atmospheric conditions at room temperature; one was kept in dark while the other was exposed to daylight. After one month CSs could be observed on surface of both films. This is important as it shows that pentacene films degrade even without presence of light. Annealing of thin pentacene films in air or oxygen atmosphere promotes formation of these CSs and growth of MRs. Our results imply that pentacene will react with oxygen even in dark. However it seems that reaction rate is small, as formation of CSs was observed after one month.

Measurement of absorbance along thickness profile before and after annealing of a film revealed a substantial decrease in its value throughout the film (Fig. 5.6). This result does not directly indicate loss of film material (sublimation) and should be taken with caution. As it will be shown later by mass and IR spectroscopy both crystallites and MRs are made of oxidized pentacene species which do not absorb light in the visible region[4]. Thus it should be understood that change in absorbance is a reflection of a change in composition.

[4] There is also a possibility that part of the incoming light was scattered by crystals, which would increase the apparent film thickness.

Optical micrographs taken along the profile of thickness showed that number density of the micro rods and small crystals is not uniform. Results (inset of Fig. 5.6) suggest that there is a connection between film thickness and density of MRs and CSs. That is, more CSs and MRs can be found with growing thickness of the film.

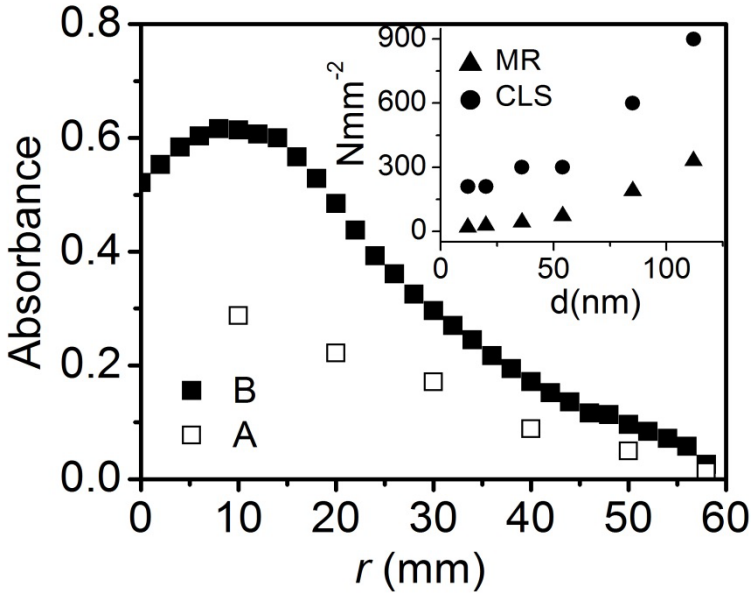

Fig. 5.6 Absorbance along pentacene film before (black squares) and after annealing (empty squares). Inset shows correlation between number of MRs and CSs per mm^2 vs. film thickness.

5.3 Characterization of MRs and CSs

For characterization and possible use of MRs and CSs it was needed to remove them from the surface of a pentacene film. Several methods were tried out and are listed as follows:

M1. Dipping a film in ultra-pure water removed MRs and CSs but also led to separation of the thin film from the substrate. This lead to a dispersion of MRs, CSs together with parts of pentacene film in water, which was unwanted.

M2. Micropipette was used to put a 10 µl drop of ultrapure water on to the annealed film and to collect it. This method proved to be successful in removing MRs but very small amount could be gathered.

M3. Dipping in ethanol did not remove the underlying pentacene film, but both MR and CSs were dissolved.

M4. Highest yield of MRs and CSs was obtained by placing a clean glass substrate over the annealed film. In this way MRs and CSs were successfully transferred to the clean substrate, from which they could then be scrapped for further use.

AFM images of MRs on annealed sample were taken in tapping mode, on an area of 12μm x 12 μm and maximum height of 2 μm. Imaging of MRs posed a problem due to few circumstances. First, the low number density of rods (300 MRs per mm^2) meant that they were hard to find in our setup[5]. Secondly freestanding rods could break the cantilever. Thirdly it was hard to find MRs that are not freestanding but rather lying on the film and even then their diameter could be larger than maximum *Z* range of AFM scanner. We successfully imaged only two MRs: their diameters were 500 nm and 1500 nm while their width was around 2000 nm (Fig. 5.7a and b). Both MRs had similar cross section, shown in the inset of Fig. 5.7c and d. It can be seen on both images that MRs have flat surfaces, again indicating their crystalline nature.

Film that was annealed for 48 h at 130 °C was imaged under scanning electron microscope in order to give better insight in shape of MRs and CSs. Sample was imaged as is, but due to the poor conductivity charge built-up at the sample surface caused braking of the MRs. Thin layer of gold (100 nm) was then evaporated over the sample to enable imaging. SEM imaging provided first clear evidences for crystal nature of grown structures. Both crystallites and MRs possess well defined facets and could be considered as single crystals (Fig. 5.7c and d). Energy-dispersive X-ray spectroscopy (EDX) analysis[6] that was performed on structures shown in Fig. 5.7c and d revealed higher oxygen content, when compared to the analysis performed on the surrounding pentacene film. This indicates presence of oxidized species in both CSs and MRs.

[5]AFM setup did not have a stage with optical microscope.

[6]Energy-dispersive X-ray analyzer is an optional part integrated with SEM.

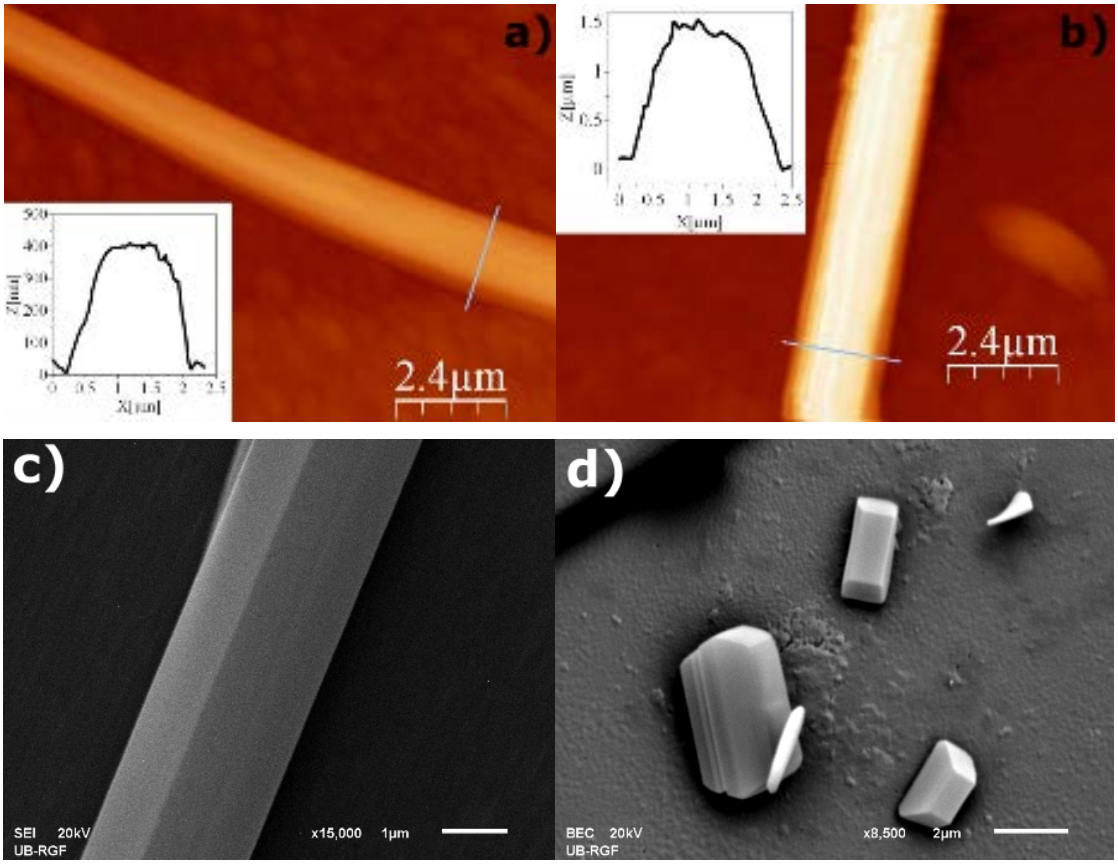

Fig. 5.7 a, b) AFM images of two MRs with lateral profiles shown in insets. SEM images of c) MRs and d) CSs.

Solubility of crystals in ethanol together with yellow luminescence and EDX analysis implied that they are not composed of pentacene. Pentacene is insoluble or has a very low solubility in most of the organic solvents and does not have yellow luminescence. In order to resolve the matter of composition ASAP mass spectroscopy was performed. For that purpose MRs and CSs were collected from annealed film by method M4 defined earlier. One spectrum was obtained from collected MRs scraped by ASAP capillary and the other from the solution of collected MRs in acetonitrile by dipping the capillary (Fig.5.8).

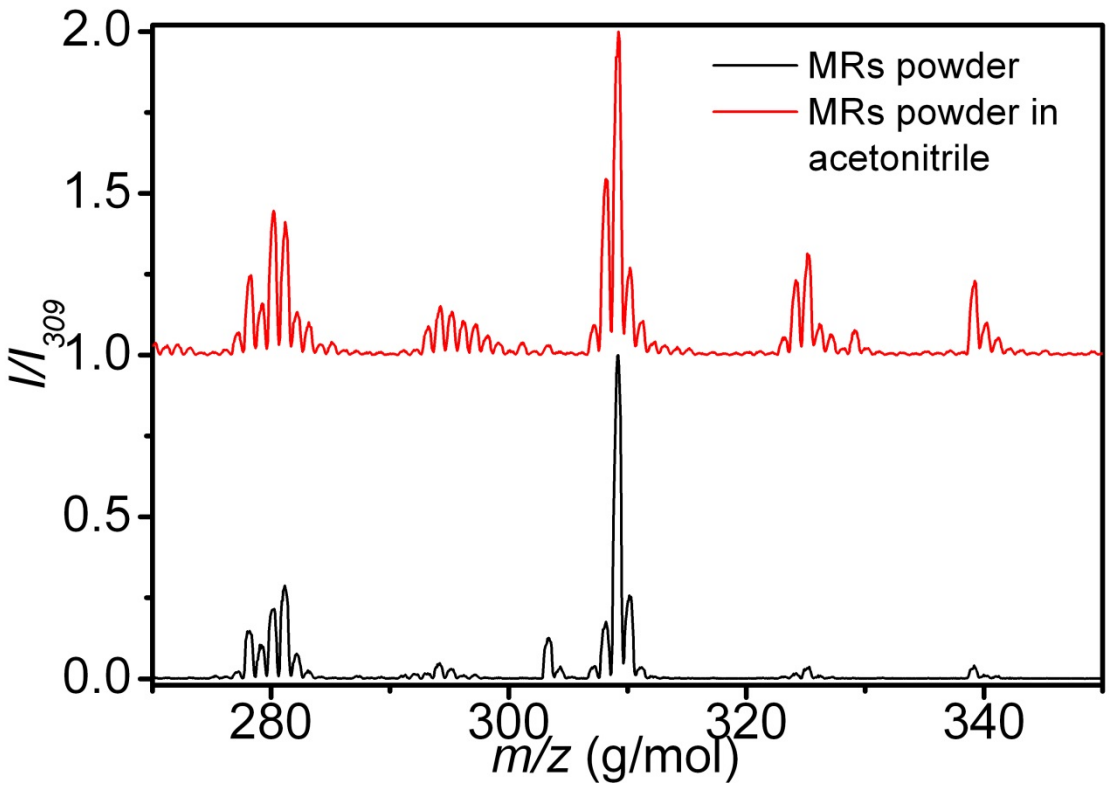

Fig. 5.8 ASAP mass spectra of MRs collected from a pentacene film (bottom curve) and MRs dissolved in acetonitrile (top curve). Spectra are normalized to the mass of 309 $gmol^{-1}$ and are offset by 1 for clarity.

In both spectra the most dominant mass is 308.3 $gmol^{-1}$ which can be attributed to 6,13-pentacenequinone. We believe that masses below 308.3 $gmol^{-1}$ belong to fragmented PQ molecule. Above that mass, two masses at 324 and 338 $gmol^{-1}$ were observed. They can be explained by addition of one and two oxygen atoms to PQ. The mass of 338 $gmol^{-1}$ corresponds to the mass of 5,7,12,14-pentacenetetrone. The mass of 324 $gmol^{-1}$ can possibly be explained by addition of -OH group to PQ molecule. At this moment the exact composition of MRs cannot be deduced and further measurements are necessary.

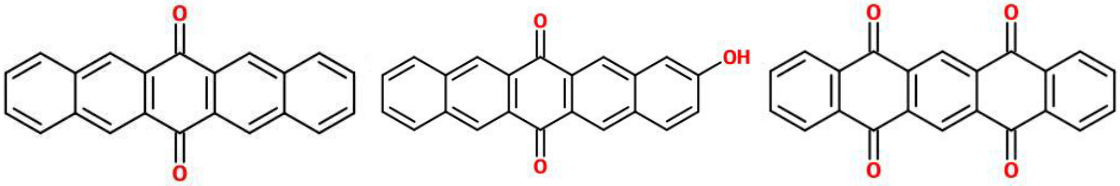

6,13-pentacenequinone PQ-OH 5,7,12,14-pentacenetetrone

Cyclotron IR spectroscopy was performed on a single MR and results are shown in Fig. 5.9. In the recorded spectra there are several features: peaks at 3000, 1680, 1590 and 1250 cm^{-1} belong to C-H,C=O,C=C and C-C bonds, respectively and the broad feature around 3300 cm^{-1}possibly belongs to -OH bond[7]. The signature of C=O bond together with results of mass spectroscopy are supporting the idea that MRs are composed of PQ and/or PT and not of pentacene. The question of composition of MRs and CSs remains, are crystals exclusively composed of PQ or PT or possibly a cocrystals [18] exist? It is interesting to note that micro rods resemble PQ that can be obtained commercially as it comes in the form of a powder that consist of large number of large rod like crystals.

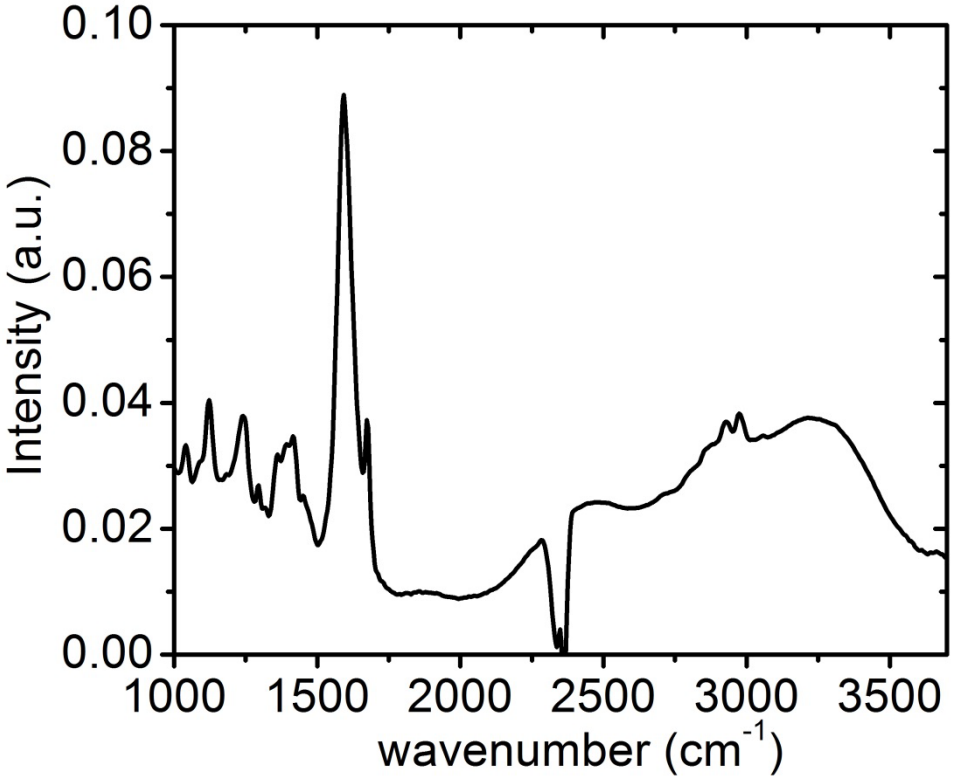

Fig. 5.9 Cyclotron IR spectrum of a single MR.

[7] Peak belonging to -OH bond is interesting and it is probably due to the presence of residual moisture as the rods were collected from a film via water droplet (method M2). Results of mass spectroscopy of both rods and crystals did not show presence of the masses that would indicate presence of -OH bonds.

XRD measurements were performed on annealed (thin film containing CSs and MRs) and reference samples (300 nm pristine thin film) in order to determine crystal structure of MRs. Information regarding the crystal structure of MRs was not obtained, probably due to low MRs to film ratio. However XRD measurements provided information about structure of annealed pentacene films. As mentioned in the previous section reference sample has shown presence of two phases, namely15.48Å and 14.69Å phase. Annealed samples showed only the presence of 14.41Å bulk phase (Fig. 5.10). Mattheus *et al*. [10] showed that annealing of thin films led to irreversible change of thin film phase to more stable bulk phase. Our results are in agreement with this observation. Origin of 14.4Å peak in our annealed samples is a result of the transformation of the thin film phase.

Characterization of MRs and CSs with AFM and SEM has shown that they have crystal nature due to well defined facets. EDX analysis together with IR and mass spectroscopy has given evidence that both structures are composed of oxidized pentacene species, namely PQ and PT and not of pentacene. However the exact composition could not be resolved. In the following subsection explanation of the crystal growth will be proposed.

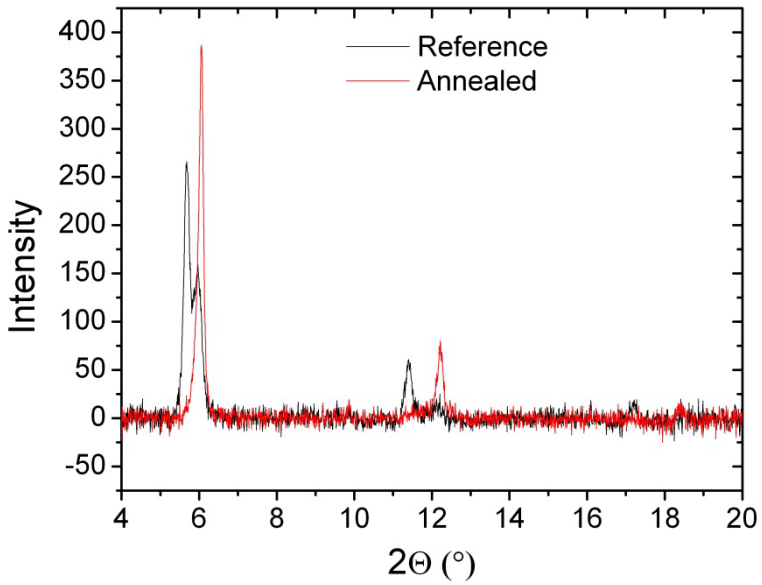

Fig. 5.10 XRD of annealed and pristine (reference) pentacene film.

5.4 Explanation of crystal growth

From the obtained results it is possible to give a reasonable explanation for the growth of crystals. We believe that formation of rods can be divided in two steps. First CSs are formed, they then serve as crystallization sites on which MRs grow. Material for formation of both CSs and MRs is provided by sublimation of material from thin film. It is not clear whether oxidation happens before or after sublimation. Sublimated molecules have a short mean free path under atmospheric conditions and the lack of temperature gradient in tube furnace means that there is no convection either, thus they return to surface of the thin film, where CSs and subsequently MRs are formed as stable structures.

There are few facts that support this claim: number density of rods is not uniform, it is thickness dependent which implies that rod formation is localized (as mentioned before there are no rods on the substrate expect near the film/substrate border). We also performed experiment in which thin film was annealed under low vacuum condition 10^{-2}Torr. As a result no MRs or CSs were formed on the surface because there was no oxygen available for oxidation process to happen and mean free path of sublimated molecules is much larger.

Characterization of thin pentacene films by UV-VIS and Raman spectroscopy, AFM and XRD has shown their polycrystalline nature. Films contain two crystalline phases as witnessed by XRD. Thickness induced effects in Raman spectra were observed, in good agreement with results found in literature [11, 15].

Annealing of these films in air leads to formation of micro and nano rods. Characterization of MRs and CSs with AFM and SEM has shown that they have crystalline nature due to well defined facets. EDX analysis together with IR and mass spectroscopy has given evidence that both structures are composed of oxidized pentacene species. However the exact composition could not be resolved. Further investigation will be needed to resolve the matter of composition.

References for Chapter 5

[1] O.D. Jurchescu, J. Baas and T. T. M. Palstra, *Effect of impurities on the mobility of single crystal pentacene*, Appl. Phys. Lett. **84** (2004) 3061.

[2] D.J. Gundlach, Y.Y. Lin, T.N. Jackson, S.F. Nelson, D.G. Schlom, *Pentacene organic thin-film transistors-molecular ordering and mobility*, Electron Device Letters, IEEE **18**(1997) 87-89.

[3] A. Vollmer, O.D. Jurchescu, I. Arfaoui, I. Salzmann, T.T.M. Palstra, P. Rudolf, J. Niemax, J. Pflaum, J.P. Rabe, and N. Koch, *The effect of oxygen exposure on pentacene electronic structure*, Eur. Phys. J. E **17**339 (2005).

[4] H. Yang,, L. Yang, M.-M. Ling, S. Lastella, D. D. Gandhi, G. Ramanath, Z. Bao, and C.Y. Ryu, *Aging Susceptibility of Terrace-Like Pentacene Films*, J. Phys. Chem. C**112**(2008) 16161-196165.

[5] H.-Y.Tsao and Y.-J. Lin, *Electronic properties of annealed pentacene films in air at various temperatures up to 400 K*, Appl. Phys. Lett. **101** (2012) 113306.

[6] V. Pandit, S. Arbuj,R. Hawaldar, P. Kshirsagar,U. Mulik, S. Gosavi, C.-J. Park and B. Kale, I*n situ preparation of a novel organo-inorganic 6,13-pentacenequinone–TiO2 coupled semiconductor nanosystem: a new visible light active photocatalyst for hydrogen generation*, J. Mater. Chem. A **3**(2015) 4338-4344

[7] Y. Kamura, I. Shirotani and H. Inokuchi, *Absorption Spectra of Oriented and Amorphous Naphthacene and Pentacene films*, Chemistry Letters, 627 (1974).

[8] L. C. Palilis, P. A. Lane, G. P. Kushto, B. Purushothaman, J. E. Anthony, Z. H. Kafafi, *Organic photovoltaic cells with high open circuit voltages based on pentacene derivatives*, Organic Electronics **9** (2008) 747–752.

[9] P.E. Burrows, Z. Shen, V. Bulovic, D.M. McCarty, S.R. Forrest, J.A. Cronin, M.E. Thompson, *Relationship between electroluminescence and current transport in organic heterojunction light-emitting devices*, J. Appl. Phys. **79** (1996) 7991-8006.

[10] C.C. Mattheus, A. B. Dros, J. Baas, G. T. Oostergetel, A. Meetsma, J. L. de Boer, T.T.M. Palstra, *Identification of polymorphs of pentacene*, Synthetic Metals **138** (2003) 475.

[11] H.-L.Cheng, Y.-S.Mai, W.-Y.Chou, L.-R.Chang and X.-W. Liang, *Thickness-Dependent Structural Evolutions and Growth Models in Relation to Carrier Transport Properties in Polycrystalline Pentacene Thin Films*, Adv. Funct. Mater. **17** (2007) 3639.

[12] L.F. Drummy and D.C. Martin, *Thickness-Driven Orthorhombic to Triclinic Phase Transformation in Pentacene Thin Films*, Adv. Mater. **17** (2005) 903.

[13] J.-W. Chang, H. Kim, J.-K.Kim, B. K. Ju, J. Jang and Y.-H.Lee, *Structure and Morphology of Vacuum-Evaporated Pentacene as a Function of the Substrate Temperature*, Journal of the Korean Physical Society **42** (2003) 647.

[14] A. C. Mayer, A. Kazimirov and G. G. Malliaras, *Dynamics of Bimodal Growth in Pentacene Thin Films*, Phys. Rev. Lett.**97** (2006)105503.

[15] Y. Furukawaa, K. Seto, K. Nakajima, Y. Itoh, J. Eguchi, T. Sugiyama, H. Fujimura, *Infrared and Raman spectroscopy of organic thin films used for electronic devices* ,Vibrational Spectroscopy, **60**,5 (2012).

[16] John R. Ferraro, Kazuo Nakamoto and Chris W. Brown, *Introductory Raman Spectroscopy*, Elsevier, (2003)..

[17] R. He, I. Dujovne, L. Chen, Q. Miao, C. F. Hirjibehedin, A. Pinczuk and C. Nuckolls, *Resonant Raman scattering in nanoscale pentacene films*, Appl. Phys. Lett. **84** (2004)987

[18] C. C. Mattheus, J. Baas, A. Meetsma, J. L. de Boer, C. Kloc, T. Siegristb and T. T. M. Palstraa, *A 2:1 cocrystal of 6,13-dihydropentacene and pentacene*, Acta Cryst. **E58** (2002) o1229-o1231

6. Conclusions

This thesis has two distinct parts, one concerning degradation under the influence of UV light of amorphous thin films of TPD and DPVBi, which are used in production of OLEDs. The other part covers annealing of polycrystalline pentacene films which are used, owing to their properties, in the production of TFTs. While they may seem unrelated, they have something in common, and that is oxidation. It will be shown that oxidation of less than a percent of TPD and DPVBi in the thin film has a dramatic influence on the optical properties, and that oxidation of pentacene leads to formation of crystal structures of oxidized molecules.

Influence of UV irradiation on morphological and optical properties of thin TPD and DPVBi films was studied. For that purpose thin films of both materials obtained by PVD were exposed to UV light in ambient, vacuum and under different oxygen pressures. Films of both DPVBi and TPD are degraded by UV light just in the case when oxygen is present. The degradation is a consequence of reaction between UV-excited molecules and oxygen. DPVBi films have much higher reaction rates and were studied more thoroughly. In the case of DPVBi it was demonstrated that thin films can be safely taken out from vacuum as long there is no UV light present and be returned to vacuum for eventual further processing with no change in composition. Further it was shown for DPVBi that reaction rates increase when oxygen concentration and UV light intensity are increased.

Mass spectroscopy of irradiated thin films of TPD and DPVBi showed the presence of new species that are result of photo-oxidation of original compounds. For TPD new species containing only one oxygen atom were detected. In the case of irradiated DPVBi films numerous new species with up to four oxygen atoms were found. Presence of oxygen was supported by the results of NMR and IR spectroscopy for TPD and DPVBi respectively.

Time needed for absorbance of DPVBi films to drop to half of its value is two orders of magnitude larger than equivalent time for PL. For the most intense UV irradiation that was used, this time for PL is about 5 s and during that time absorbance drops only for a few tenths of percent. There is a non-trivial quenching mechanism of PL: it is a consequence of exciton diffusion form excited DPVBi to impurity molecule,

where it is assumed that excitons move via Förster resonant energy transfer by hopping. Thus, only a small fraction of percent of photo-oxidized species is sufficient to quench the luminescence in amorphous DPVBi films.

While this type of study was not performed for TPD films it would be reasonable to assume that quenching of PL in TPD films could be explained by mechanism that was found for thin DPVBi films.

Influence of UV irradiation in the presence of air on formation of morphologies was tested, for TPD it proved to be beneficial (as previously reported), while in the case of DPVBi crystallization was stopped only temporarily. Having in mind that both materials are used as emissive layer in OLEDs and effect that UV irradiation had on PL such treatment would not be recommended.

Findings of DPVBi study are important because they show that even a small amount of oxygen that penetrates a DPVBi layer would impair luminescence efficiency of a device. Moreover, the absorption of own radiation (for DPVBi and TPD both) would additionally contribute to the rate of degradation of a device. It is reasonable to expect that transport properties would also be affected when materials are used as a hole-transporting layer in OLEDs.

Polycrystalline thin pentacen films were obtained by combinatorial PVD. Micro rods (MRs) and crystallites (CSs) form on the surface of pentacene annealed in air and dark. Both MRs and CSs have well defined facets, as witnessed by AFM and SEM, implying that they have single-crystalline structure. EDX analysis revealed presence of oxygen in MRs and CSs. Mass and IR spectroscopy of MRs and CSs showed that they are composed of oxidized pentacene molecules. Further experiments are needed in order to resolve the exact chemical composition and the structure of micro rods. If it turns out that the MRs are composed solely of 6,13-pentacenequinone, they could be easily integrated in devices (due to their shape and size).

Appendix A: Assignation of NMR peaks

Measured and calculated spectra of TPD are shown in Fig. A1. The line width of calculated spectrum is adjusted in such way to match the experimental one as much as possible. There are some discrepancies between calculated spectra and measured spectra regarding the number of peaks and chemical shifts. Complete assignation of all of the observed resonances of a pristine TPD film was done with the aid of calculated proton NMR spectra of TPD molecule [1] and calculations done by hand using the known chemical shifts of various molecular fragments/groups [2] and experimental results [3].

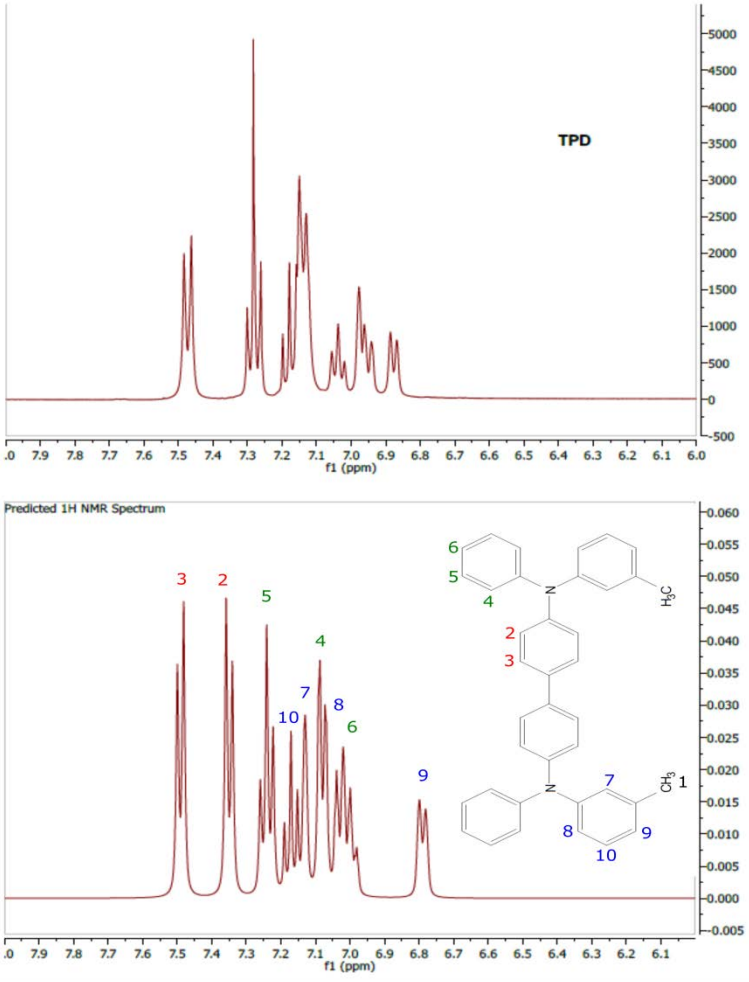

Fig.A.1 Measured (E) ^{1}H NMR spectrum of TPD powder (top) and calculated (T) ^{1}H NMR spectra of TPD (bottom).

In order to solve the problem of assignation a good point to start is calculated spectra of triphenylamine (TPA) shown in Fig. A2.Presence of N atom shifts the electron density and removes the degeneracy from protons, which is present in benzene where all protons have the same chemical shift. There are three distinct protons (labeled 6, 4 and 5) which results in three groups of peaks located around 7, 7.08 and 7.24 ppm. Two of these groups are observable in the experimental (**E**) spectra of TPD near their predicted positions at 7.04 and 7.28 ppm. It is clear that they belong to the protons 5 and 6 from the outer phenyl ring without a methyl group. The values are shifted for 0.04 ppm which means that the third group should be at 7.12 ppm, however it is not obvious that the peak located there in **E** spectrum should be assigned to proton 4.

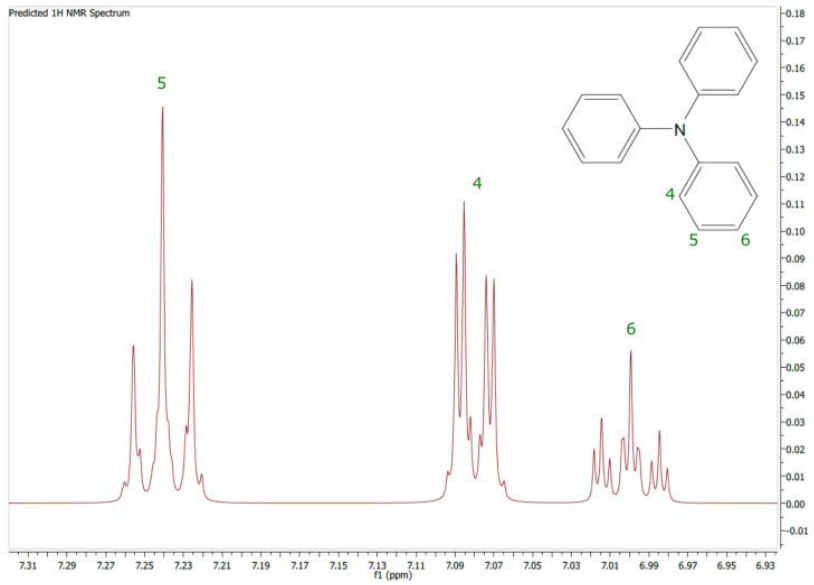

Fig.A.2 Predicted NMR spectrum of triphenylaimine (TPA).

The phenyl ring with the methyl group has four distinct protons (labeled 7, 8, 9 and 10) due to the influence of methyl group and N atom. Their predicted positions from the calculated spectra of TPD are 7.08, 7.02, 6.85 and 7.19 respectively. In the **E** spectrum two peaks can be observed at 6.88 ppm and they can be assigned to proton 9 and peaks at 7.18 ppm to proton 10. This leaves two unassigned protons for this ring. The center phenyl ring has two distinct protons (labeled 2 and 3) and gives two groups of peaks predicted at 7.29 and 7.43 ppm. Again only one group can be observed in the **E** spectrum located at 7.48 ppm and it can be assigned to proton 3. In order to complete

the assignation of the remaining protons (2, 4, 7, 8) an experimental spectra of irradiated TPD film (Fig.A3) was used as it was recorded with a higher resolution. The careful examination of the large group of 7.12 ppm reveals that peaks that belong to proton 4 are there as predicted however they are superimposed with another group. The two peaks in this group have the same symmetry and peak to peak distance as the group predicted for the proton 2, so they are assigned to it. The difference of predicted and observed value is 0.17 ppm. The predicted values for two remaining protons 7 and 8 are 7.08 and 7.02 ppm. However they could not be found in the experimental spectrum. The previous values obtained for shifts in the outer phenyl ring and the values given in reference [2] for shifts caused by methyl group on a phenyl ring are used to hand calculate the shifts for these protons. Obtained values for protons 7 and 8 are 6.95 and 6.93 ppm which is closer to the observed values.

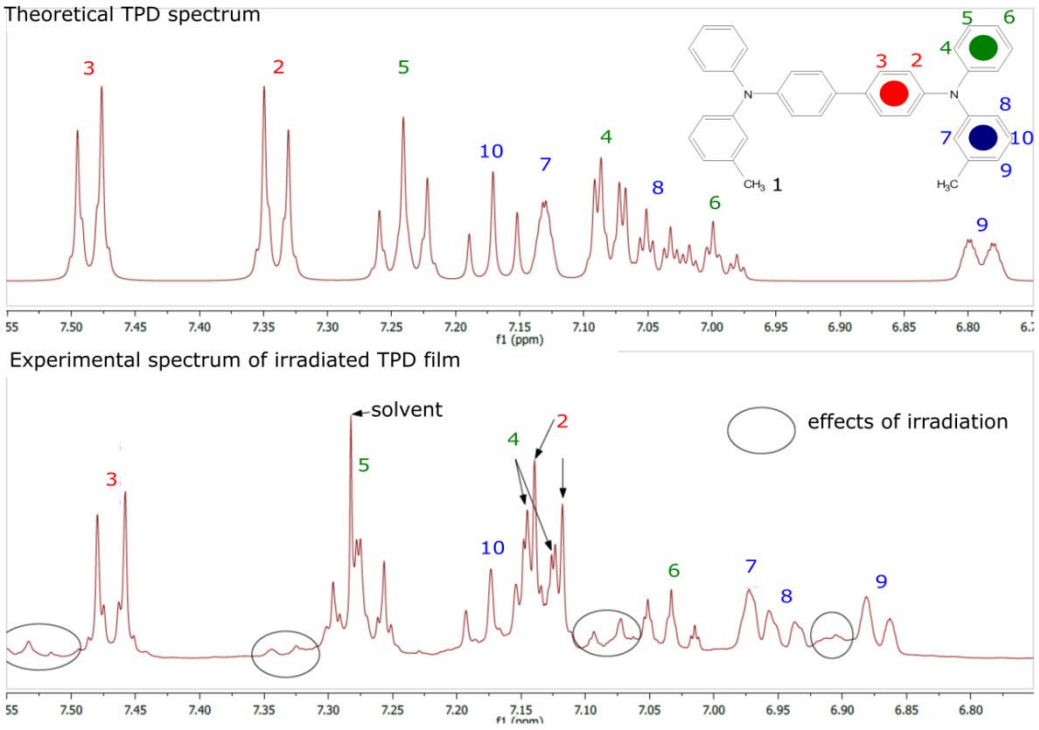

Fig.A3 Theoretical spectrum of TPD and high resolution experimental spectrum of irradiated TPD film.

The final results of assignation for non-irradiated TPD film and spectrum of irradiated film are shown in Fig.A1. Only the unique protons are labeled for clarity. From previous discussion it is clear that resonance at 2.3 ppm belongs to protons (1)

from two methyl groups while a large number of resonances centered at 7 ppm belong to protons (2–7) from phenyl rings.

References for Appendix A

[1] M.R. Willcott, *MestReNova*, J. Am. Chem. Soc. **131** (2009) 13180.

[2] M. Balci, *Basic ^{1}H- and ^{13}C-NMR Spectroscopy*, Elsevier, Amsterdam, 2005.

[3] Results regarding ^{1}H NMR of TPA can be found at following address: http://www.hanhonggroup.com/nmr/nmr_en/B37299.html

Appendix B: Evidences for formation of complexes upon irradiation of DPVBi films with UV light in air

B.1 Evidence for formation of complexes found in PL spectra

Evidence for existence of excited complexes was not found in absorbance. Very reasonable explanation for this would be small quantity which could not be detected. However some changes could be observed when PL spectra obtained for different irradiation times were compared to the spectrum of pristine sample. PL spectra for different irradiation times and that of pristine sample normalized to maximum value are shown in Fig. B.1 (left) and their difference in Fig B.1 (right). Results show that there is a small shift of emission maximum and that new broad peak appears and its intensity grows with irradiation time. This broad peak can be regarded as a hallmark for presence of complexes.

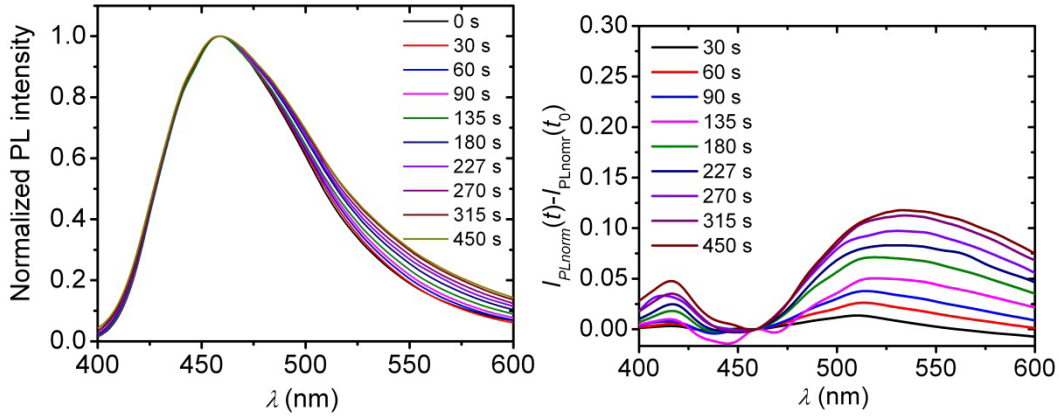

Fig. B.1 Normalized PL spectra for different UV light exposure times (left). Difference between normalized spectra for different UV exposure times and spectrum of pristine sample.

B.2 Evidences for formation of complexes observed by Raman spectroscopy

Presence of complexes can also provide explanation for background signal that was observed in the Raman spectra of irradiated DPVBi films. As it can be seen from the results, this background signal resembles photoluminescence, and its intensity grows

with irradiation time (Fig. B.2). Origin of this background signal is interesting, as from absorbance spectra it is clear that DPVBi nor the species that are created during irradiation process do not absorb at the wavelength of the He-Ne laser. If several Raman spectra were taken one after another, that is if laser irradiation was prolonged, a decrease of the background signal was observed. In order to prove that the irradiation with laser light is responsible for bleaching of the background signal following experiment was performed: two separate spots of the thin film were irradiated with UV light, then Raman spectra were recorded every minute, the first spot was continuously irradiated by the laser for ten minutes and the other was irradiated 10 x 1 min with one minute pauses in between.

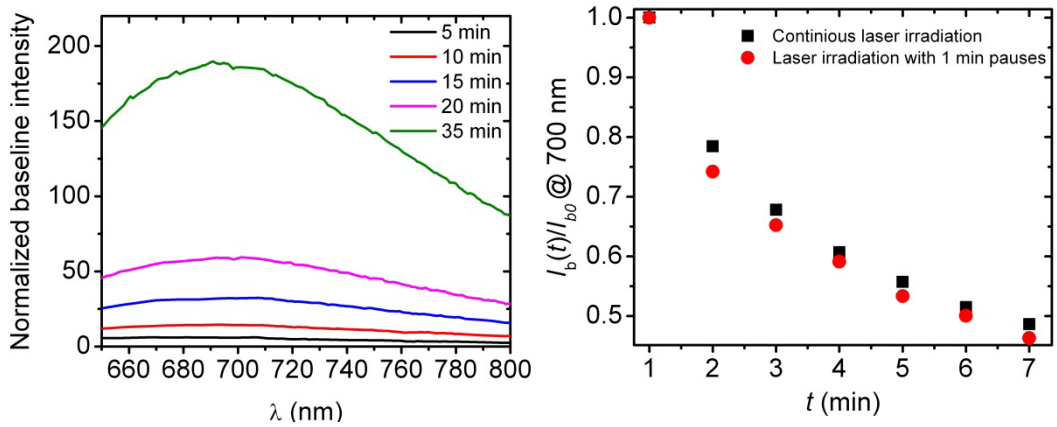

Fig.B.2 Raman background signal for different UV exposure times (left). Bleaching of the background signal with He-Ne laser with continuous exposure and with pauses.

Background signal was bleached for the same amount in both cases thus proving that the laser irradiation is responsible for this effect. This type of behavior suggests either reversibility of some chemical reaction or presence of complexes. While in fluids there is no ground state of exciplex as it is equal to dissociation, according to Birks [1] this does not have to be the case in the solid state. That is there is a possibility that a ground state could exist under the influence of surrounding molecules. It is possible that laser light could excite complex from the ground state which and their emission is responsible for the background signal. Also irradiation with laser light could also provide sufficient energy for dissociation of the complexes which would result in the bleaching of the background signal.

B.3 Partial reversibility of photoluminescence

It was shown that keeping irradiated film under vacuum for approximately one hour did not result in the recovery of the photoluminescence. However if the previously degraded part was irradiated in vacuum a partial recovery of PL was observed as presented in Fig. B.3.

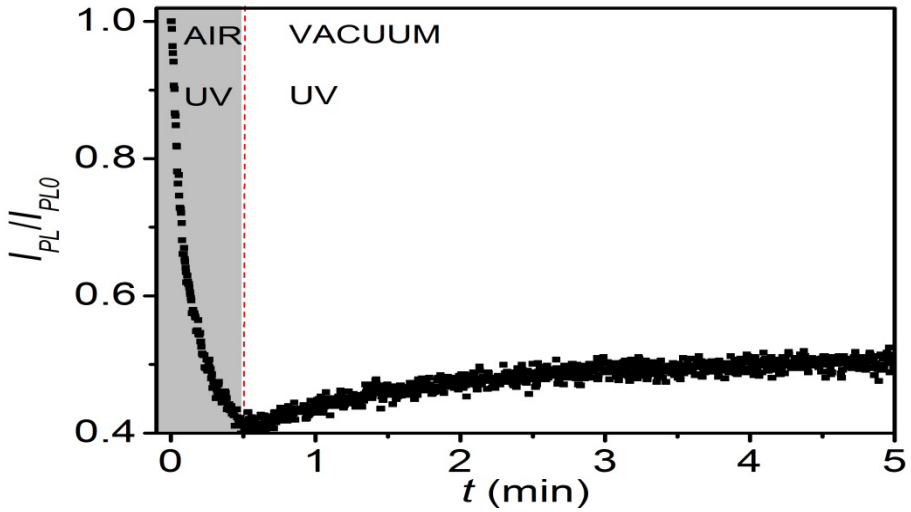

Fig.B.3 Partial reversibility of photoluminescence as a result of UV irradiation in vacuum.

First the film exposed to UV light in air for 30 s which resulted in loss of 60 % of its PL, and then the chamber was quickly pumped down to 10^{-2} Torr. After five minutes of exposure under vacuum 10 % of initial PL signal has been recovered. This can be explained by the reversibility of some chemical reaction or by dissociation of formed charge transfer complexes. Possible explanation for this phenomenon lays in the formation of exciplex between excited DPVBi and oxygen molecules. They would form a bound state with lower energy that would be in the visible region. Irradiation in vacuum possibly supplies energy for dissociation of complex and removal of oxygen from film.

References for Appendix B

[1] Edited by M. Gordon, *The Exciplex*, Acad. Press, New York, 1975.

Appendix C: Raman and IR spectra of TPD and DPVBi

Raman and IR spectra of pristine DPVBi and TPD films are shown in Fig. C1. Most prominent feature of the Raman spectra of both molecules is located at 1605 cm^{-1} and can be attributed to C=C stretch in the phenyl ring [1]. Several smaller features that can be found in the spectral range of 1000-1300 cm^{-1} for both molecules are consequence of C-H in plane vibrations.

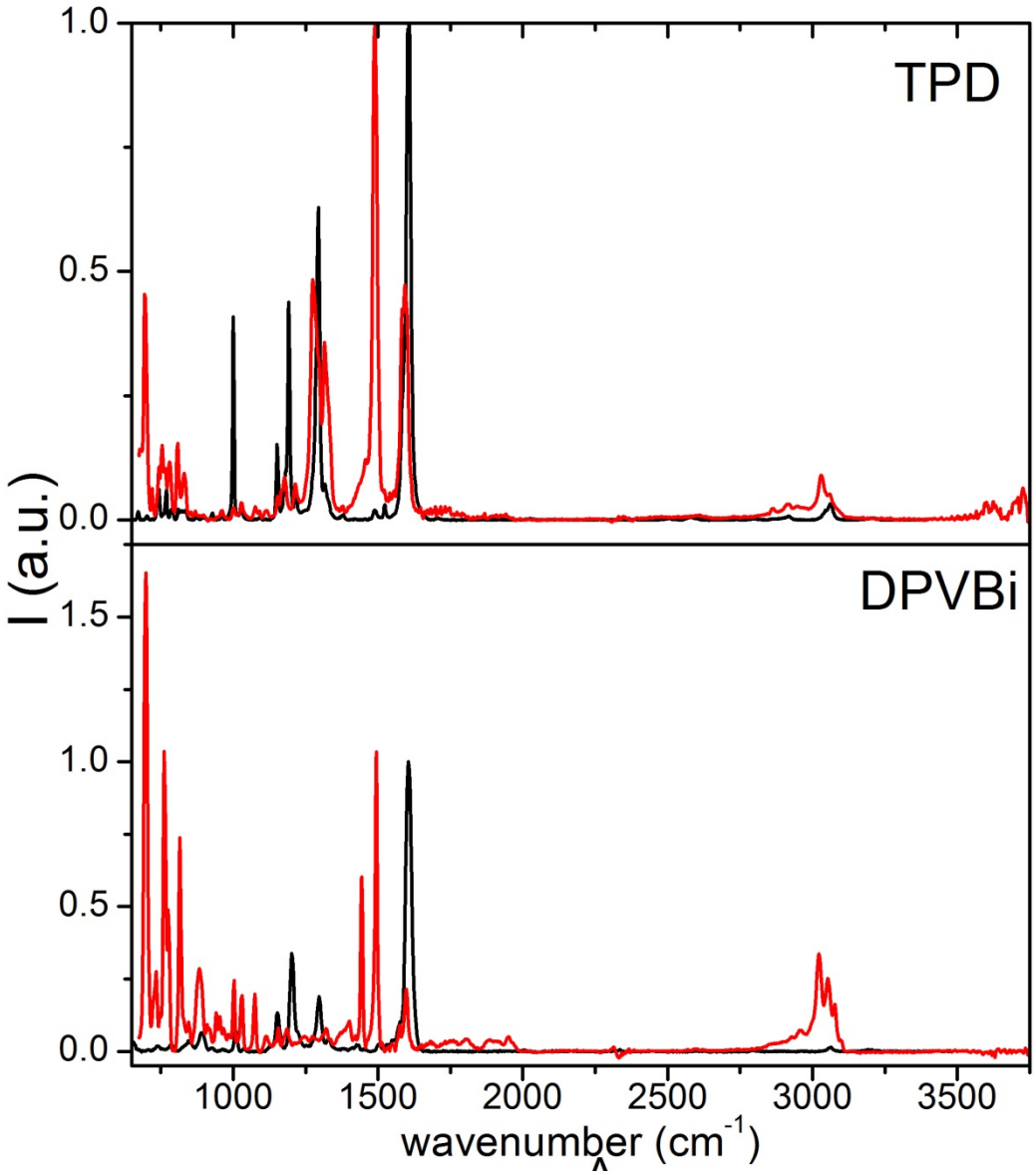

Fig.C1 Raman (black line) and IR (red line) spectra of a pristine DPVBi and TPD films.

IR spectrum of TPD was compared to the experimental spectrum of TPA [2] found in literature and the peaks are assigned according to it. Features in the region 754-831 cm^{-1} are due to out of plane C-H vibrations, as are the features in DPVBi spectrum

ranging from 761 to 880 cm^{-1}. The rest of the peaks in the TPD spectrum is connected to the following vibrations: 1274 cm^{-1} (C-N stretch), 1319 cm^{-1} (C-N stretch, C-N-C bend, R stretch), 1494 cm^{-1} (C-N, R stretch, C-H bend) and 1599 cm^{-1} (R stretch) [2]. While the remaining features in 1444-1599 cm^{-1} are due to C=C stretching vibrations [1].

References for Appendix C

[1] G. Sorcrates, *Infrared and Raman Characteristic Group Frequencies: Tables and Charts*, 3rd edition, John Willey and Sons, 2004.

[2] I. Reva, L. Lapinski, N. Chattopadhyay and R. Faustoa, *Vibrational spectrum and molecular structure of triphenylamine monomer: A combined matrix-isolation FTIR and theoretical study*, Phys. Chem. Chem. Phys. **5** (2003) 3844–3850.

Прилог 1.

Изјава о ауторству

Потписани-а Александар Ж. Томовић

број уписа _____

Изјављујем

да је докторска дисертација под насловом

Electronic properties and morphologies of thin films of organic molecules obtained by combinatorial deposition from gaseous phase

- резултат сопственог истраживачког рада,
- да предложена дисертација у целини ни у деловима није била предложена за добијање било које дипломе према студијским програмима других високошколских установа,
- да су резултати коректно наведени и
- да нисам кршио/ла ауторска права и користио интелектуалну својину других лица.

Потпис докторанда

У Београду, 25.06.2015.

Александар Томовић

Прилог 2.

Изјава о истоветности штампане и електронске верзије докторског рада

Име и презиме аутора ____Александар Ж. Томовић_____

Број уписа _____

Студијски програм __Физика кондензоване материје и статистичка физика_____

Наслов рада __ **Electronic properties and morphologies of thin films of organic molecules obtained by combinatorial deposition from gaseous phase**_____

Ментор __др Владимир П. Јовановић, научни сарадник_____

Потписани ___Александар Ж. Томовић_____

изјављујем да је штампана верзија мог докторског рада истоветна електронској верзији коју сам предао/ла за објављивање на порталу **Дигиталног репозиторијума Универзитета у Београду.**

Дозвољавам да се објаве моји лични подаци везани за добијање академског звања доктора наука, као што су име и презиме, година и место рођења и датум одбране рада.

Ови лични подаци могу се објавити на мрежним страницама дигиталне библиотеке, у електронском каталогу и у публикацијама Универзитета у Београду.

Потпис докторанда

У Београду, 25.06.2015.

Александар Томовић

Прилог 3.

Изјава о коришћењу

Овлашћујем Универзитетску библиотеку „Светозар Марковић“ да у Дигитални репозиторијум Универзитета у Београду унесе моју докторску дисертацију под насловом:

Electronic properties and morphologies of thin films of organic molecules obtained by combinatorial deposition from gaseous phase

која је моје ауторско дело.

Дисертацију са свим прилозима предао/ла сам у електронском формату погодном за трајно архивирање.

Моју докторску дисертацију похрањену у Дигитални репозиторијум Универзитета у Београду могу да користе сви који поштују одредбе садржане у одабраном типу лиценце Креативне заједнице (Creative Commons) за коју сам се одлучио/ла.

1. Ауторство

2. Ауторство - некомерцијално

3. Ауторство – некомерцијално – без прераде

4. Ауторство – некомерцијално – делити под истим условима

5. Ауторство – без прераде

6. Ауторство – делити под истим условима

(Молимо да заокружите само једну од шест понуђених лиценци, кратак опис лиценци дат је на полеђини листа).

Потпис докторанда

У Београду, 25.06.2015.

Александар Томовић